

EUR 5002 e

COMMISSION OF THE EUROPEAN COMMUNITIES

TRINO VERCELLESE NUCLEAR POWER PLANT RESEARCH PROGRAMME FOR THE DEVELOPMENT OF CLOSED-CYCLE WATER REACTOR TECHNOLOGY

Final Technical Report (1966-1972)

LIBRARY

1974



Report prepared by ENEL
Ente Nazionale per l'Energia Elettrica, Rome - Italy

Euratom Contract No. 071-66-6 TEEI

LEGAL NOTICE

This document was prepared under the sponsorship of the Commission of the European Communities.

Neither the Commission of the European Communities, its contractors nor any person acting on their behalf:

make any warranty or representation, express or implied, with respect to the accuracy, completeness, or usefulness of the information contained in this document, or that the use of any information, apparatus, method or process disclosed in this document may not infringe privately owned rights; or

assume any liability with respect to the use of, or for damages resulting from the use of any information, apparatus, method or process disclosed in this document.

This report is on sale at the addresses listed on cover page 4

at the price of B.Fr. 185.—

**Commission of the
European Communities
D.G. XIII - C.I.D.
29, rue Aldringen
L u x e m b o u r g**

September 1974

This document was reproduced on the basis of the best available copy.

EUR 5002 e

COMMISSION OF THE EUROPEAN COMMUNITIES

POWER PLANT DEVELOPMENT OR TECHNOLOGY

EUR 5002 e

TRINO VERCELLESE NUCLEAR POWER PLANT RESEARCH
PROGRAMME FOR THE DEVELOPMENT OF CLOSED-CYCLE WATER
REACTOR TECHNOLOGY
Final technical report (1966-1972)

Commission of the European Communities
Report prepared by the Ente Nazionale per l'Energia Elettrica, Rome (Italy)
Euratom Contract No. 071-66-6 TEEI
Luxembourg, September 1974 - 138 Pages - 57 Figures - B.Fr. 185.—

The present report covers the activities performed within the framework of the Research Program on the Trino Vercellese Nuclear Power Plant for the Development of Closed-Cycle Water Reactor Technology (EURATOM-ENEL Contract 071-66-6 TEEI). (June 1, 1966 to November 30, 1972.)

Task 1: to develop a zero-dimensional calculation model to study the core reactivity behaviour in various operating conditions. *Task 2*: to study the effect of main coolant pH changes on reactivity and on power and temperature

1972)

EUR 5002 e

TRINO VERCELLESE NUCLEAR POWER PLANT RESEARCH
PROGRAMME FOR THE DEVELOPMENT OF CLOSED-CYCLE WATER
REACTOR TECHNOLOGY
Final technical report (1966-1972)

Commission of the European Communities
Report prepared by the Ente Nazionale per l'Energia Elettrica, Rome (Italy)
Euratom Contract No. 071-66-6 TEEI
Luxembourg, September 1974 - 138 Pages - 57 Figures - B.Fr. 185.—

The present report covers the activities performed within the framework of the Research Program on the Trino Vercellese Nuclear Power Plant for the Development of Closed-Cycle Water Reactor Technology (EURATOM-ENEL Contract 071-66-6 TEEI). (June 1, 1966 to November 30, 1972.)

Task 1: to develop a zero-dimensional calculation model to study the core reactivity behaviour in various operating conditions. *Task 2*: to study the effect of main coolant pH changes on reactivity and on power and temperature

Report prepared by ENEL
Ente Nazionale per l'Energia Elettrica, Rome - Italy

Euratom Contract No. 071-66-6 TEEI

ABSTRACT

The present report covers the activities performed within the framework of the Research Program on the Trino Vercellese Nuclear Power Plant for the Development of Closed-Cycle Water Reactor Technology (EURATOM-ENEL Contract 071-66-6 TEEI). (June 1, 1966 to November 30, 1972.)

Task 1: to develop a zero-dimensional calculation model to study the core reactivity behaviour in various operating conditions. *Task 2*: to study the effect of main coolant pH changes on reactivity and on power and temperature reactivity coefficients. *Task 3*: to develop a neutron noise technique for the surveillance of reactor vessel internal structures. *Task 4*: to determine the gamma activity distribution among the fuel assemblies in order to evaluate fuel burnup and/or end-of-cycle power distributions. *Task 5*: to study the behaviour of the steam generators at various power levels and in different operating conditions in order to determine the steam generator ultimate capability. *Task 6*: to determine the significant core physics characteristics in various operating conditions with the aim of providing a check of the calculating techniques. *Task 7*: to determine the content of heavy isotopes in the fuel as function of burnup, initial enrichment, and neutron spectrum; to determine fuel burnup; to check the accuracy of calculating methods.

CONTENTS

INTRODUCTION	9
SUMMARY OF PLANT OPERATION	17
CONCLUSIONS	22
1. TASK No. 1: Reactivity Balances	22
2. TASK No. 2: pH Effect	23
3. TASK No. 3: Neutron Noise Analysis	23
4. TASK No. 4: Gamma Scanning of Selected Fuel Assemblies	24
5. TASK No. 5: Steam Generator Potential	25
6. TASK No. 6: Core Physics Characteristics	26
7. TASK No. 7: Post-Irradiation Examinations	26
8. ORIGINAL TASKS Nos. VI, VII, VIII and XII: Power Distributions, Flow Rate Through the Core and Flow Distributions, DNB Ratios, Core Protection and Control Systems.	28
9. ORIGINAL TASK No. IX: Flux Synthesis Techniques.	29

LIST OF FIGURES

- Fig. 1 Load diagram and integrated cycle burnup for Cycle 1
- Fig. 2 Load diagram and integrated cycle burnup for Cycle 2 and Cycle 3
- Fig. 2.1 pH and boron concentration values during the second pH test
- Fig. 3.1 Normalized power and cross power spectral densities of ion chambers RIC6 and RI10 (Trino Vercellese)
- Fig. 3.2 Normalized power and cross power spectral densities of ion chambers RIC4 and RIC5 (Trino Vercellese)
- Fig. 3.3 Normalized power and cross power spectral densities of ion chambers RIC3 and RIC7 (Trino Vercellese)
- Fig. 3.4 Normalized power and cross power spectral densities of ion chambers RIC8 and RI11 (Trino Vercellese)
- Fig. 3.5 NPSD value at the peak vs. azimuthal position of the ion chambers (Trino Vercellese)
- Fig. 3.6 Noise signal phases (Trino Vercellese)
- Fig. 3.7 Normalized power and cross power spectral densities of ion chambers LPR11 and LPR9 (Chooz)
- Fig. 3.8 Normalized power and cross power spectral densities of ion chambers (J. Cabrera)
- Fig. 3.9 Normalized power and cross power spectral densities of ion chambers E2 and E8 (J. Cabrera)
- Fig. 3.10 NPSD plots of the ion chamber RI-11 at 30% power for different configurations of the reactor internals (Trino Vercellese)

- Fig. 3.11 Normalized power and cross power spectral densities of ion chambers C9 and C2 (Garigliano)
- Fig. 4.1 Comparison between experimental and calculated gamma activity distributions
- Fig. 4.2 Axial gamma activity distribution in fuel assembly N. 91
- Fig. 4.3 Assemblywise power distribution comparison between Ge-Li scan and theoretical values
- Fig. 4.4 Assemblywise power distribution. Comparison between Ge-Li and gross gamma scan values.
- Fig. 4.5 Axial power distribution comparison between experimental values from Ge-Li and gross gamma scans.
- Fig. 4.6 Correlation between burnup and Cs-137 activity at the end of cycle 2 (Ge-Li gamma scanning data, assembly averages).
- Fig. 4.7 Correlation between burnup and Cs-137 activity at the end of Cycle 2.
- Fig. 5.1 Steam generator schematization for the F.111 RID code analysis.
- Fig. 5.2. a) Simplified diagram of high pressure steam lines of the Trino Vercellese plant.
- Fig. 5.2. b) Equivalent electric network for the ARIA code.
- Fig. 5.3 Time variation of steam flow rate, steam quality and liquid velocity in the first element (940 MWt).
- Fig. 5.4 Time variation of steam flow rate, steam quality and liquid velocity in the first element (1100 MWt).
- Fig. 5.5 Feedwater temperature (Tfw), feedwater flow rate (Wfw) and secondary pressure (Ps) vs. power.

- Fig. 5.6 Time variation of water level (Y), steam quality (Xout), steam flow rate (Wg) and liquid velocity (U) in the first element (940 MWt).
- Fig. 5.7 Time variation of water level (Y), steam quality (Xout), steam flow rate (Wg) and liquid velocity (U) in the first element (1100 MWt).
- Fig. 5.8 Time variation of steam flow rate, steam quality and liquid velocity in the first element (1200 and 1250 MWt).
- Fig. 5.9 Amplitudes of steam generators level oscillations (normalized to steam generator A oscillation at 825 MWt) versus power.
- Fig. 5.10 Amplitudes of steam generators level oscillations (normalized to steam generator A oscillation at 825 MWt and nominal level set point) versus power. + 30 cm level set point.
- Fig. 5.11 Overall heat transfer coefficient vs. power.
- Fig. 5.12 Experimental T_p vs. power
- Fig. 5.13 Secondary pressure (P_s) vs. power
- Fig. 5.14 Steam pressure and heat transfer coefficient vs. primary avg. temperature for various power levels.
- Fig. 5.15 Overall heat transfer coefficient vs. power for various average temperatures (T_m)
- Fig. 5.16 Steam pressure vs. power

- Fig. 6.1 Moderator temperature coefficient vs. boron concentration (hot, zero power, beginning of cycle).
- Fig. 6.2 Moderator temperature coefficient vs. moderator temperature (hot, zero power, beginning of cycle).
- Fig. 6.3 Control group differential worth.
- Fig. 6.4 Differential control rod worth.
- Fig. 7.1 Total gamma-activity, part of typical rod.
- Fig. 7.2 Total gamma activity, typical rod.
- Fig. 7.3 Comparison of experimental and theoretical axial burnup distributions in two fuel rods at the end of cycle 1
- Fig. 7.4 a) Isotopic production and depletion vs. burnup for the inner core region.
- Fig. 7.4 b) Isotopic production and depletion vs. burnup for the intermediate core region.
- Fig. 7.4 c) Isotopic production and depletion vs. burnup for the outer core region.
- Fig. 7.5 Correlation between burnup and U-235/U-238
- Fig. 7.6 Correlation between U-235/U-238 and Pu-240/Pu-239
- Fig. 7.7 Correlation between uranium depletion and Kr-84/Kr-83.
- Fig. 7.8 Correlation between Pu/U and Xe-131/Xe-134.
- Fig. 7.9 Correlation between Pu/U and Cs-137, Ce-144, Ru-106 specific activities.

- Fig. 7.10 Correlation between Pu/U and Cs-134/Cs-137 activity ratio
- Fig. 7.11 Correlation between burnup and Cs-134/Cs-137 activity ratio
- Fig. 8.1 Normalized power density distribution changes during core lifetime.
- Fig. 8.2 Assemblywise radial power distributions at 3330 MWD/MTU and at end of cycle (11,500 MWD/MTU) (full power, data normalized to unit average)
- Fig. 8.3 Axial burnup distribution of a central fuel assembly at end of cycle (average assembly burnup; 12,500 MWD/MTU)
- Fig. 8.4 Effect of an average temperature change on normalized axial power density distribution at end of cycle.
- Fig. 8.5 Effect of power level change on normalized power density distribution at end of cycle.

INTRODUCTION

The present report covers the activities performed within the framework of the Research Program on the Trino Vercellese Nuclear Power Plant for the Development of Closed-Cycle Water Reactor Technology (EURATOM-ENEL Contract No. 071-66-6 TEEI (RD) for the period June 1st, 1966 - November 30th, 1972. Originally, the program consisted of 12 tasks. However, in April 1969, a re-arrangement of the program took place: the tasks were then reduced to 7.

Between Cycles 1 and 2 the plant was shutdown for an extended period (April 29, 1967 - January 20, 1970) for reactor pressure vessel internals repairs and modification which required the removal of the Aeroball In-Core Instrumentation System. When plant operation was resumed, some of the original tasks appeared obsolete. Some other tasks such as Task No. VI (Power Distributions) had to be discontinued because of the removal of the Aeroball System.

A list of the original and of the revised tasks follows:

<u>Original Tasks</u>	<u>Revised Tasks</u>
I Reactivity Balances	1 Unchanged
II pH tests	2 Unchanged
III Surface Boiling	3 Neutron Noise Analysis
IV Litium and Potassium Tests	- Cancelled
V Materials Behaviour	4 Gamma Scanning 7 Post-Irradiation Examinations
VI Power Distributions	- Discontinued

<u>Original Tasks</u>	<u>Revised Tasks</u>
VII Flow Rate Through the Core and Flow Distributions	- Discontinued
VIII DNB Ratios	- Discontinued
IX Flux Synthesis Techniques	- Closed
X Steam Generator Potential	5 Unchanged.
XI Core Physics Characteristics	6 Unchanged.
XII Core Protection and Control Systems	- Closed.

The basic objectives of the various tasks are as follows:

Revised Tasks

- Task No. 1: To develop a zero-dimensional calculation model to study the core reactivity behaviour in various operating conditions.
- Task No. 2: To study the effect of main coolant pH changes on reactivity and on power and temperature reactivity coefficients.
- Task No. 3: To develop a neutron noise technique for the surveillance of reactor vessel internal structures (modified from the original objective, i.e. to study the surface boiling phenomenon).
- Task No. 4: To determine the gamma activity distribution among the fuel assemblies in order to evaluate fuel burnup and/or end-of-cycle power distributions.
- Task No. 5: To study the behaviour of the steam generators at various power levels and in different operating conditions in order to determine the steam generator ultimate capability.

Task No. 6: To determine the significant core physics characteristics in various operating conditions with the aim of providing a check of the calculating techniques.

Task No. 7: To determine the content of heavy isotopes in the fuel as function of burnup, initial enrichment, and neutron spectrum; to determine fuel burnup; to check the accuracy of calculating methods (modified from the objective of original Task No. V).

Original Tasks

Task Nos. VI, VII, VIII and XII: To determine the ultimate capability of the core with the aid of the in-core instrumentation (Aeroball System).

Task No. IX: To investigate a simple method for determining a three-dimensional power distribution from calculated radial power distributions and Aeroball data.

No activity has been performed on Task No. IV, since this task appeared already obsolete by the time the technical work had started (June 1966) following contract negotiations. This task was originally conceived when the boron hide-out phenomenon was a source of concern for the chemical shim operation of PWRs.

In the course of the program, 25 Quarterly Progress Reports were issued, starting October 1st, 1966, and ending November 30th, 1972. Reports 22 and 23 were published in a single volume in April 1972. Following Quarterly Progress Report No. 13, all reports were issued in English (earlier reports were written in Italian).

Six Annual Reports were published respectively in July 1967, 1968, 1969, 1970, 1971 and 1972 (the last three reports in English).

Table I indicates the quarterly and annual progress reports dealing with the various tasks.

The following Topical Reports (all in English) were issued at various times during the program:

- Neutron Flux Distributions During First Operating Cycle of Trino Vercellese Reactor, by G. P. Battista and S. Valenziani (ENEL), 1967 and Addendum 1
- Comparison Between Theoretical and Experimental Physics Data for Trino Core No. 1, by R. Bannella (ENEL) and A. Fedrighini (FIAT), 1969
- Report on the Operations Performed at the C. C. R. EURATOM of Ispra on Three Irradiated Fuel Assemblies, by A. Costantino (ENEL), 1970
- A Computer Code for Calculating Reactivity Balances, by P. Fornaciari and M. Gatto (ENEL), 1970
- In-Service Monitoring of Core Structures and Reactor Internals by Neutron Noise Measurements, by M. Calcagno and F. Cioli (ENEL), 1970
- Core Power Distribution at the End of Cycle 2 from La^{140} Activity Measurements, by A. Agostinelli (ENEL) et al., 1972
- Neutron Noise Measurements at the Jose` Cabrera Reactor (Zorita), by M. Calcagno, D. Castaldi, F. Cioli and C. A. Ottaviani (ENEL), 1972.

TABLE 1: REFERENCES

Report	Task N° 1	Task N° 2	Task N° 3	Task N° 4	Task N° 5	Task N° 6	Task N° 7	VI-VII VIII-XII	IX
APR-1	*	*	*		*	*	*	*	
APR-2	*	*	*	*	*	*		*	*
APR-3	*		*			*	*	*	
APR-4	*		*			*	*		
APR-5	*	*	*	*	*	*	*		
APR-6			*	*	*	*	*		
QPR-1	*	*			*	*	*	*	
QPR-2	*	*			*	*	*	*	
QPR-3		*	*		*	*	*	*	
QPR-4	*	*	*		*	*	*	*	
QPR-5	*	*	*	*	*	*		*	
QPR-6		*	*	*	*			*	
QPR-7			*	*				*	*
QPR-8	*	*	*	*	*	*		*	*
QPR-9								*	
QPR-10	*					*		*	
QPR-11	*		*			*	*		
QPR-12	*		*			*	*		
QPR-13	*		*			*	*		
QPR-14	*		*			*	*		
QPR-15	*		*			*	*		
QPR-16	*		*			*	*		
QPR-17		*	*				*		
QPR-18	*	*	*			*	*		
QPR-19			*	*			*		
QPR-20			*	*	*		*		
QPR-21			*	*	*	*	*		
QPR-22			*	*	*	*	*		
QPR-23									
QPR-24			*	*	*		*		
QPR-25			*			*	*		
QPR-26			*						

APR = Annual Progress Report
 QPR = Quarterly Progress Report

Over the same period of validity of the ENEL program, an integrative research program has been performed by FIAT, Sezione Energia Nucleare (1).

The main objective of this integrative program was to provide an interpretation of the experimental results obtained through the ENEL program, to make theoretical predictions, and to compare experimental and theoretical results.

Thirteen Progress Reports were issued in the course of this program plus the following Topical Reports:

- Topical Report No. 1: Post-Irradiation Examination of Trino Vercellese Core 1 Fuel Elements: Four Group Cross Section Libraries Evaluation as Function of Burnup, FN-E-112 (1970)
- Topical Report No. 2: Trino Vercellese Core One Post-Irradiation Analysis: Interpretation of the Experimental Results and Theoretical Predictions, by M. De Serafini et al., FN-E 118 (1971).

A summary of the work performed by FIAT is contained in "Research Program Integrative of the ENEL Program on the Trino Vercellese Reactor: Final Report", by F. Basile et al., EUR 5003, 1973.

The experimental portion of Task No. 7 (Post-Irradiation Fuel Examinations) was carried out mainly by EEC personnel of the

(1) FIAT has performed additional work on Tasks No. 5 and 7 under a subcontract with ENEL.

Joint Research Center (JRC) at Ispra. The task included two series of measurements: analyses of selected rods removed from three assemblies discharged at the end of Cycle 1, and analyses of selected rods from one assembly discharged at the end of Cycle 2.

The results of the first series of measurements are given in: "Post-Irradiation Analyses of Trino Vercellese Reactor Fuel Elements", by J. Biteau et al. (JRC Ispra - Karlsruhe), Doc: EUR/4909/e, 1972.

The second series of analyses is still under way: the JRC will publish a second report at the completion of the work (late 1973). The theoretical portion of Task No. 7 was carried out by FIAT. The results are given in Topical Reports Nos. 1 and 2 already mentioned. In the frame of Task No. 7 the computer code CONDOR-3 (refined version of CONDOR-2) was prepared by Applicazioni e Ricerche Scientifiche (ARS) of Milan.

The activities related to Task No. 3 (Neutron Noise Analysis) were closely coordinated with the work performed under a EURATOM Study Contract with ENEL and four other parties named "On-load Surveillance Techniques of Nuclear Plant Components", EURATOM Contract No. 043-71-10-ECIC.

A report was issued by the five participants to this Contract in 1972, with the title "On-load Surveillance of Nuclear Power Plant Components by Noise and Vibration Analyses".

The results of the work performed under EURATOM-ENEL Contract No. 071-66-6 TEEI (RD) (subject of this Final Report) and under the above-mentioned EURATOM-FIAT Contract No. 098-66-6 TEEI were presented to the Commission and to various experts of the Community at the following six meetings:

1. May 18, 1967, Bruxelles
2. January 23, 1968, Bruxelles
3. February 6, 1970, Bruxelles
4. November 25, 1970, Bruxelles
5. October 29, 1971, Ispra
6. June 15, 1972, Torino.

SUMMARY OF OPERATION

The reactor was first brought to criticality on June 21, 1964.

Power production began on October 22, 1964.

The reactor is now in its third cycle of operation, scheduled to end on March 30, 1973.

A summary of the operation is presented in Table II. The load diagram and integrated cycle burnup for the years 1964-1972 are plotted in Figs. 1 and 2.

A summary of the main operation events follows.

Cycle 1

During the design stage, it was decided that the reactor power level (originally established at 615 MW(th) could be stretched up to 825 MWth.

Therefore the installation of a second turbogenerator unit was decided to bring total station electric power rating from 182 MWe to 257 MWe.

Operation started with only unit No. 1, and during Cycle 1 a shutdown of three months (June 6 - August 30, 1965) took place to tie in unit No. 2. At the increased power level of 825 MWth, the main coolant average temperature was reduced from 282°C to 278°C.

A second shutdown of about seven weeks took place in mid 1966 for unit No. 1 inspection and maintenance.

At the end of the cycle, a stretch-out operation was performed in two steps; First, rods were completely withdrawn and the full power was kept constant by letting the average temperature drop from 278°C to 274°C (this allowed 11 more days at full

power after the end of the nominal cycle).

Finally unit No. 1 was shutdown and the reactor power was cut to 300 MWth allowing two additional weeks of operation on unit No. 2.

Cycle 1 ended on April 28, 1967.

Shutdown after Cycle 1

During the shutdown, it was found that some of the vessel internals were damaged. The same type of problem was experienced at the SENA plant at Chooz, which is of the same design as Trino. As a result of these damages, the thermal shield and the in-core instrumentation (Aeroball System and thermocouples) were removed from the vessel. Extensive repairs and modification took place and only in January 1970 the plant was ready for tests at reduced power on the repaired internals.

These tests were performed for some weeks in January and February, then the plant was shutdown again for inspection. During Cycle 1, some debris from the damaged vessel internals had become stuck inside some fuel assemblies. The assemblies themselves were in good conditions, but to avoid thermal-hydraulic problems due to flow blockage in subsequent cycles, it was decided to discharge from the core, in addition to the 40 assemblies of the scheduled discharge batch, 12 more assemblies originally intended for two or three cycles of irradiation.

Then only 44 fresh assemblies were reloaded in the core thus lowering the core loading from 120 to 112 square assemblies.

TABLE II
SUMMARY OF PLANT OPERATION

Cycle	1	2	3
Duration	22.10.64/28.4.67 ⁽¹⁾	20.5.70/9.7.71 ⁽²⁾	9.9.71/30.3.73 ⁽³⁾
Burnup (MWD/MTU)	11,590	8,189	8,552 ⁽³⁾
Gross power production (GkWhe)	3,388 ⁽⁴⁾	2,197	2,388 ⁽³⁾
On-line capacity factor	...	94.4%	80.8% ⁽³⁾
Core loading (No. of square assemblies)	120	112 ⁽⁵⁾	112

(1) Two extended shutdowns took place during the cycle for installation of the TG unit No. 2 (6.6/31.8.65) and for maintenance and inspection of unit No. 1 (21.5/11.7.66)

(2) Tests at power were performed in January and February 1970, following vessel internals repairs.

(3) As of Dec. 31, 1972.

(4) Not available because of plant uprating during cycle.

(5) Loading was reduced in order to limit fast neutron flux at vessel wall after thermal shield removal.

This loading reduction was decided to reduce fast neutron flux at the vessel wall after thermal shield removal.

Cycle 2

Notwithstanding the loading reduction, the rated power level for Cycle 2 was kept at 825 MWth. The main coolant average temperature was further reduced from 278°C to 269°C.

Initially, the plant operated at 30% of full power, then after three weeks from startup, following authorization of the Licensing Authority, the full power level was achieved.

Cycle 2 operation was very smooth: load reductions or short shutdowns occurred only in July 1970 and March 1971 for maintenance and/or minor troubles. This is reflected in the high on-line capacity factor during the cycle (94.4%).

Cycle 3

After a three-month shutdown for refueling and maintenance, the reactor was brought to criticality on September 9, 1971. Full power was reached on September 25, 1971. Also during Cycle 3 the main coolant average temperature was kept at 269°C.

Cycle 3 is scheduled to end on March 30, 1973.

The main events during the cycle are the following:

- Oct. 1 - Nov. 6, 1971: shutdown for repairs of the low-pressure pumps of the emergency core cooling system;
 - April 7 - May 9, 1972: unit No. 1 outage for turbine repairs.
- Up to Dec. 31, 1972, Cycle 3 on-line capacity factor was 80.8%.

Throughout the three cycles of operation, the fuel performance was entirely satisfactory: no fuel clad failures were experienced with very low fission product activities in the coolant.

CONCLUSIONS

The following general conclusions can be drawn:

- a. As a result of the research work, new and modern techniques, such as neutron noise analysis and isotopic gamma scanning were satisfactorily developed or improved.
- b. A series of experimental data on reactor physics was collected and a detailed understanding of reactor behaviour was gained.
- c. The post-irradiation examinations performed at the Joint Research Laboratories (Ispra and Karlsruhe) provided new information on fuel isotopics and its dependence on neutron spectrum.
- d. The integrative program performed by FIAT allowed the development of a calculation technique which proved to be quite satisfactory for interpreting and predicting the reactor and plant performance.

The following specific conclusions for the single tasks can be drawn:

Task No. 1: Reactivity Balances

The work performed proves that a simple zero-dimensional model with two energy groups can predict fairly well the reactivity behaviour of the reactor.

Task No. 2: pH Effect

- a. The difference between the power defects at normal and reduced pH is fairly close to the reactivity loss experienced at full power upon pH reduction. This confirms that the power defect change accounts for the entire pH reactivity effect.
- b. The mechanism through which the pH affects the power coefficient appears to be a change of heat transfer characteristics between fuel and coolant, due to modifications induced by pH change of the crud deposits on fuel clad surfaces.

Task No. 3: Neutron Noise Analysis

- a. The neutron noise technique has proved fully successful for revealing pendular oscillations of the lower vessel internals package of PWRs.
- b. No other oscillations of the internals have been firmly evidenced.
- c. By comparing the neutron spectra before and after the repairs of the reactor vessel internals in Trino, the conclusion may be drawn that the noise analysis technique is potentially capable of detecting changes in the structural integrity of the reactor internals thus providing a means for surveillance and incipient failure detection.
- d. For a better understanding of the noise phenomena, a continuous monitoring of the neutron noise spectra of a given reactor over a long period of time is recommendable. A correlation of changes in the neutron spectra with varying

plant operating conditions should be investigated, possibly by concurrently analyzing the noise of physical parameters other than the neutron flux.

Task No. 4: Gamma Scanning of Irradiated Fuel Assemblies

a. Gross-gamma scanning five months after the end of Cycle 1

The good agreement between the radial and axial gamma activity distributions measured and those calculated starting from data of the in-core instrumentation (Aeroball System) confirms the accuracy of the calculation of the burnup distribution.

b. Gamma scanning at the end of Cycle 2

i. The overall standard deviation of the measurements was found to be 2.0%.

ii. The mean square deviation between calculated and measured values is 2.2%.

No particular trends in the deviations were evidenced: the discrepancies are statistically distributed between the core center and the periphery, low and high enrichments, low and high burnup assemblies.

iii. The mean square deviation between Ge-Li and gross gamma data is 2.8%. The gross gamma scan produced lower power values for the peripheral assemblies.

iv. In general, the measurements demonstrated the validity of Ge-Li gamma scanning as an accurate method for determining end-of-cycle power distributions.

On the other hand, the gross gamma scan still provides

useful information for PWR's because the power distribution does not change substantially during the last two or three months of the cycle.

c. Gamma scanning nine months after the end of Cycle 2

- i. It was confirmed that the Cs-137 activity is a good burnup indicator.
- ii. A linear correlation was found between the Cs-134/Cs-137 activity ratio and the Pu/U mass ratio in the fuel.

Task No. 5: Steam Generator Potential

- a. Two main phenomena could result in limiting the steam generator capability and thus the plant power capability:
 - i. Thermohydraulic instability of the steam generator recirculation loop.
 - ii. Acoustic resonance phenomena in the secondary steam circuit of the plant.

No limits are imposed by average temperature oscillations which are certainly self-limited in a PWR-type plant.

- b. The power level corresponding to the threshold of thermohydraulic instability was found to be at about 1200 MW(t). Thus, future power upratings up to 1020 MW(t) (being presently planned) will not be prevented because of thermohydraulic instability phenomena in the steam generator recirculation loop.

c. Very large oscillations on the steam generator secondary variables could take rise for plant power levels higher than the nominal one (825 MW(t)) if a coincidence between the acoustic resonance frequency of the steam circuit and the frequency of the thermohydraulic loop preferential mode of oscillation should be permitted.

A + 30 cm liquid level set point is required in order to damp the acoustic oscillations. In this case, a quite stable behaviour can be predicted up to at least 1020 MW(t).

Task No. 6: Core Physics Characteristics

a. Core physics measurements were performed at the startup of each cycle and during the cycles when other special tests were in progress. Reactivity coefficients, boron worth and control rod differential and integral worths were measured several times.

b. Of special interest are the results obtained for the control rod differential worth at power: it was found that the differential worth depends on initial rod position, i. e. initial axial distribution, and it is affected by the axial Xenon transient initiated by the rod movement itself.

c. The axial burnup distribution was found to affect the shape of the control rod differential worth curve.

Task No. 7: Post-Irradiation Examinations (first series of measurements)

a. The visual examination of the fuel rods confirmed that the clad had no defects.

- b. Metallographic examination of the fuel confirmed that, besides the cracking of the fuel, there was no particular modification in the microstructure.

The microstructure of the cladding was homogeneous.

- c. Absolute values of burnup for 21 fuel samples were determined utilizing three distinct destructive methods:

- gamma scanning of dissolved fuel solutions
- mass spectrometry of fuel samples for heavy isotopes concentration measurements
- mass spectrometry of fuel samples for Nd-148 concentration measurements.

A fourth determination of burnup was obtained from non-destructive Cs-137 activity measurements (Ge-Li gamma spectrometry).

The results obtained with the four methods agree among themselves within $1 \pm 4\%$.

- d. The mass spectrometric analysis provided data of isotopic fuel composition versus burnup in the range 3000 \pm 18000 MWD/MTU. There is a good agreement between calculated and experimental results.
- e. Various linear correlations were observed between concentration ratios of fission products and/or heavy isotopes. All the observed correlations proved the consistency of the experimental data.

Original Task No. VI: Power Distributions

- a. The axial power density distributions through Cycle 1 reflect the hystory of the control rod operation.
In the first part of the cycle with the control group inserted by 30-40%, the distribution was skewed toward the bottom. In the middle part of the cycle, following rod withdrawal from 30-40% to approximately 4%, the distribution shifted toward the upper portion of the core. In the last part of the cycle, the axial power density profile was noticeably flat.
- b. The flat power density profile at cycle end is the result of a balance between the accumulated axial burnup distribution and the moderator temperature distribution along the height of the core. In fact, due to initial insertion of control rods, the burnup profile is slightly skewed toward the bottom; this makes the lower portion of the core less reactive, thus compensating the negative reactivity effect in the upper portion where the water is hotter.
- c. The radial power distribution becomes flatter with progressing irradiation; the peak decreased during Cycle 1 from 1.23 to 1.17 and the power increased in the outer region of the core.
- d. The effect on the axial power density distribution due to variations in average coolant temperature and power was evidenced during Cycle 1 by means of the Aeroball System. When the coolant temperature was decreased from 276 to 271°C, the axial power density profile, previously flat, became skewed toward the top of the core.

Obviously, the temperature decreased both in the lower and in the upper portions of the core, but the reactivity gain was higher in the upper portion, because of the non-linearity of the temperature coefficient. This fact was experienced only at the end of the cycle when an equilibrium in terms of reactivity between the normal temperature gradient and the axial burnup distributions had been reached and when the temperature coefficient is higher.

- e. A similar effect is caused by a power level change occurring at constant average temperature. A power reduction from 825 MW(t) to 260 MW(t) caused again the power density distribution to skew toward the top. Following the power reduction, the temperature actually increased in the lower half of the core and decreased in the upper half with the reactivity rising at the top and decreasing at the bottom.
- f. The accuracy of the Aeroball System during the first part of Cycle 1 could not be systematically assessed. Toward the end of the cycle, a repeatability test was conducted covering several Aeroball runs. All the experimental points fell within a $\pm 2\%$ interval.

Original Task IX: Flux Synthesis Techniques

- a. Full separability of the three-dimensional power distribution into radial and axial components has been demonstrated to hold for almost the entire core without control rods (only for two small regions located at the top and at the bottom of the core and for the peripheral assemblies, no firm conclusions about separability could be drawn).

- b. The separability holds for all burnup levels throughout Cycle 1, according to the analysed data.
- c. The power density synthesis can be easily performed in the unrodded region. For the core with control rods partially inserted, two cases were considered:
 - i. Asymptotic conditions of the power density distribution are reached in both the rodded and unrodded axial region.
 - ii. Asymptotic conditions of the power density distribution are reached only in the unrodded axial region.
- d. For case i., a method of power density synthesis was developed which avoids the discontinuities at the interface between the axial zones. This method could not be checked against experimental results, since during Cycle 1 control rods were not inserted deeply enough to allow the attainment of asymptotic conditions of the power density distribution in the rodded region.
- e. For case ii., no generally applicable method of power density synthesis could be developed.

Integrative Program Performed by FIAT - Sezione Energia Nucleare

- a. During Cycle 1, FIAT developed a calculational method for PWR core physics evaluation. The method was set up and checked with the aid of the experimental data collected by ENEL. The finalized method was then employed to provide theoretical predictions of the results of all subsequent physics tests performed at Trino.

- b. The post-irradiation examination data were also analyzed with methods provided by FIAT.
- c. In general, the calculational methods developed by FIAT proved to be in agreement with the experimental data.

1. TASK No. 1: Reactivity Balances

1.1 Objective

To develop a zero-dimensional model to study the core reactivity behaviour in various reactor operating conditions.

1.2 Experimental Work

No experimental work was performed for this task. Available operating and experimental data were employed for the analysis.

1.3 Analytical Work

1. A digital code was developed. It is described in the Topical Report "A Computer Code for Calculating Reactivity Balances". The code utilizes the two-group theory with a zero-dimensional model of the reactor core which takes into account the core regions by means of statistical weighting factors.
2. The cross sections are obtained through polynomial expansions of cross sections calculated for selected values of the variables with the LEOPARD Code.
3. The code makes a reactivity balance between two situations: an initial and a final one (the two situations may coincide and the code will compute reactivity coefficients for the given situation). The code calculates the various reactivity coefficients in the initial conditions and uses them to evaluate the in-

dividual reactivity changes due to the various operating parameters between the initial and the final conditions.

4. The output of the code consists of the reactivity coefficients and of the value of a selected operating variable (usually the boron concentration in the primary coolant) which closes the reactivity balance.
5. The code has been tested and is actually operative on the UNIVAC-1108.

1.4 Summary of Results and Conclusions

1. The work performed proves that a simple zero-dimensional model with two energy groups can predict fairly well the reactivity behaviour of the reactor.
2. The code was initially conceived with the purpose of monitoring the reactivity changes in relation to the feared boron hide-out phenomenon associated with the chemical shim operation and was intended to determine the core reactivity behaviour both at steady state and during operational transients. However, the difficulty to express the cross sections and the other nuclear constants within wide range of the main operating variables limited the range of correct application of the program to the field of normal operating conditions.

3. All the LEOPARD calculations, on which the polynomial expansions are based, are valid for Cycle 1. An extension to Cycle 2 would have required a new set of LEOPARD calculations, new polynomial expansions and new statistical weights. This made the extension of the code to subsequent operating cycles quite time-consuming.
4. Other limitations of the code are the following:
 - a. Spatial effects are considered only through radial statistical weights
 - b. Rapid transients are not treated: the code performs a reactivity balance between stationary conditions (however, Xenon transients can be followed)
 - c. The control rod worth is calculated using a formula that interpolates the experimental data as function of burnup and initial rod group position (all other reactivity coefficients are calculated using theoretical formulae of the two-group theory)
 - d. The code is accurate only in a range of temperatures centered around the rated value.
5. The work performed was presented at a meeting of EEC experts in Bruxelles. It was concluded that the results obtained are satisfactory but no need was envisaged to extend the code to subsequent cycles

and to program it on the plant process PRODAC-510 computer.

Actually, this matter lost much of its interest because of the discovery that the anomalous reactivity changes which occurred in the Yankee plant (and in general in the early PWRs) were in all cases slow (time constants of the order of hours), thus not impairing the safety of the operation.

2: pH Effect

jective

Following the discovery of a number of anomalous reactivity changes at the Yankee plant, an experimental program was performed at Trino to study the effect of main coolant pH changes on reactivity and on power and temperature reactivity coefficients.

Experimental Work

1. Two pH tests were performed, one during Cycle 1 (October 1966) and the other during Cycle 2 (October 1970).
2. In each test, the coolant pH was reduced from the normal value (7.3 in hot condition) to zero alkali value (5.5 in hot condition) and the resulting reactivity loss was measured.
3. Power and temperature swings were made (by control rod motion in the first test and by boron concentration change in the second test) and the respective reactivity coefficients were measured in the two pH conditions. In Table 2.1, the main test conditions and the experimental results of both tests are summarized.

2.3 Analytical Work

1. During the course of the tests, reactivity balances were performed at the time of boron concentration measurements with Xenon close to (or at) its equilibrium value.

Table 2.1 - Operating Conditions and Test Results

pH Tests	pH Range (Hot)	Burnup MWD/MTU	Boron Concentr. ppm	Thermal Power MW	Temperature °C	CG Position step	pH Reactivity pcm	Temperature Coefficient pcm/°C	Power Defect pcm
I (Oct. 1966)	7.33-5.60	11.000	348	824	277.5	220	320	- 30.9 (at 275°C)	300
II (Oct. 1970)	7.24-5.50	3025 (II cycle)	603	825	267.9	240	285	- 27.0 (at 266°C)	280

2. The analysis of temperature coefficient measurements was straight-forward and only minor corrections were applied to take into account small power changes during the measurements (especially for the test performed through a boron-temperature exchange).
3. The analysis of power defect measurements required some care, especially with regard to the correct rod worth and Xenon reactivity.

2.4 Summary of Results and Conclusions

1. Reactivity loss starts immediately after pH reduction and is complete after a few days (Fig. 2.1).
2. Upon alkali addition to restore normal pH value, about 75% of the lost reactivity is regained in 20 hours and the remaining 25% is recovered very slowly over a period of several days.
3. pH reactivity effect is about 300 pcm between the two pH values of 7.3 and 5.5.
4. pH changes do not cause variations in the moderator temperature coefficient
5. pH changes do influence the integral power coefficient.
6. The difference between the power coefficients at different pH values is close to the reactivity loss experienced at full power upon pH reduction. This suggests that the increase of the integral power coefficient (power defect) can fairly justify the entire pH reactivity effect.

7. The mechanism through which the pH affects the power coefficient appears then to be a change of the heat transfer characteristics between the fuel and the coolant, due to modifications induced by pH changes of the crud deposits on fuel clad surfaces.
8. Measurements carried out on other PWRs confirm the above results, in particular for what concerns items 4 and 5 above.

3. TASK No. 3: Neutron Noise Analysis

3.1 Objective

To develop a neutron noise technique for the surveillance of reactor vessel internal structures.

3.2 Experimental Work

1. The experimental work was performed on the following reactors:

- Trino Vercellese (Italy)
- Chooz (SENA, France)
- José Cabrera (Spain)

Table 3.1 lists the measurements performed on these reactors.

2. The instrumentation normally used consisted of the following:

- neutron detection
- current to voltage conversion
- filtering
- amplification.

3. The neutron detectors of the normal reactor instrumentation were used. This is an attractive feature of the neutron noise technique: the installation of additional sensors and cables is usually unnecessary.

4. The conversion from current to voltage was usually performed by picoammeters.

As an alternative, conversion was accomplished by

Table 3.1 - Summary of Measurements

DATE	REACTOR	POWER % OF RATED	CYCLE	DETECTORS EMPLOYED	REFERENCES (*)
October, 1966	Trino	100 + 30	2/3 of 1st	RI-10; RI-11	QPR No. 3-12
March, 1967	Trino	100 + 30	end of 1st	RI-11	QPR No. 3-5-11; APR No.1
January, 1970	Trino	30	beginning of 2nd	RIC-6; RIC-8; RI-10; RI-11	QPR No. 15-16; APR No. 4
September, 1970	Trino	100	1/3 of 2nd	All detectors	QPR No. 14
October, 1970	Trino	100 + 40	1/2 of 2nd	All detectors	QPR No. 20
November, 1970	Trino	100 + 1	1/2 of 2nd	All detectors	QPR No. 18-19
February, 1971	Trino	100	2/3 of 2nd	All detectors	QPR No. 19
April, 1971	Josè Cabrera	100 + 1	end of 1st	Out-of-core and in-core	Topical Report
June, 1971	Chooz	100 + 1	end of 1st	All detectors	Topical Report
September, 1971	Trino	100	beginning of 3rd	All detectors	QPR No. 21
March, 1972	Trino	100	1/3 of 3rd	All detectors	QPR No. 22-23
March, 1972	Garigliano	100	-	Out-of-core and in-core	QPR No. 22-23-24
October, 1972	Trino	100	2/3 of 3rd	All detectors	QPR No. 26

(*) QPR = Quarterly Progress Report
 APR = Annual Progress Report

passing the detector current through a resistor. In this case, a limitation is imposed, however, because the resistance must be sufficiently low to avoid, in the frequency range of interest, low-pass filtering resulting from this resistance and the combined capacitance of the cable connecting the detector to the resistor and of the detector itself. When picoammeters are used, the d. c. component of the detector current was suppressed either before or after conversion using a high-pass filter.

5. A high-pass filter at 0.1 Hz was used either to eliminate the d. c. component or the residual component whenever the suppression was performed before the conversion stage.

An active low-pass filter was used when needed to reduce the 50 Hz network noise.

6. D. c. differential amplifiers, having very low noise, were normally used to adjust the noise signal to the optimum value for the recorder.

3.3 Analytical Work

1. The spectral analysis was the type of analysis more commonly used. Off-line digital analysis was preferred for its accuracy and speed.
2. The analysis was performed in the 0 + 50 Hz range since this frequency interval includes both the range of interest for the surveillance of reactor internals

and the range where the white noise is the predominant component.

In the above frequency range, 512 points were deemed adequate for the precise definition of the neutron noise spectra.

The time required for the analysis was considerably reduced by adopting a playback-tape speed higher than the recording speed.

3. The Normalized Power Spectral Densities (NPSDs) of two detectors, the modulus and the phase of their cross spectrum, and the coherence function are generally computed at the same time. Sophisticated criteria were used for plotting the phase values in order to avoid oscillations of the curve in the frequency range where the noise signals are in phase opposition.
4. A part of the research effort was devoted to the development of a theory of neutron flux noise in power reactors.

The main possible sources of neutron noise in a power reactor have been identified as follows:

- reactivity noise
- attenuation noise
- white detection noise
- correlated noise due to fission-branching processes
- detector movement noise
- instrumentation noise.

For each of the above noise sources, the mathematical relationship between the noise level, in terms of Power Spectral Density (PSD), of the neutron detector signal and the physical parameters governing the source of the noise have been developed.

Such relationship provided a basis for quantitative determination on the physical mechanisms generating the noise. Moreover, they made it possible to assess the sensitivity of the surveillance technique based on neutron noise monitoring, with respect to the various phenomena that may cause fluctuations in the neutron detector signals.

3.4 Summary of Results

1. A summary of the most significant results obtained during the program on the Trino, Chooz, and José Cabrera reactors is given in Figs. 3.1 + 3.9.
2. Figs. 3.1 + 3.4 show the spectra of neutron noise signals coming from 8 out-of-core ion chambers of the Trino reactor. Each of these figures refers to a pair of ion chambers at diametrically opposed locations with respect to core centerline. The NPSDs of signals from these two chambers, the normalized modulus and phase of their cross-spectrum, and their coherence function are plotted in each figure.
3. In the neutron noise spectra of Figs. 3.1 + 3.4, two main resonance peaks at about 4.5 and 5.5 Hz can be distinctly noted.

4. The height of these peaks versus the circumferential position around the core is plotted in Fig. 3.5. The experimental points can be interpolated with a sine-squared function.
5. Fig. 3.6 shows the phases of the cross spectra, in the frequency range associated with the 4.5 and 5.5 Hz peaks, between the noise signals of various ion chambers.
6. The behaviour evidenced in Figs. 3.5 and 3.6 can be theoretically predicted by assuming that the 5.5 Hz peak is due to pendular oscillations of the lower reactor vessel internals package along a given direction. The actual direction of oscillation is also identified.
7. On the contrary, no firm interpretation of the 4.5 Hz peak was given so far, since this peak is dependent on the power level (the 5.5 Hz peak is not affected at all by it). Actually, at power levels less than full power, the 4.5 Hz peak changes its frequency: at 30% or less power levels, the spectra show only one peak, i. e. the two peaks, 4.5 and 5.5 Hz, become coincident.
In addition, the frequency and height of the 4.5 Hz peak continue to vary for about 20 days, if full power is attained after a shutdown or prolonged operation at some lower power levels. This behaviour has not yet been understood.

Although even the 4.5 Hz peak seems originated by a pendular movement of the lower reactor internalspackage, no firm conclusion can be drawn.

8. Figs. 3.7 and 3.8 give the normalized power and cross power spectral densities of out-of-core ion chambers diametrically opposed, for the Chooz and Josè Cabrera reactors. In these figures, two distinct resonance peaks can be noted, one at 5.5 Hz (Chooz) and the other one at 11 Hz (Josè Cabrera), both peaks having characteristics equal to those of the 5.5 Hz peak found in the Trino reactor, i. e. :
 - a. Equal height in the two autospectra of noise signals from ion chambers diametrically opposed
 - b. Opposition of phase, in the frequency range associated to the peaks
 - c. Peak height and frequency independent of the power level.

As for the Trino reactor, these peaks can be satisfactorily explained by assuming a pendular oscillation of the internals package.

9. In Figs. 3.1, 3.2, 3.3, 3.4, 3.7 and 3.8, other narrow peaks can be observed. In particular, those at 24.6 Hz in Trino and Chooz, and 16.5 Hz in Josè Cabrera are due to periodical signals with a frequency equal to the rotational frequency of the main coolant pumps.

10. In the José Cabrera reactor, noise signals from in-core ion chambers have also been analyzed (Fig. 3.9). The 11 Hz peak is obviously attributable to the pendular oscillation of the lower internals package.
11. Fig. 3.10 shows the changes apparently caused in the neutron spectra by different configurations of the reactor vessel internals for the Trino Reactor. The upper spectrum was obtained in March 1967 with the original arrangement of the internals, although already damaged. The January 1970 spectrum was obtained subsequently to internals repair but with the secondary core support still provisional. The July 1970 spectrum was obtained with the internals in the present arrangement^(*).

(*) The repairs consisted of the following:

- a. The thermal shield was eliminated because of difficulties in rejoining the three sectors into a solid assembly and in fastening this assembly to its support at the pressure vessel wall.
- b. All the bolts of the barrel joint were replaced with high strength Inconel X-750 bolts of improved design.
- c. The tie-rods connecting the lower barrel and the lower support casting were eliminated and replaced with bolts of high-strength material (316 SS cold worked) to anchor the core plate to the barrel.
- d. A secondary core support was added at the periphery of the lower support casting.

The March 1967 spectrum shows a peak about 3 Hz wide, whereas the spectra after the repairs show narrower peaks. This would indicate a higher damping coefficient of the oscillations in March 1967. In addition, the amplitude of the oscillation, which is proportional to the square root of the area under the peak, was greater in March 1967. Both the higher damping and the greater amplitude seem indicative of a structure having a bolted joint near failure, which was actually the case in March 1967. In July 1970, the lower support casting was heavier than in January 1970 by about 10% due to the substitution of the provisional secondary core support with the final one. This may be interpreted as the cause of the shift of the peak frequency in the January and July 1970 spectra.

12. In the course of the program, an on-line code (FOURIA) capable of calculating the neutron noise power spectral density was developed^(*). Unfortunately, this code was never programmed on the on-line PRODAC 510 process computer at Trino. The purpose of the code is to monitor the neutron spectra on a continuous basis and possibly to correlate changes of these spectra with variations in the plant operating conditions.

(*) Cf. Quarterly Progress Reports No. 12, Appendix A and No. 13.

13. For sake of comparison, Fig. 3.11 shows the NPSD for the Garigliano reactor which is a boiling water reactor. Because of the different arrangement of the vessel internals package in this reactor, no peak attributable to a pendular oscillation is observed.

3.5 Conclusions

1. The neutron noise technique has proved fully successful for revealing pendular oscillations of the lower vessel internals package of PWRs.
2. No other oscillations of the internals have been firmly evidenced.
3. By comparing the neutron spectra before and after the repairs of the reactor vessel internals in Trino, the conclusion may be drawn that the noise analysis technique is potentially capable of detecting changes in the structural integrity of the reactor internals thus providing a means for surveillance and incipient failure detection.
4. For a better understanding of the noise phenomena, a continuous monitoring of the neutron noise spectra of a given reactor over a long period of time is recommendable. A correlation of changes in the neutron spectra with varying plant operating conditions should be investigated, possibly by concurrently analyzing the noise of physical parameters other than the neutron flux.

4. TASK No. 4: Gamma Scanning of Selected Fuel Assemblies

4.1 Objective

To determine the gamma activity distribution among the fuel assemblies to be used for evaluating the end-of-cycle burnup and/or power distributions.

4.2 Experimental Work

Four gamma scannings were performed:

1. Gross gamma scanning of 48 square fuel assemblies (40% of the core) performed on September 1967, five months after the end of Cycle 1, using a movable ionization chamber running inside a central channel of the fuel assemblies.
2. Gross gamma scanning of 42 square fuel assemblies performed on July 1971, at the end of Cycle 2, using ionization chambers as above.
3. Spectrometric gamma scanning of 34 square fuel assemblies performed with a Ge-Li detector (to measure La-140 activity) on August 1971, at the end of Cycle 2. Nine axial measurements were made for each corner of each assembly. The 34 assemblies were also subjected to the gross scan indicated in 2 above. These measurements were aimed at determining end-of-cycle power distributions.

An extensive description of these measurements, analysis methods, and results is given in Topical

Report "Core Power Distributions at the End of Cycle 2 from La-140 Activity Measurements", June 1972.

4. Spectrometric gamma scanning of 12 square fuel assemblies performed with a Ge-Li detector (to measure long-lived fission product activity) on April 1972, nine months after the end of Cycle 2. The measurements were performed with the intent of demonstrating the feasibility and practicality of on-site scanning to determine burnup distributions and of verifying a linear correlation between the Cs-134/Cs-137 activity ratio and the Pu/U mass ratio in the fuel.

The activity of Cs-137, Cs-134, Zr-Nv-95, Eu-154, Ce-Pr-144, Ru-Rh-106 was measured.

For each assembly four complete gamma spectra were collected, one for each corner, at nine axial locations.

The assemblies examined had initial enrichments of 3.13 and 3.90 w/o and average assembly burn-up in the range 19,000 - 22,000 MWD/MTU.

The facility used for the Ge-Li gamma scanning consists of the collimator system (installed in a hole bored through the wall of the spent fuel pool), a transfer system to move the assembly in front of the collimator, and a pre-fabricated shed installed outside the spent fuel pool building where the measuring equipment is located. This facility was expressly designed and installed for this task.

4.3 Analytical Work

1. Gross gamma scanning, five months after the end of Cycle 1.

The Manganese activity distributions obtained with the Aeroball system were converted into power distributions by means of a factor calculated according to a two-energy group formula as function of initial enrichment and irradiation.

Cycle 1 was divided in 15 time intervals in which the power level and the control rod position were approximately constant. For each period, an Aeroball run representative of the power distribution in that period was selected. By an integration procedure, the burnup distribution at the end of the cycle was determined.

To check indirectly the accuracy of this method of burnup calculation, the gamma activity of the various assemblies at the time of the gamma scanning was calculated and compared with the experimental results.

2. Gamma scanning at the end of Cycle 2

The experimental La-140 activity data were converted into relative power data using theoretical factors (one for each corner) to account for the mutual gamma shielding of the fuel rods as seen by the Ge-Li detector and the particular geometry of the fuel assemblies. The method adopted

for this data reduction was found to be adequate (cf. the Topical Report mentioned in 4.2 item 3). The BURSQUID, PISUA and TRIGAM codes were employed for the calculations.

The results of the Ge-Li gamma scanning were compared with theoretical predictions and with gross gamma scan data.

3. Gamma scanning nine months after the end of Cycle 2

The burnup and the Pu/U mass ratio were calculated by means of the BURSQUID code.

4.4 Summary of Results and Conclusions

1. Gross gamma scanning five months after the end of Cycle 1

Figs. 4.1 and 4.2 show how good is the agreement between the radial and axial gamma activity distributions measured and those calculated starting from data of the in-core instrumentation (Aeroball system). This confirms indirectly the accuracy of the calculation of the burnup distribution.

2. Gamma scanning at the end of Cycle 2

- a. The overall standard deviation of the measurements was found to be 2.0%.
- b. Fig. 4.3 shows a comparison between experimental (Ge-Li) and theoretical radial power

distributions. The mean square deviation between calculated and measured values is 2.2%. No particular trends in the deviations were evidenced: the discrepancies are statistically distributed between the core center and the periphery, low and high enrichments, low and high burnup assemblies.

- c. Figs. 4.4 and 4.5 give a comparison of radial and axial power distributions derived respectively from gross gamma and Ge-Li data.

The mean square deviation between Ge-Li and gross gamma data is 2.8%. The gross gamma scan produced lower power values for the peripheral assemblies. This could be due to differences between isotope yields from U-235 and Pu-239 fissions (peripheral assemblies contain less Pu than central ones).

- d. In general, the measurements demonstrated the validity of Ge-Li gamma scanning as an accurate method for determining end-of-cycle power distributions.
- e. On the other hand, the gross gamma scan provides useful information for PWR's because the power distribution does not change substantially during the last two or three months of the cycle. Actually, the main contributions to

gross gamma activities, even at short times after shutdown, come from fission products with half-lives of 30 to 60 days. The Ge-Li scan, which can discriminate the La-140 activity (half-life 12.8 days), does provide more accurate end-of-cycle power distributions.

3. Gamma scanning nine months after the end of Cycle 2

- a. The results obtained indicated that there is a linear correlation between the Cs-134/Cs-137 activity ratio and the Pu/U mass ratio in the fuel. Fig. 4.6 shows the calculated Pu/U mass ratio as function of the measured Cs-134 (796 + 801 keV)/Cs-137 (662 keV) activity ratio.
- b. In addition, the results confirmed that the Cs-137 activity is a good burnup indicator. Fig. 4.7 gives the calculated assembly burnup versus the measured Cs-137 (662 keV) activity. Although the burnup range is limited, it appears that the measured activity is correlated with burnup.

5. TASK No. 5: Steam Generator Potential

5.1 Objective

To study the behaviour of the steam generators of the Trino plant at various power levels and in different operating conditions, in order to determine the steam generator ultimate capability.

5.2 Experimental Work

The experimental part of this task was completed in July 1971. The results of the work are described in FIAT's Topical Report "Theoretical and Experimental Analysis of Steam Generator Performance at ENEL's Trino Vercellese Nuclear Power Plant", FN-C-5, April 1972.

The following main activities were carried out:

- a. Detection and recording (on magnetic tape) of the main variables characterizing the behaviour of the steam generators.
- b. Frequency analysis of the recorded signals.
- c. Experimental program performed to obtain, through proper temperature measurements, an experimental check of the calculated steam generators recirculation ratios (not successful).

5.3 Analytical Work

1. Three areas were investigated:
 - a. Stability of the internal recirculation loop of the steam generators
 - b. Acoustic resonance phenomena in the secondary steam circuit.
 - c. Heat transfer capability of the steam generators.
2. The theoretical analysis of the stability of the internal recirculation loop of the steam generators was carried out by means of the F111-RID digital code, expressly developed by FIAT for this task. The main purpose of the code is to study the preferential mode of oscillation of the upper part of the downcomer region of the steam generator. A detailed description of the model and the code is given in the Topical Report FN-C-5, already mentioned.

The mathematical model is based upon a two dimensional representation of a two-phase flow, assuming the length along the flow path and the time as independent variables.

The recirculation loop was divided into a finite number of elements, each having a uniform cross section. The length of an element is sufficiently small so that the properties in each element could be considered uniform everywhere; expansions and contractions in flow cross section are assumed to

be located at the inlet or outlet of each element (Fig. 5.1). To each element of this model the conservation equations, i. e. continuity, energy and momentum equations, and the primary to secondary coolant thermal exchange equation for those elements located in the heated region were applied.

In the energy equation for the coolant flow in the recirculation loop, the effect of potential and kinetic energies, as well as the contribution of frictional losses, pressure time derivative and pressure gradient, were neglected.

In the derivation of momentum equations, however, the effect of frictional forces was considered and the contribution of frictional losses was incorporated in form of empirical pressure drop relationships.

The equivalent length concept was used for the calculation of pressure drop in the U-tube support plate, swirl vane steam separator and U-turns.

The thermal power distribution along the steam generator tube bundle was assigned as a spatial function.

The numerical method used to solve the fundamental equations is the "modified - Euler" integration process (with automatic control of integration step width).

The mathematical model and the numerical techniques outlined above, are programmed in the digital Code F111-RID by using the FORTRAN automating coding language for the 1108-UNIVAC digital computer.

3. The acoustic resonance phenomena on the secondary steam circuit were studied by means of the A.R.I.A. code, expressly developed for this task and described in FIAT's Topical Report FN-C-5 already mentioned. The A.R.I.A. (Acoustic Resonance Analysis) code was developed to study pressure resonances in a perfect gas of a complex network comprehending pipes and tanks, connected to simulate (by means of an electric analogy) high pressure steam system of the Trino plant.

Fig. 5.2 shows a simplified diagram of the Trino Vercellese high pressure steam system and the equivalent electric network.

By setting to zero the sum of the currents at the junctions, 9 linear equations are established with 9 unknown quantities (the pressures at the junctions), which can be solved as function of frequency. In particular, the A.R.I.A. code calculates the transfer functions (amplitude in decibels and phase in degrees) between the pressure excitation and the pressure fluctuations in any junction and at the steam generators drums.

5.4 Summary of Results and Conclusions

1. Two main phenomena could result in limiting the steam generator capability and thus the plant power capability:
 - a. Thermohydraulic instability of the steam generator recirculation loop

- b. Acoustic resonance phenomena in the secondary steam circuit of the plant.

No limits are imposed by average temperature oscillations which are certainly self-limited in a PWR-type plant.

A further limit for the plant power capability could be imposed by core and turbine operating limits (i. e. maximum avg. coolant temperature and minimum steam pressure, respectively, when associated with the steady state heat transfer capability of the steam generators).

2. The steam generator thermohydraulic stability was studied by means of the F111-RID code. The steam generator behaviour at 940 and 1100 MW(t) were first determined (present nominal rating: 825 MW). Figs. 5.3 and 5.4 show the results of the stationary condition search calculations corresponding to these two power levels, the input data relative to the secondary pressure and to the feedwater temperature being those indicated in Fig. 5.5. The system response to a + 1 ft perturbation in the liquid level is shown in Figs. 5.6 and 5.7: in each case a stable behaviour is predicted by the code.

In order to find the power level corresponding to the threshold of instability, further calculations were made at 1200 and 1250 MW(t). As can be seen in Fig. 5.8, during the steady state search

calculations the oscillations become divergent for the 1250 MW(t) case. These last calculations were made by imposing the same steam pressures and feedwater temperatures extrapolated for the 1100 MW(t) calculations.

The power level corresponding to the threshold of instability can then be fixed at about 1200 MW(t). Thus, future power upratings up to 1020 MW(t) (being presently planned) will not be prevented because of thermohydraulic instability phenomena in the steam generator recirculation loop.

3. Very large oscillations on the steam generator secondary variables could take rise for plant power levels higher than the nominal one (825 MW(t)) if a coincidence between the acoustic resonance frequency of the steam circuit and the frequency of the thermohydraulic loop preferential mode of oscillation should be permitted.

Fig. 5.9 shows that the experimental increase of the oscillation peaks with increasing power levels (with nominal set point and constant primary system average temperature) can be, on the average, approximated by the theoretical increase trend calculated by A. R. I. A.. In these conditions, increases in the operating power levels (with respect to the present 825 MW(t) power level) could determine, as it results by an extrapolation of the A. R. I. A. data, too large oscillations of the operating liquid

level, steam pressure, and steam flow rate to permit a stable and safe operation.

A + 30 cm liquid level set point will be very useful in order to damp the acoustic oscillations. In this case, a quite stable behaviour can be foreseen up to at least 1020 MW(t) (Fig. 5.10).

4. The heat transfer characteristics of the steam generator can result in a limitation for the plant power capability due to the limits on the maximum average coolant temperature (influencing core capability) and the minimum steam pressure (fixed by the turbine). An effort was made in order to define a reliable set of curves correlating the average coolant temperature, the steam pressure, and the plant power level.

A semi-empirical evaluation of the steam generator heat transfer coefficient h was first tried by introducing the measured values in the classical heat exchanger equation.

As shown by Fig. 5.11, quite scattered values resulted for the two instrumented steam generators (A and C), mainly due to measurement errors. Interpolated experimental h values were then obtained in Fig. 5.11 by interpolating with respect to measured values of the power level, of the inlet to outlet primary coolant temperature difference, and of the steam pressure (Figs. 5.12 and 5.13).

In order to permit the necessary extrapolations for different power levels and average temperatures, two theoretical hypotheses for calculating h (Jens-Lottes and Rohsenow-Clark correlations for the secondary side) were compared to the experimental one.

The two resulting theoretical behaviours are given in Fig. 5.11. It can be seen that the Jens-Lottes correlation is more effective in reproducing the experimental values and more conservative (cf. also Fig. 5.13).

Thus, it was concluded that the heat transfer coefficient theoretically calculated with the Jens-Lottes correlation can be used for extrapolation purposes. Figs. 5.14, 5.15 and 5.16 show the results of these extrapolations which are indicative of the plant power capability as defined by the steam generator steady state heat transfer capability.

Since all of the above calculations were made assuming that the secondary heat transfer mechanism is always of the local boiling type, it was verified that, in the zones with lower heat flux, a local boiling heat transfer regime is actually prevailing and that in the zones with maximum heat flux, no film boiling occurs.

Both assumptions were demonstrated adequate.

6. TASK 6: Core Physics Characteristics

6.1 Objective

To determine the significant core physics characteristics in various reactor operating conditions with the aim of providing a check of the calculating techniques.

6.2 Experimental Work

1. Physics tests were performed at beginning of every cycle both at zero and full power. The measurements concerned the following parameters:
 - moderator temperature coefficient as function of boron concentration and moderator temperature;
 - differential rod worth as function of power level, Xenon concentration and initial rod position;
 - average differential boron worth.
2. At various times during the cycle and at cycle end the following measurements were carried out:
 - moderator temperature coefficient;
 - differential rod worth curves vs. burnup;
 - boron concentration vs. burnup;
 - power defect and power coefficient vs. power level.

6.3 Analytical Work

Experimental data were reduced and analyzed with the usual procedures.

Theoretical predictions were performed by FIAT, Sezione Energia Nucleare^(*).

6.4 Summary of Results and Conclusions

1. The trend of the moderator temperature coefficient as function of boron concentration and moderator temperature is given in Figs. 6.1 and 6.2, respectively. It should be noted that the measurements were in general performed with the control group inserted. This resulted in a measured coefficient more negative than it would be in all-rods-out condition.

Theoretical and experimental values were found in good agreement.

2. The differential control rod worth, at beginning of Cycle 1, as function of power level, Xenon concentration, and initial rod position is given in Fig. 6.3. The initial position of the control group affects its differential worth through the associated Xenon axial distribution.

(*) Cf. Quarterly Progress Reports of FIAT Integrative Research Program and the Topical Report prepared jointly by ENEL and FIAT mentioned in 6.4, item 7.

3. The average differential boron worths, measured at beginning of cycles for various temperatures, boron concentrations, and rod insertions, are given in Table 6.1.
4. In Table 6.2, the moderator temperature coefficient measured at power during core life is shown.
5. In Fig. 6.4, a comparison among differential rod worths, measured at beginning of each cycle, is given. The curves for Cycles 2 and 3 show a "saddle" shape, probably due to the axial burnup distribution in the core at the burnup level considered.
6. Measurements of power defect, power coefficient, critical boron concentration were also carried out during the first three cycles. The experimental values have been compared with the theoretical ones. In most cases the agreement is fairly good.
7. In the Topical Report "Comparisons Between Theoretical and Experimental Physics Data for Trino Core No. 1" prepared jointly by ENEL and FIAT, an extensive and systematic comparison of calculated and measured data related to Cycle 1 is given.

Table 6.1 - Average Differential Boron Worth at Beginning of Various Cycles

CYCLE	I		II	III
Boron Worth $\frac{\text{pcm}}{\text{ppm}}$	- 10	- 7.1	- 7.3	- 6.7
Average Temperature, °C	38-43	282-285	269	269
Boron Concentration, ppm	1800	1240-1840	1230-1454	1351-1657
Control Group Position, % ins.	0-85-286 steps	73-194 steps	-	0-100

Table 6.2 - Moderator Temperature Coefficient Measurements at Power

Cycle	T pcm/°C	C _B ppm	Cycle Burnup MWD/MTU	Avg. Temp. °C	CG Position Step
1	- 30.6	348	8,200	273 - 277.4	220 - 205
	- 36.2	52-133	10,770	276 - 261	263
2	- 26	614-628	2,492	268 - 264	240

7. TASK No. 7: Post-Irradiation Examinations

7.1 Objective

1. To determine the content of heavy isotopes in the fuel as function of burnup, initial enrichment, and neutron spectrum.
2. To determine the burnup distribution in the core.
3. To check the accuracy of the calculating methods by means of comparison of theoretical and experimental data.

7.2 Experimental Work

1. The experimental program was conducted by JRC (Ispra and, at a lesser extent, Karlsruhe) personnel. In the first part (August 1969), three assemblies discharged at the end of Cycle 1 were dismantled⁽¹⁾ at JRC Laboratories of Ispra. The results were presented in the Topical Report "Post-Irradiation Analysis of Trino Vercellese Reactor Fuel Elements", by J. Biteau et al., EUR 4909/e, 1972.
In the second part (August 1972), one assembly discharged at the end of Cycle 2 was dismantled and subjected to examinations which are still underway. A Topical Report will be issued by JRC and FIAT, upon completion of the work.

(1) The special equipment necessary for dismantling the fuel assemblies and for removing the fuel rods to be subjected to post-irradiation examinations was designed and procured by ENEL. This equipment is described in detail in the Topical Report "Operations Performed at the JRC Laboratories of Ispra on Three Irradiated Fuel Assemblies" March 1970.

2. The following activities were common to the two series of experiments:
 - a. Transportation of the fuel assemblies from Trino to the pool of the ESSOR reactor at the JRC Laboratories of Ispra.
 - b. Cutting of the assembly box.
 - c. Removal of the assembly upper end and extraction of the rods to be examined.
 - d. Closing of the assemblies with a temporary plate and shipping to the reprocessing plant.

3. The following laboratory activities were performed during the first part of the program on 8 rods removed from three square fuel assemblies:
 - a. Visual rod examination.
 - b. Non destructive gamma-scanning and gamma-spectrometry. The total gamma activity was measured with a NaI detector along the rod at intervals of 0.5 mm.
The gamma-spectra were determined with a Ge-Li detector at six levels for each rod.
 - c. Metallurgical and metallographic examinations of cladding and fuel.
 - d. A number of dissolution tests of UO_2 .

- e. Several purifications of U and Pu with different solvents (TBP for uranium and TTA for plutonium) from solutions of irradiated uranium diluted with U-233 and Pu-242.
 - f. Neodymium purification by resins from a solution of irradiated uranium in nitric acid. Some mass spectrometric measurements of the Nd-148/Nd-150 ratio were performed.
 - g. Destructive gamma spectrometry measurements utilizing a Ge-Li detector for five samples.
 - h. Determination of uranium and plutonium isotopic compositions by means of mass spectrometric analysis.
4. The selection of fuel assemblies, rods and samples for post-irradiation examinations was based on the following criteria:
- wide range of initial enrichments (2.72, 3.13, 3.90 w/o)
 - wide range of burnup values (3000 ± 18000 MWD/MTU)
 - different neutron spectra⁽¹⁾ due to different assembly location within the core and different rod location within the assemblies
 - different axial location of samples along the rods.

(1) I. e. asymptotic or unperturbed spectrum when the rods were entirely surrounded by fuel rods; perturbed spectrum for corner rods; intermediate spectrum for rods near the center of the assembly, i. e. near the water hole left vacant for the in-core instrumentation thimble.

7.3 Analytical Work

The theoretical calculations were performed by FIAT, Sezione Energia Nucleare utilizing the computer codes PHANTOM, SQUIRREL and CONDOR 3. CONDOR 3 was especially developed by ARS (Milan) for these theoretical evaluations (Cf. "CONDOR-3, a Two Dimensional Reactor Lifetime Program with Local and Spectrum Dependent Depletion" by E. Salina, Nov. 1969 and "Valutazione dettagliata del livello d'irraggiamento e della composizione isotopica locale alla prima scarica del combustibile di Trino Vercellese" di A. Moncassoli-Tosi and P. G. Rama, January 1972).

7.4 Summary of Results and Conclusions (First Part of the Program)

1. The ~~visual~~ examination of ~~the fuel rods~~ confirmed that the clad had no defects.
2. Figs. 7.1 and 7.2 show some results of non-destructive gamma-scanning and gamma-spectrometry. In Fig. 7.1 the well pronounced minima of activity are due to the interface of different fuel pellets. All fuel rods show a decrease of activity near the grid positions (Fig. 7.2).
3. Metallographic examination of the fuel confirmed that, besides the cracking of the fuel, there was no particular modification in the microstructure. The microstructure of the cladding was homogeneous.

4. Absolute values of burnup for 21 fuel samples were determined utilizing three distinct destructive methods:
 - gamma scanning (by a Ge-Li detector) of dissolved fuel solutions for Cs-137 absolute activity measurements;
 - mass spectrometry of fuel samples for heavy isotopes concentration measurements (the code BURNUP was utilized to treat these data);
 - mass spectrometry of fuel samples for Nd-148 concentration measurements.

A fourth determination of burnup was obtained from non-destructive Cs-137 activity measurements (Ge-Li gamma spectrometry). These relative burnup measurements were normalized on the basis of the destructive gamma spectrometry to obtain absolute values of burnup.

The results obtained with the four methods agree among themselves within $1 \pm 4\%$.

Fig. 7.3 shows a comparison between experimental and theoretical axial burnup distributions.

5. The mass spectrometric analysis provided data of isotopic fuel composition versus burnup in the range 3000 ± 18000 MWD/MTU for the three enrichments. Some data for the 2.72 w/o enrichment are presented in Fig. 7.4. The figure shows a good agreement between calculated and experimental results.

6. Several linear correlations have been observed (Figs. 7.5 & 7.11) between concentration ratios of fission products, heavy isotopes and burnup values.

All the observed correlations proved the consistency of the experimental data.

7. An exhaustive illustration of experimental techniques and test results is given in "Post-Irradiation Analysis of Trino Vercellese Reactor Fuel Elements" by J. Biteau et al. (EUR 4909/e, 1972).

8. Original Tasks VI, VII, VIII and XII. Power Distributions.
Flow Rate Through the Core and Flow Distributions.
DNB Ratios, Core Protection and Control Systems.

8.1 Objective

To determine the ultimate capability of the core with the aid of the in-core instrumentation system (Aeroball System).

8.2 Experimental Work

An extensive series of Aeroball runs was performed at various times during Cycle 1 and in various operating conditions.

A list of these runs and a complete presentation of raw and analysed data are given in Topical Report "Neutron Flux Distributions During First Operating Cycle of Trino Vercellese Reactor" by G. P. Battista and S. Valenziani, May 1967 and in Addendum 1 to this Report, October 1967.

At the end of Cycle 1, failures of several channels of the Aeroball system were discovered.

During the extended plant shutdown which occurred at the end of Cycle 1 for modifications of the reactor vessel internals, it was decided to remove the in-core instrumentation system. Therefore, the only Aeroball data available are those related to Cycle 1.

8.3 Analytical Work

The Aeroball data reduction was performed according to the methods described in the Topical Report already mentioned.

8.4 Results and Conclusions

1. The most significant results obtained with the Aero-ball system during Cycle 1 are summarized in Figs. 8.1 + 8.5.
2. The axial power density distributions through Cycle 1 reflect the history of the control rod operation. In the first part of the cycle (up to 2600 MWD/MTU) with the 10 rods of the control group inserted by 30-40%, the distribution was skewed toward the bottom. In the middle part of the cycle, following rod withdrawal from 30-40% to approximately 4%, the distribution shifted toward the upper portion of the core. In the last part of the cycle, the axial power density profile was noticeably flat.
3. Typical axial power density profiles at full power are shown in Fig. 8.1, which also presents a profile taken with control rods inserted by 70% at a power level of 270 MW(t). The flat power density profile at cycle end is the result of a balance between the accumulated axial burnup distribution and the moderator temperature distribution along the height of the core. In fact, due to initial insertion of control rods, the burnup profile is slightly skewed toward the bottom; this makes the lower portion of the core less reactive, thus compensating the negative reactivity effect in the upper portion where the water is hotter.

4. Radial maps of relative assemblywise power distributions are presented in Fig. 8.2. The radial power distribution becomes flatter with progressing irradiation: the peak decreases from 1.23 to 1.17 and the power increases in the outer region of the core.
5. Fig. 8.3 gives the burnup distribution at the end of the cycle derived from the axial power density profiles by means of an integrative procedure. These data have been indirectly confirmed by the results of a gamma scanning performed on selected fuel assemblies at the end of the cycle (cf. 4.3).
6. The effect on the axial power density distribution due to variations in average coolant temperature and power was evidenced by means of the Aeroball system.
7. Fig. 8.4 shows the effect of an average temperature change at full power. When the coolant temperature was decreased from 276 to 271°C, the axial power density profile, previously flat, became skewed toward the top of the core. Obviously, the temperature decreased both in the lower and in the upper portions of the core, but the reactivity gain was higher in the upper portion, because of the non-linearity of the temperature coefficient. This fact was experienced only at the end of the cycle when an equilibrium in terms of

reactivity between the normal temperature gradient and the axial burnup distributions had been reached and when the temperature coefficient is higher.

8. A similar effect (Fig. 8.5) is caused by a power level change occurring at constant average temperature (278°C). The power reduction from 825 MW(t) to 260 MW(t) caused again the power density distribution to skew toward the top. Following the power reduction, the temperature actually increased in the lower half of the core and decreased in the upper half with the reactivity rising at the top and decreasing at the bottom.
9. No significant trends have been observed in the radial power distributions following the temperature and power changes described above.
10. The accuracy of the Aeroball system during the first part of Cycle 1 could not be systematically assessed. Toward the end of the cycle, a repeatability test was conducted covering several Aeroball runs. All the experimental points fell within a $\pm 2\%$ interval.
11. No significant work has been actually performed on the original tasks VII, VIII and XII because the removal of the in-core instrumentation system at the end of Cycle 1 made impossible to collect all the experimental data needed to carry on these tasks.

9. Original Task IX: Flux Synthesis Techniques

9.1 Objective

To investigate a simple method for determining a three-dimensional power distribution starting from:

- a. Radial power distributions calculated for the asymptotic regions (defined as the core regions in which the radial distributions are the same at all axial levels)
- b. Aeroball activity (axial) distributions.

9.2 Experimental Work

No experimental work has been carried out expressly for this task. Available data of various Aeroball runs were used.

9.3 Analytical Work

The method proposed is described in Appendix A of Quarterly Progress Report No. 7 "Application of the Flux Synthesis Method to In-Core Instrumentation Data Analysis" by K. Fisher and Y. Paternot.

9.4 Summary of Results and Conclusions

1. Full separability of the three-dimensional power distribution into radial and axial components has been demonstrated to hold for almost the entire core without control rods.
2. Only for two small regions located at the top and

at the bottom of the core and for the peripheral assemblies, no firm conclusions about separability could be drawn.

3. The separability holds for all burnup levels throughout Cycle 1, according to the analysed data.
4. The power density synthesis can therefore be easily performed in the unrodded region.
5. For the core with control rods partially inserted, two cases were considered :
 - a. Asymptotic conditions of the power density distribution are reached in both the rodded and unrodded axial regions.
 - b. Asymptotic conditions of the power density distribution are reached only in the unrodded axial region.
6. For case a., a method of power density synthesis was developed which avoids the discontinuities at the interface between the axial zones. This method could not be checked against experimental results, since during Cycle 1 control rods were not inserted deeply enough to allow the attainment of asymptotic conditions of the power density distribution in the rodded region.
7. For case b, no generally applicable method of power density synthesis could be developed.

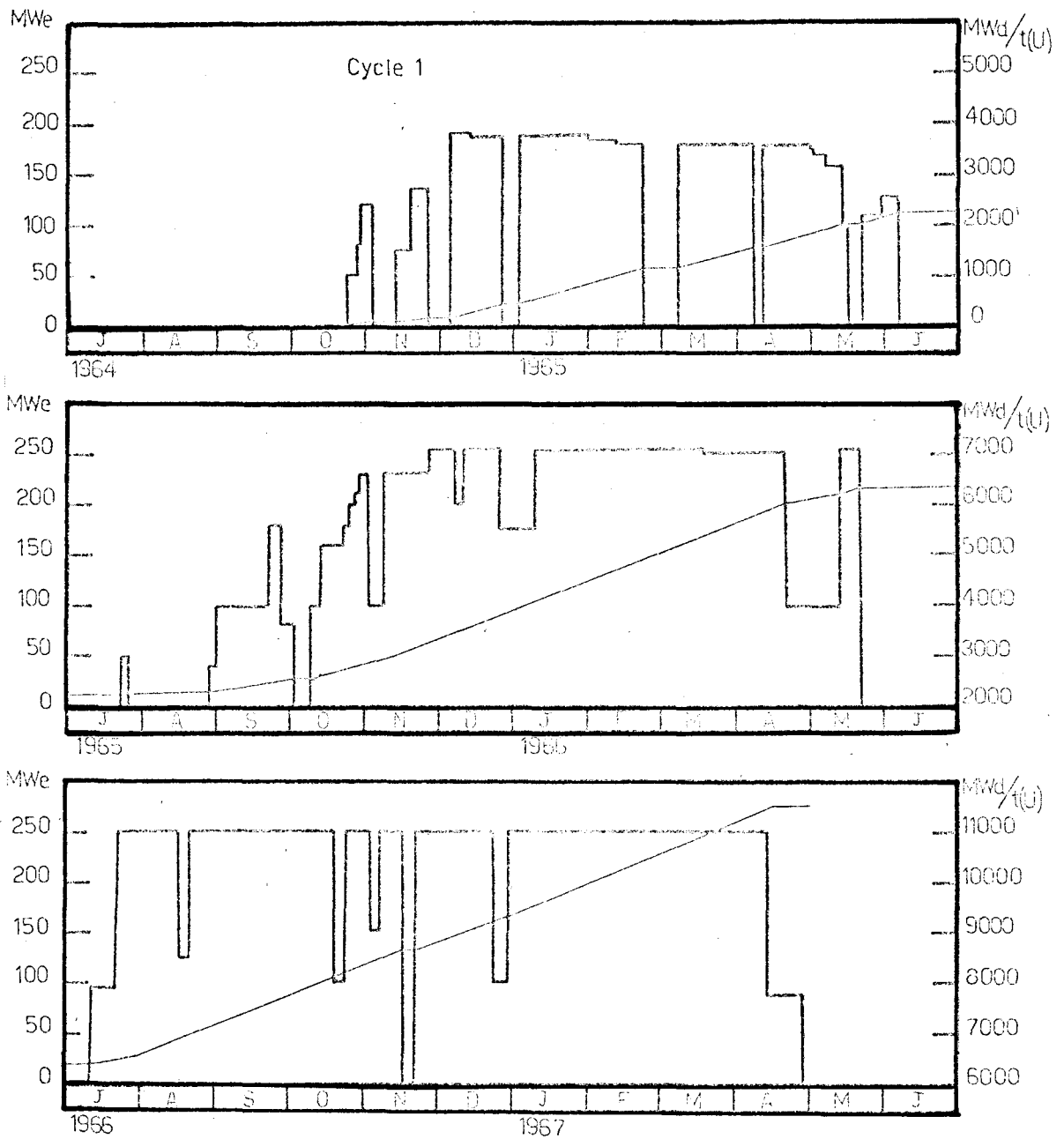


[Fig. 1: Load Diagram and Integrated Cycle Burnup for Cycle 1

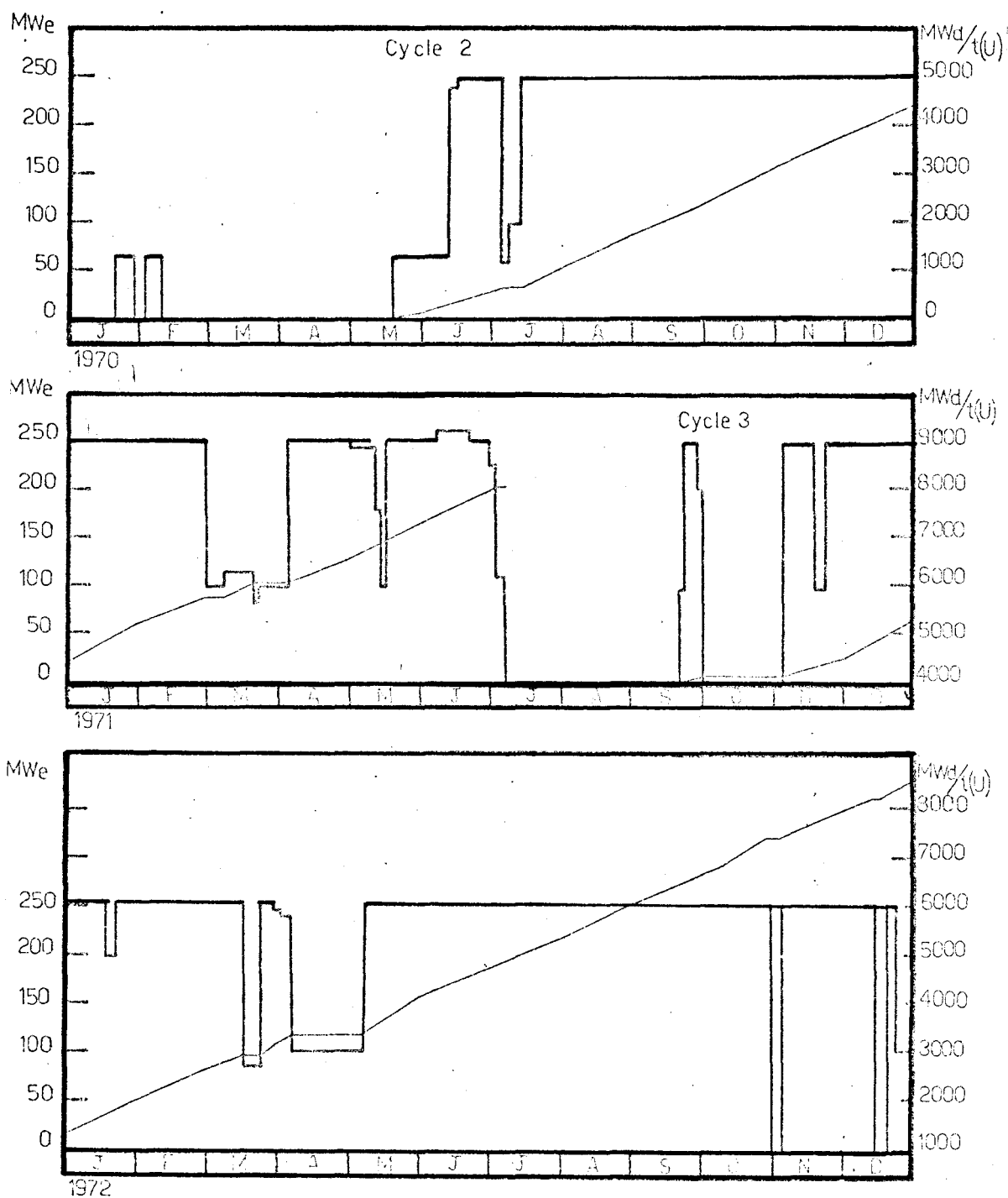


Fig. 2 : Load Diagram and Integrated Cycle Burnup for Cycle 2 and Cycle 3

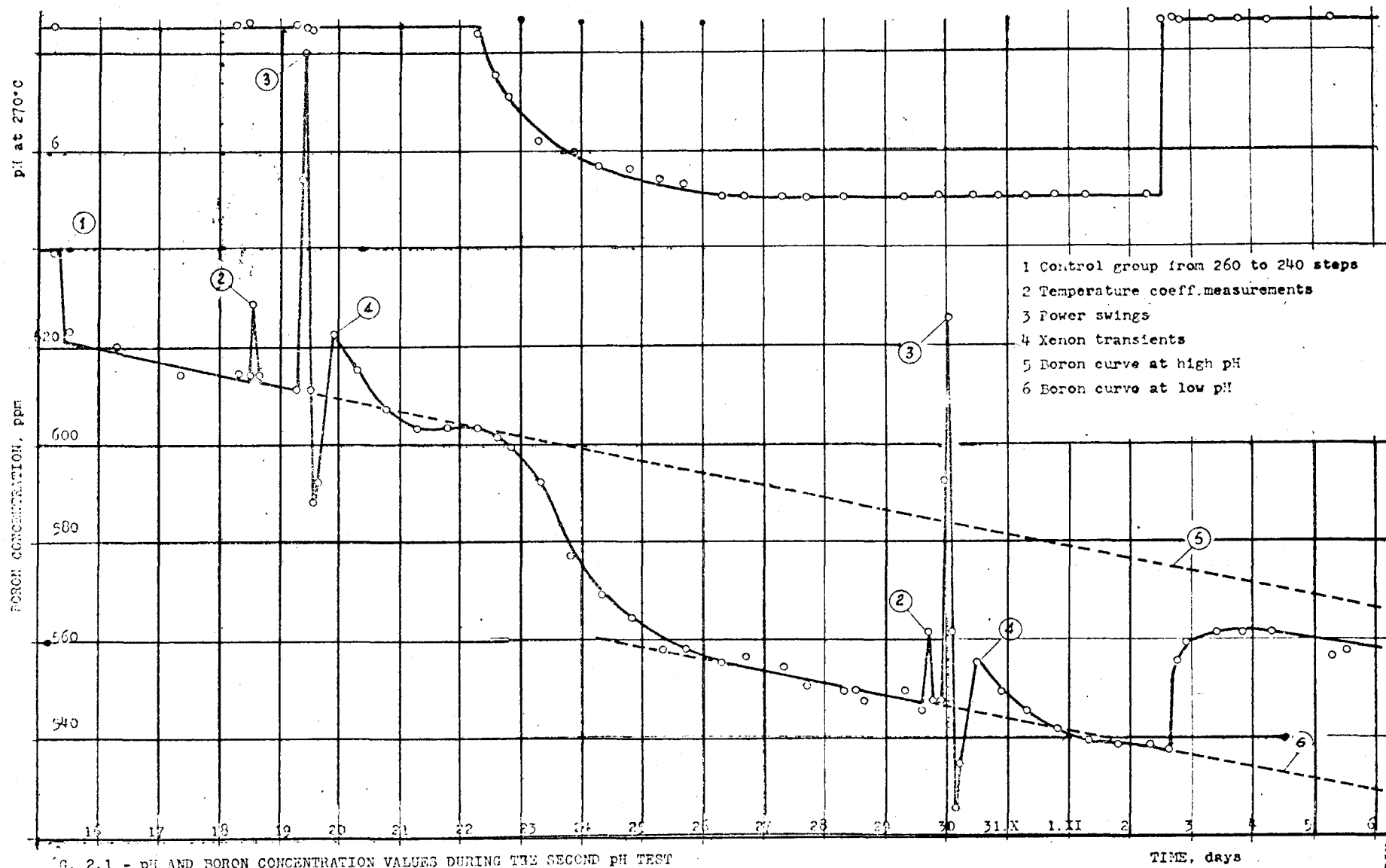
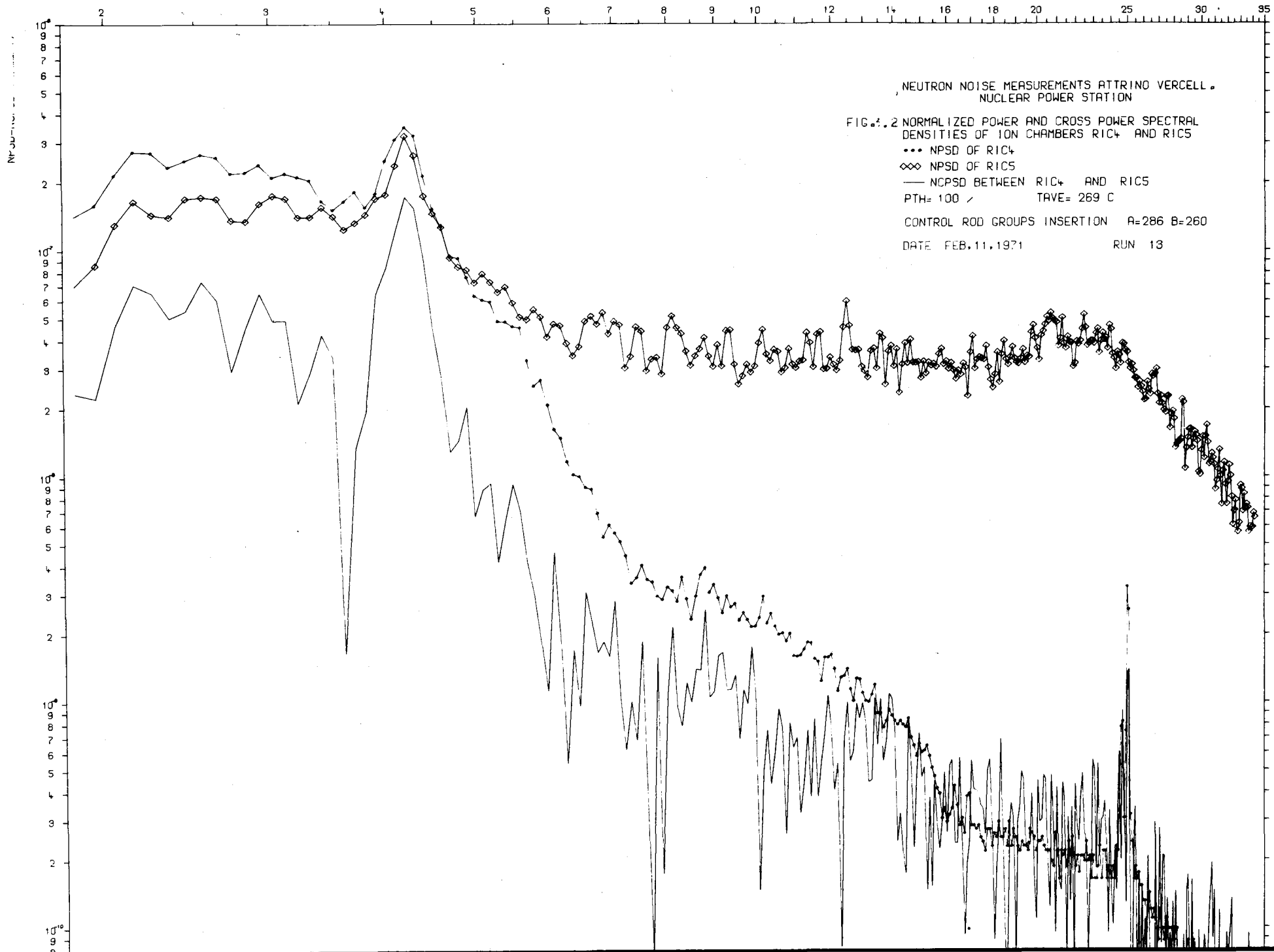
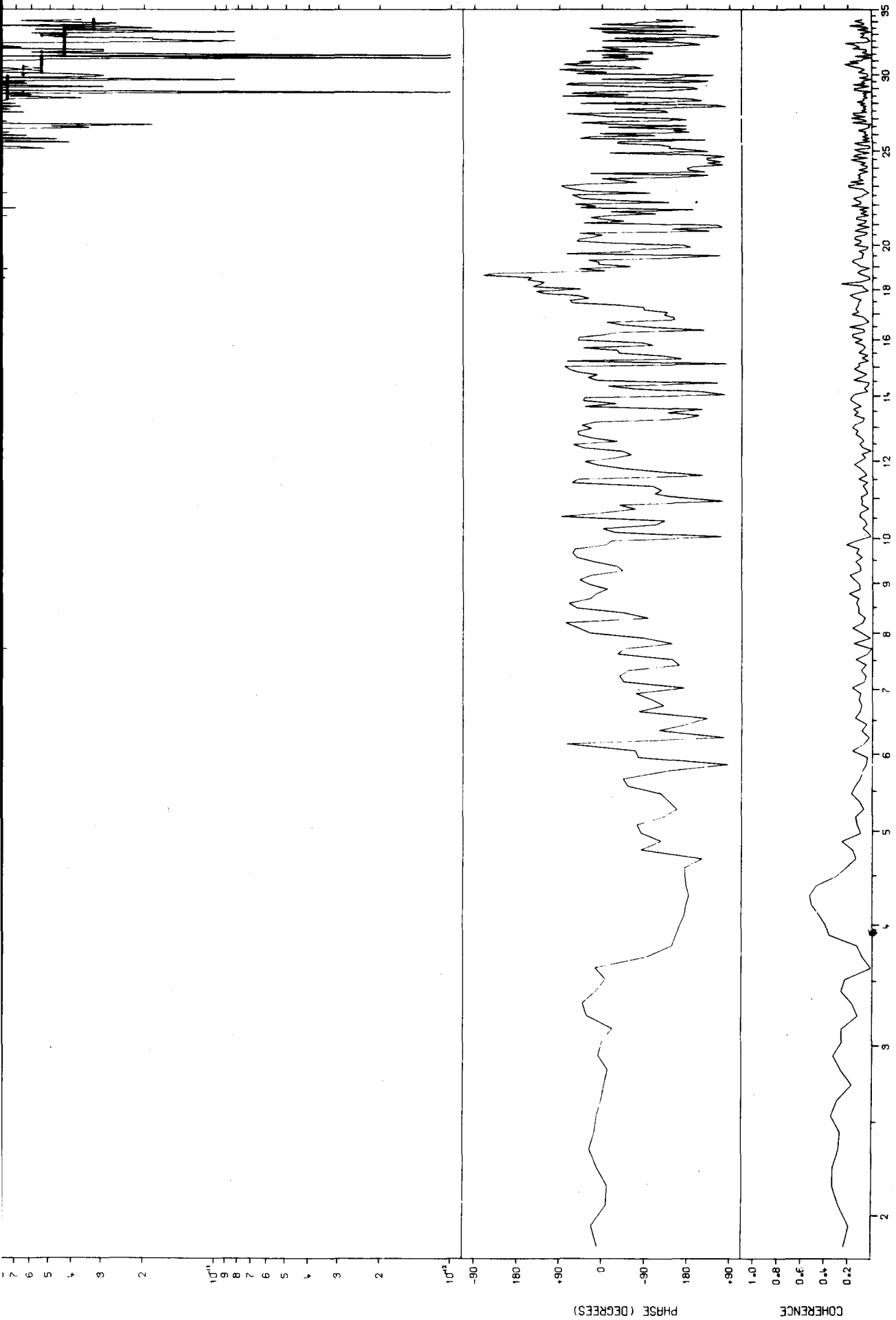
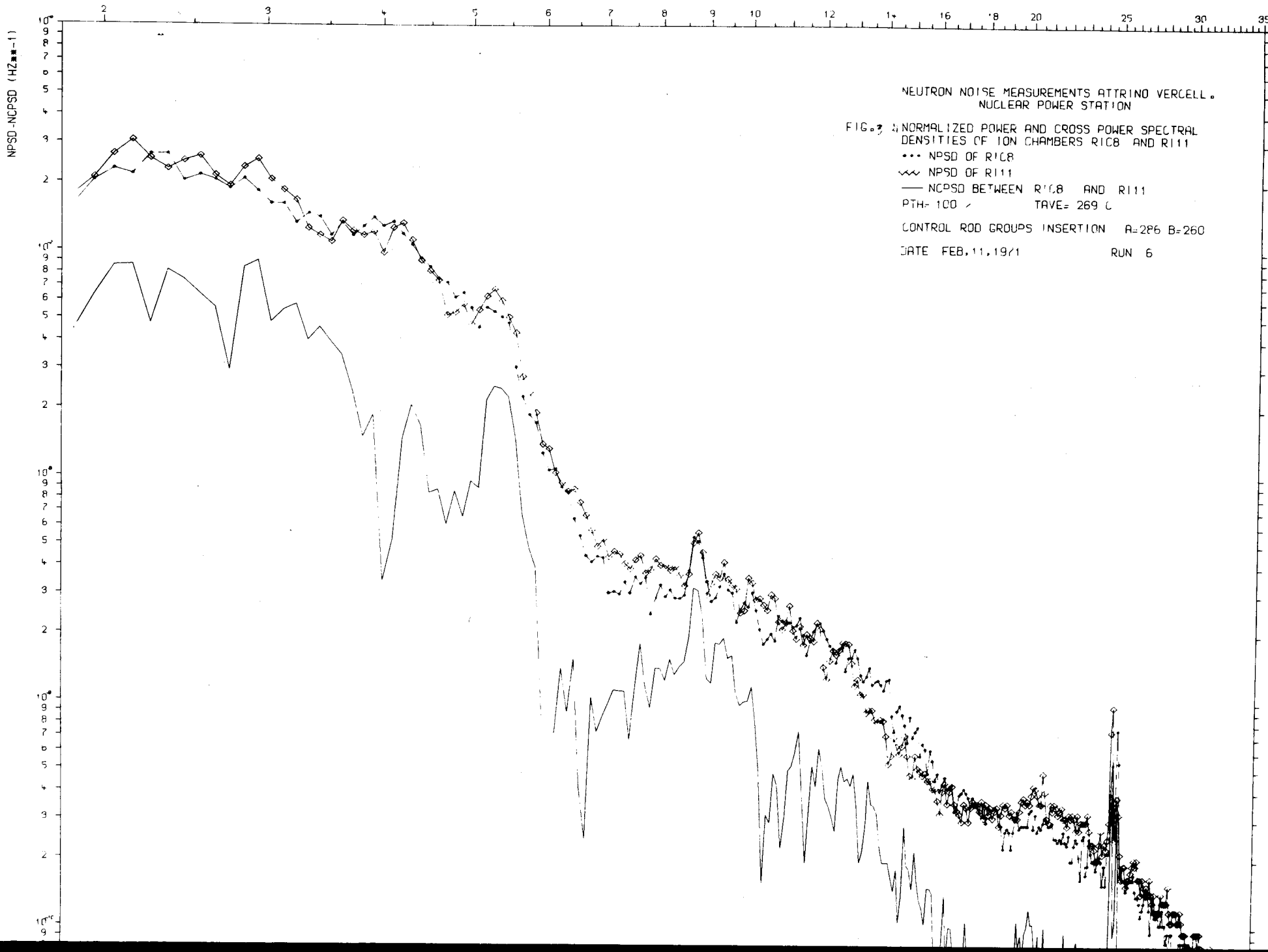
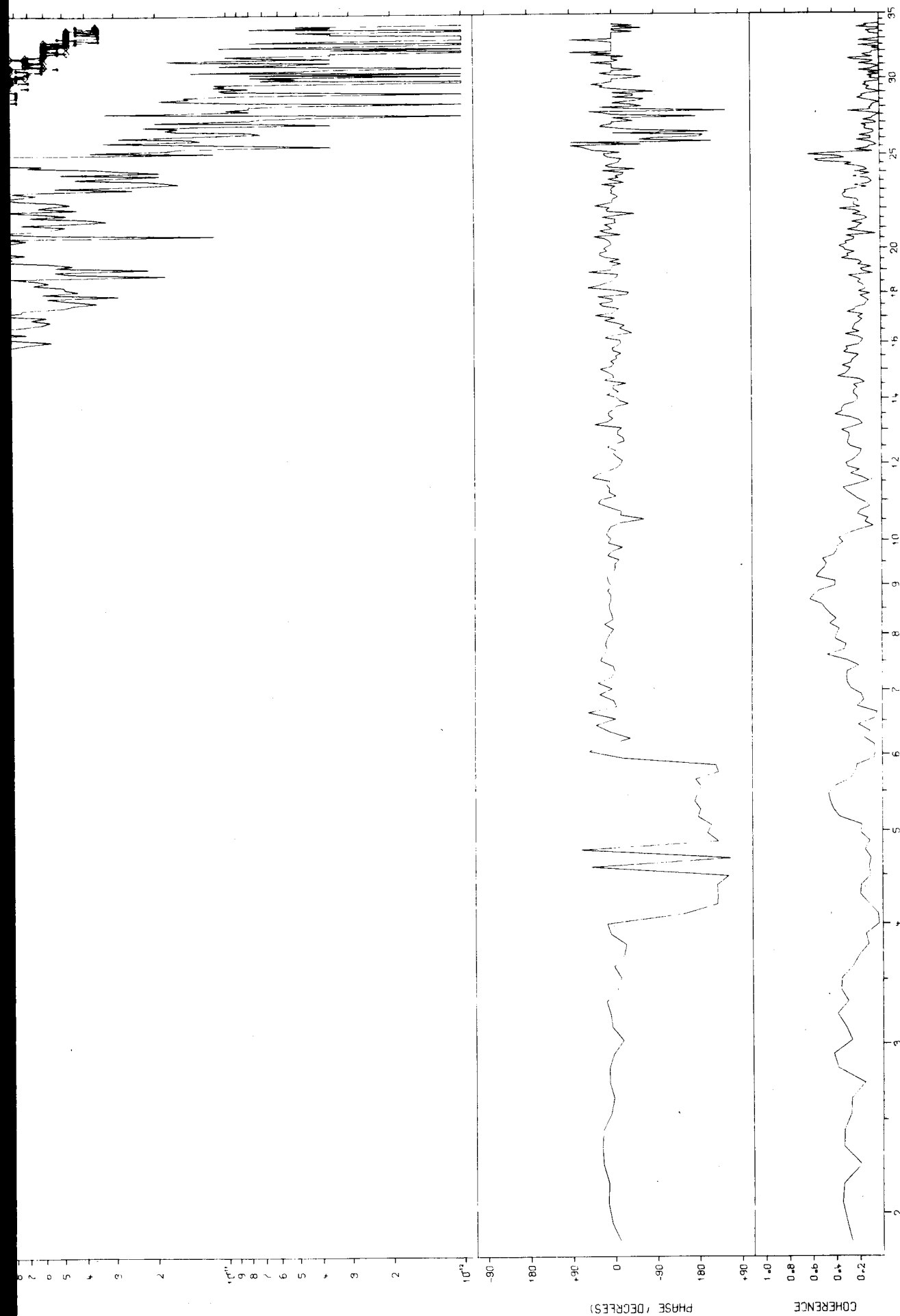


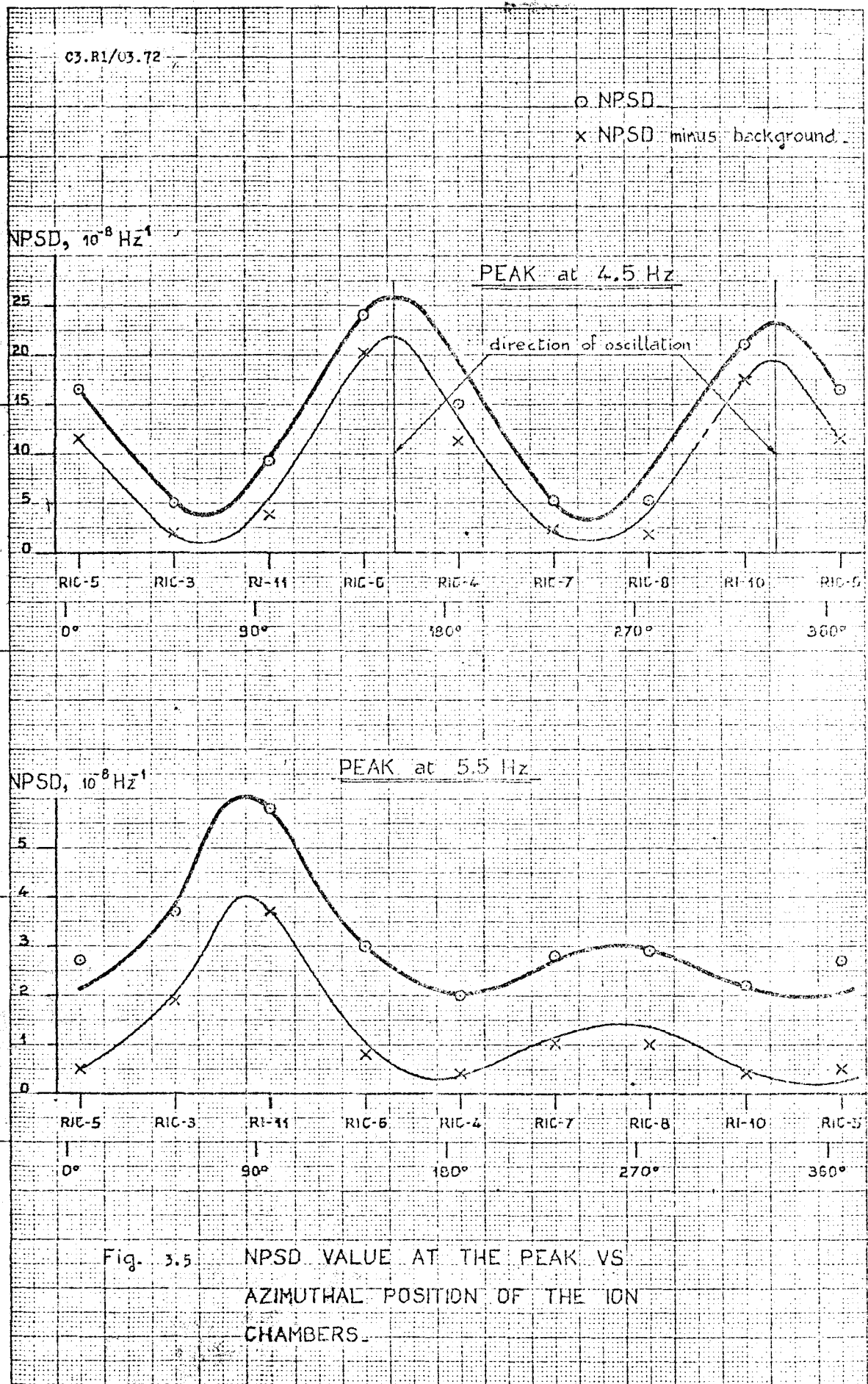
Fig. 2.1 - pH AND BORON CONCENTRATION VALUES DURING THE SECOND pH TEST





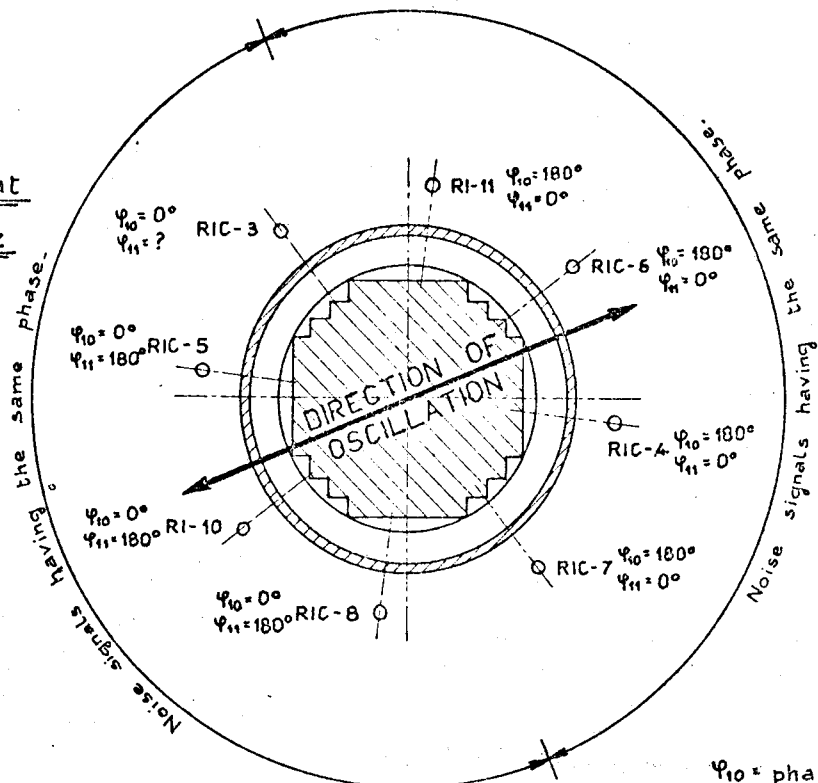






C3.R1/03.72

PEAK at
4.5 Hz



ψ_{10} = phase respect to RI-10.
 ψ_{11} = phase respect to RI-11.

PEAK at
5.5 Hz

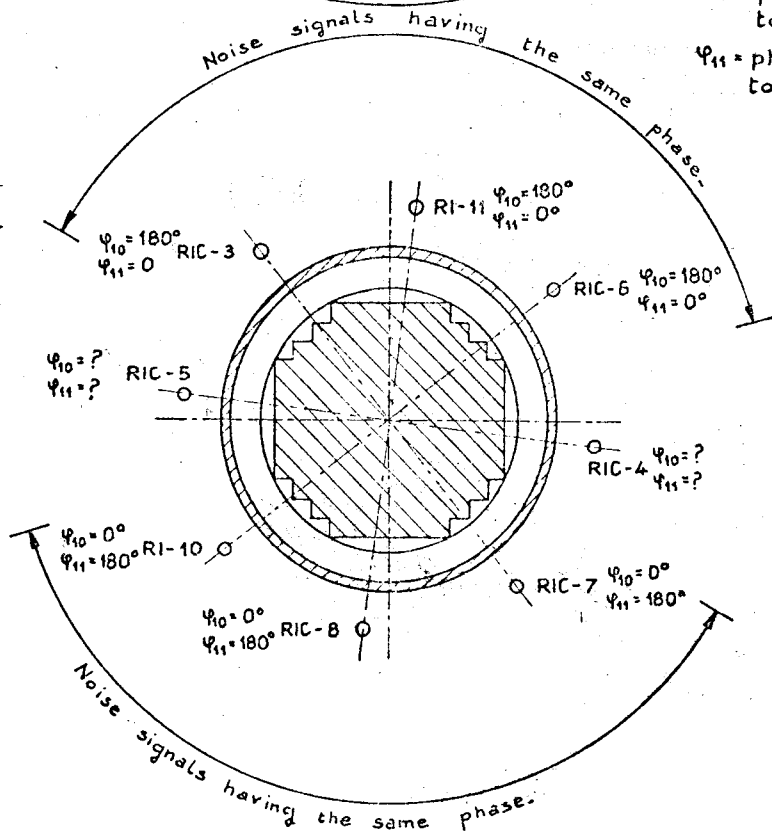
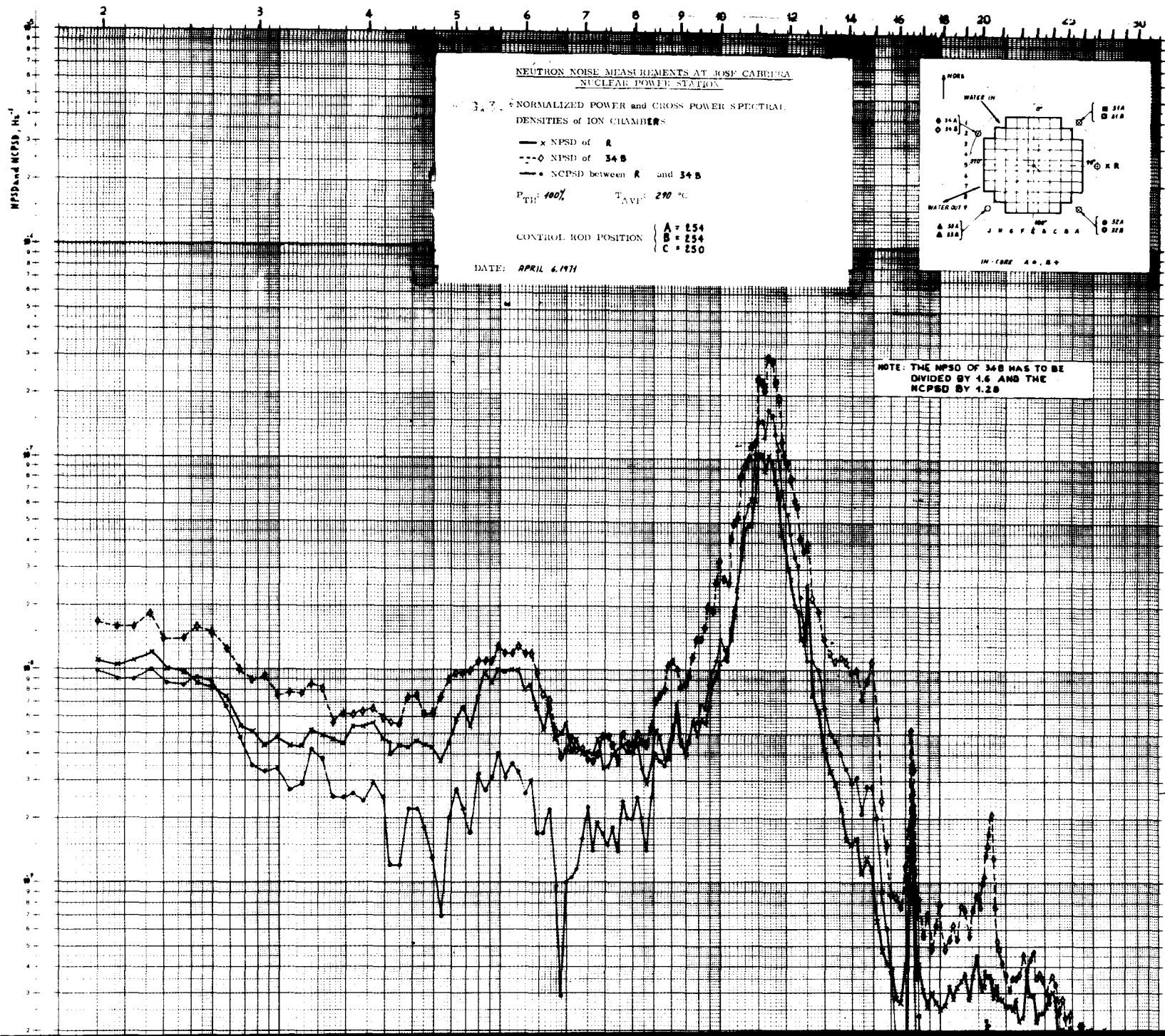


Fig. 3.6 - NOISE SIGNAL PHASES



NEUTRON NOISE MEASUREMENTS AT JOSE CABRERA
NUCLEAR POWER STATION

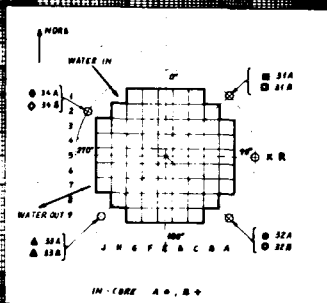
3.7. NORMALIZED POWER and CROSS POWER SPECTRAL DENSITIES of ION CHAMBERS

—x NPSD of R
 ---◇ NPSD of 34B
 —• CPSD between R and 34B

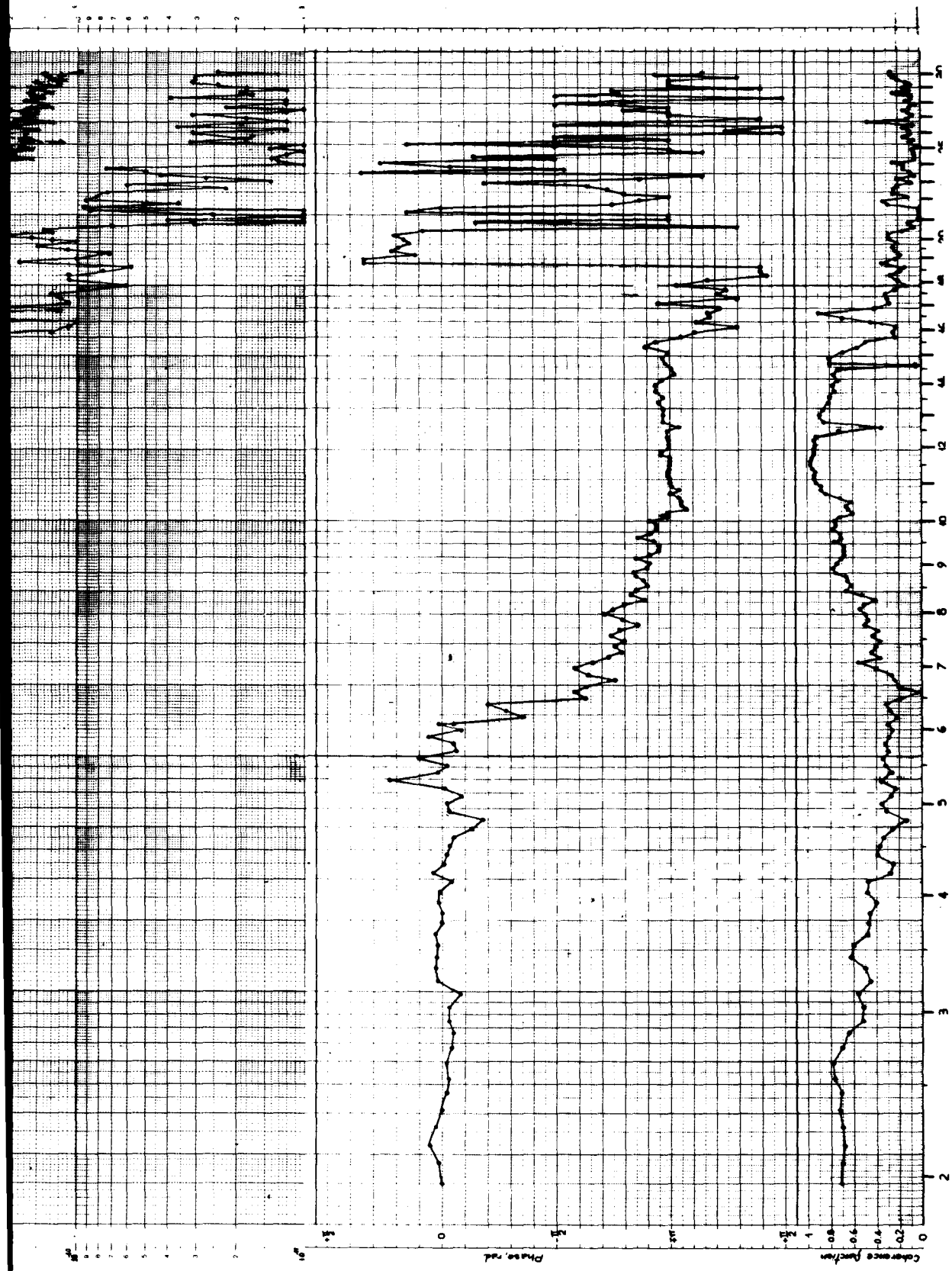
P_{TH} : 100% T_{AVG} : 290 °C

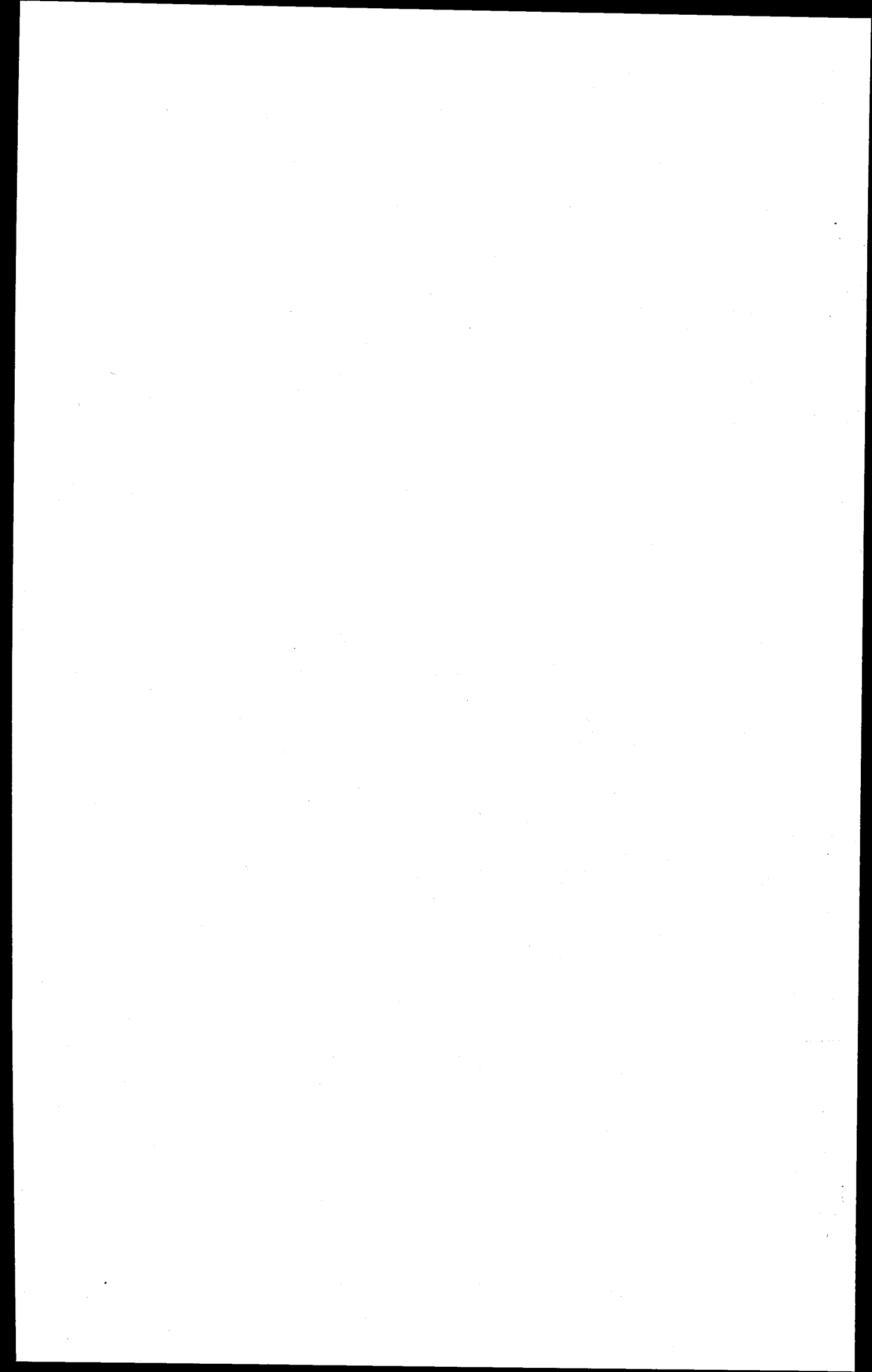
CONTROL ROD POSITION { A = 254
 B = 254
 C = 250

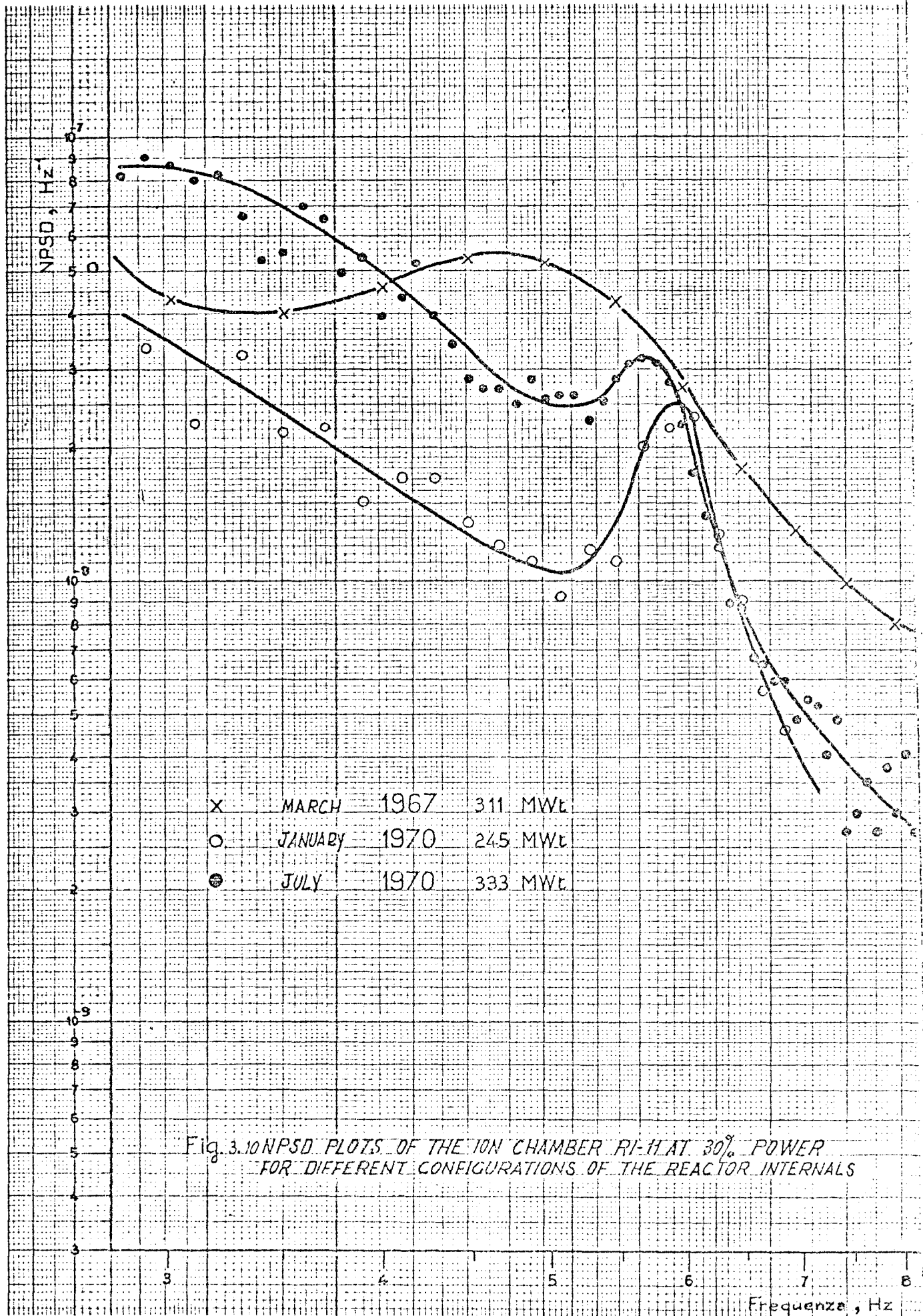
DATE: APRIL 6, 1971

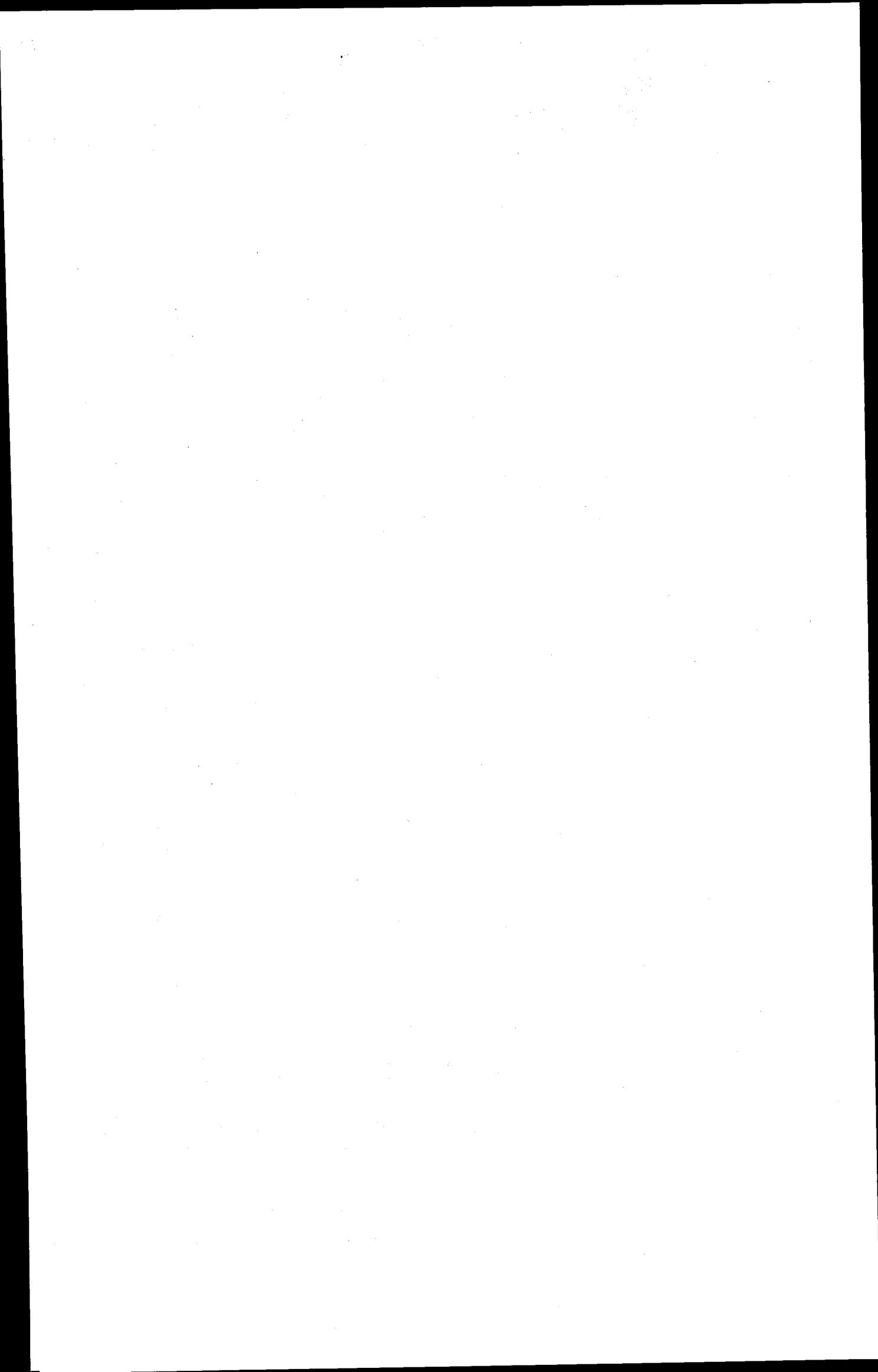


NOTE: THE NPSD OF 34B HAS TO BE DIVIDED BY 1.6 AND THE CPSD BY 1.28









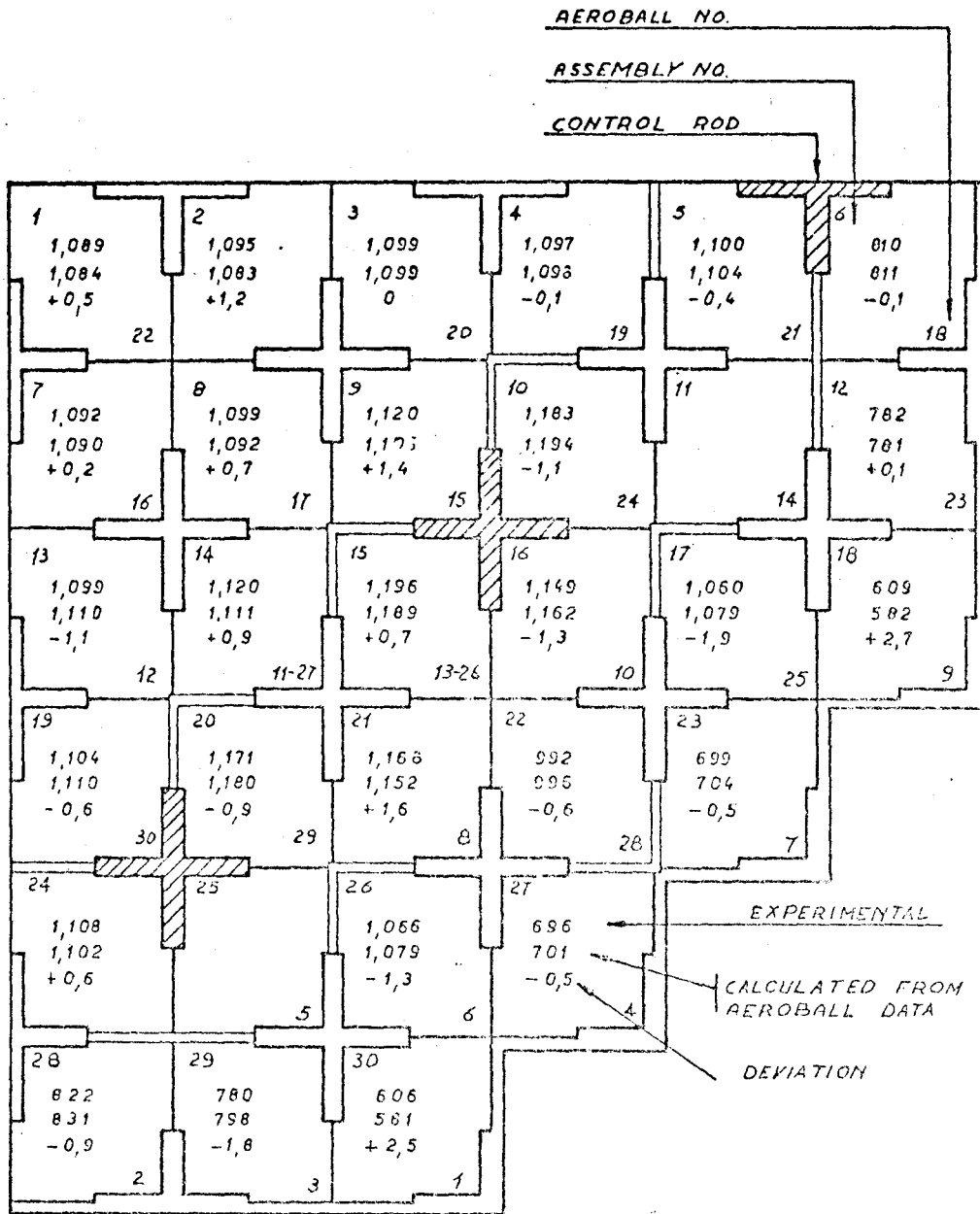


FIG. 4.1 - COMPARISON BETWEEN EXPERIMENTAL AND CALCULATED GAMMA ACTIVITY DISTRIBUTIONS

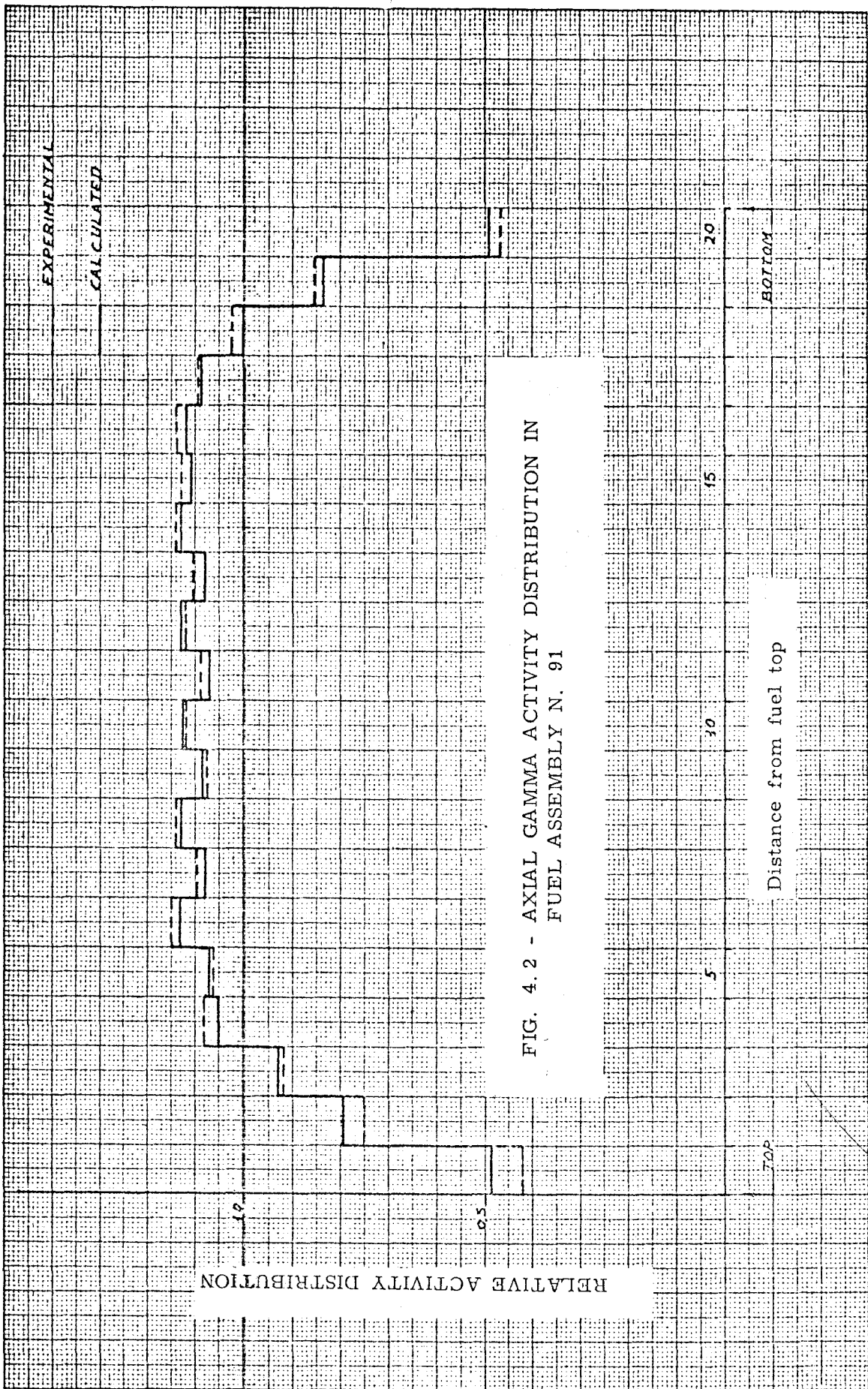
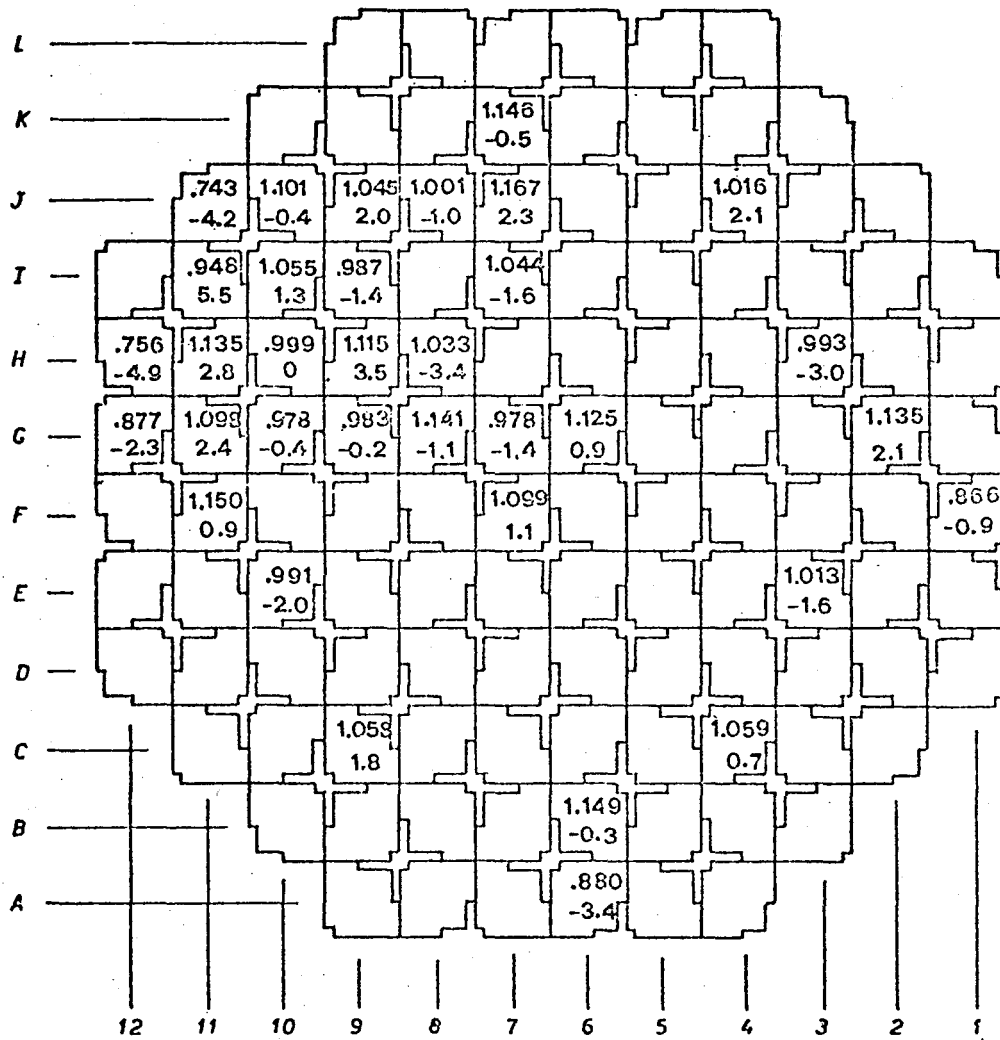


FIG. 4.2 - AXIAL GAMMA ACTIVITY DISTRIBUTION IN FUEL ASSEMBLY N. 91



x.xxx
x.x

 Power distribution data from La^{140} activity scanning by Ge-Li.
 $(T-E/T) \times 100$ $\sigma = \pm 2.33\%$

Fig. 4.3 - ASSEMBLYWISE POWER DISTRIBUTION COMPARISON BETWEEN Ge-Li SCAN AND THEORETICAL VALUES

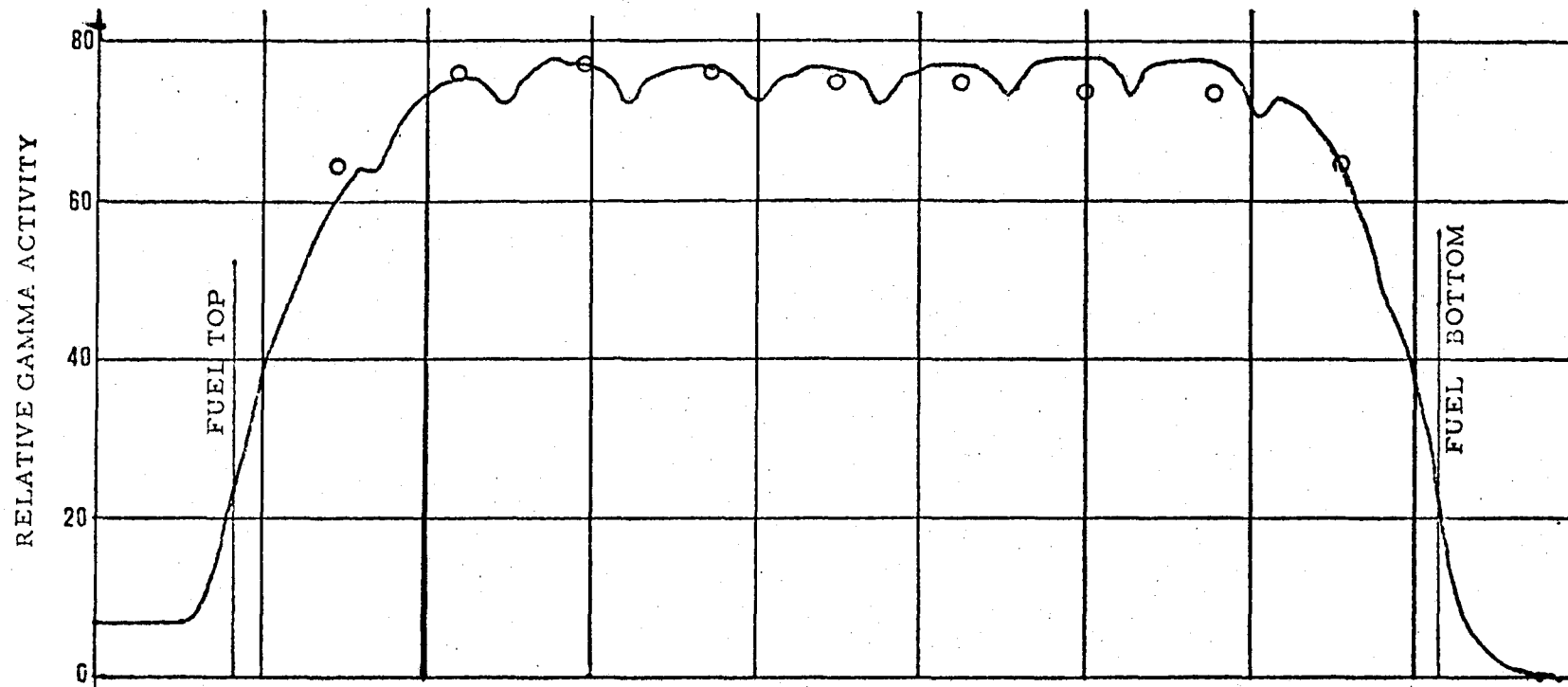


Fig. 4.5. - AXIAL POWER DISTRIBUTION COMPARISON BETWEEN EXPERIMENTAL VALUES FROM Ge-Li AND GROSS GAMMA SCANS

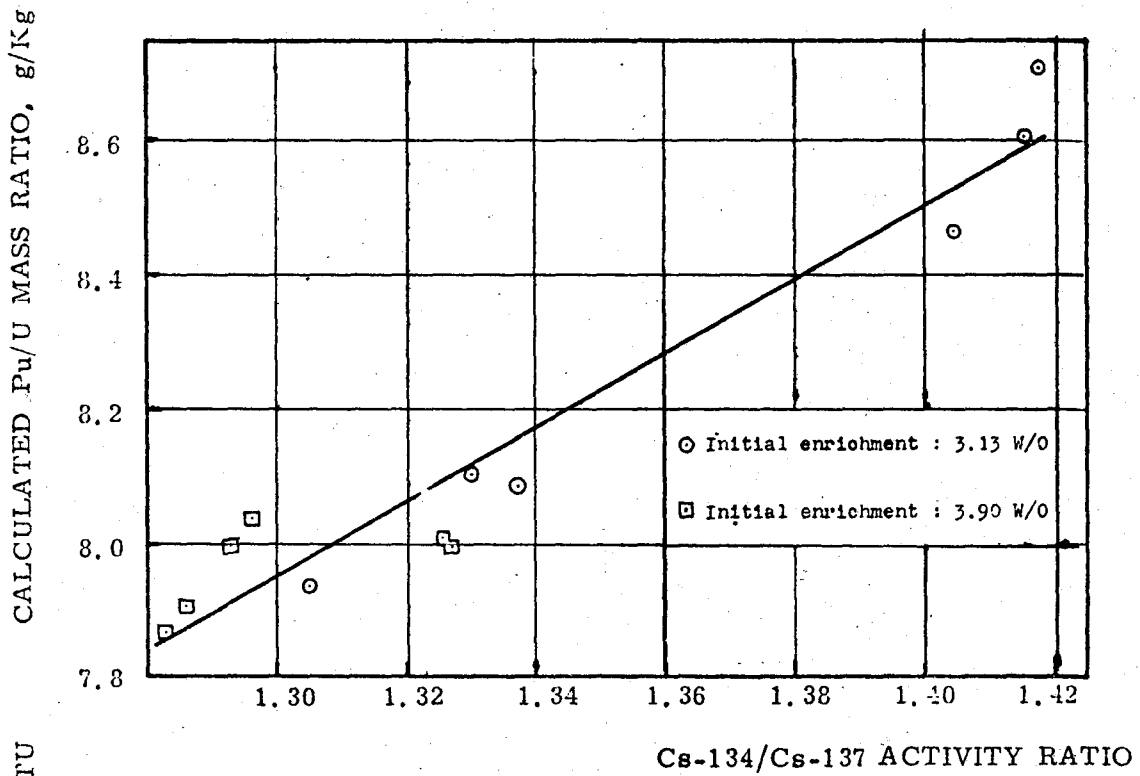


Fig. 4.6- CORRELATION BETWEEN Pu/U RATIO AND Cs-134/Cs-137 ACTIVITY RATIO AT THE END OF CYCLE 2 (Ge-Li Gamma Scanning Data, Assembly Averages)

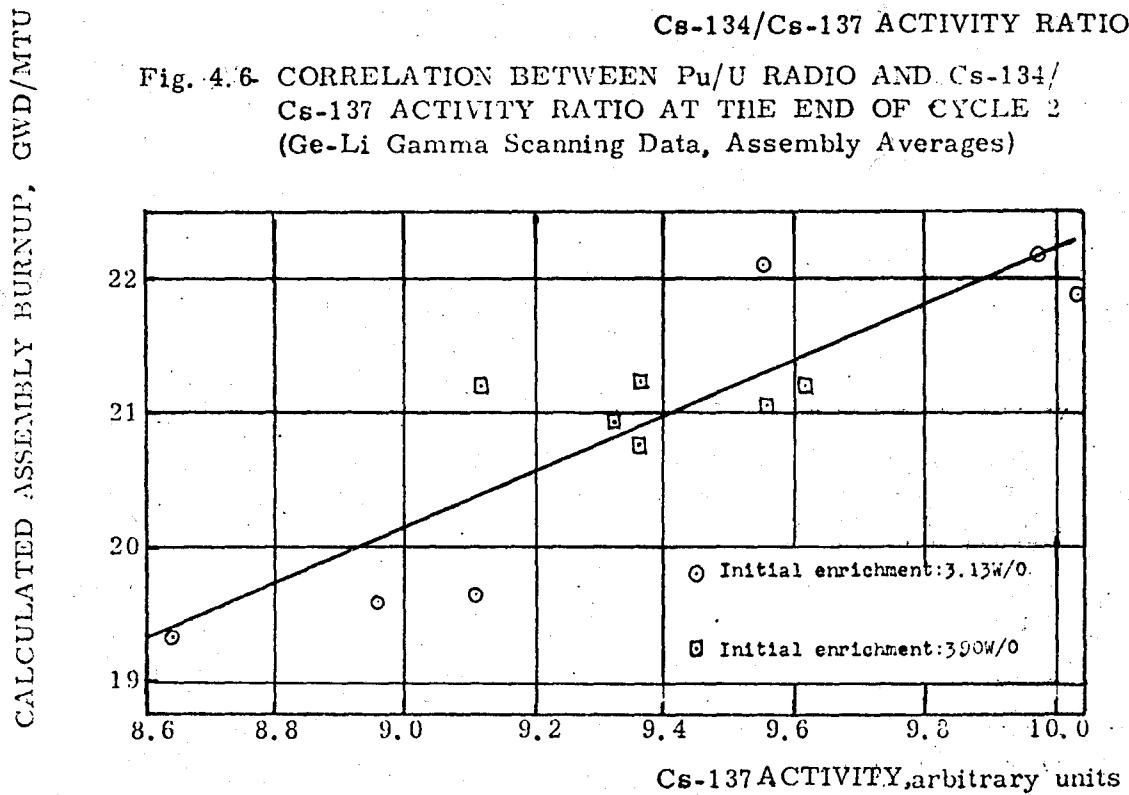


Fig. 4.7- CORRELATION BETWEEN BURNUP AND Cs-137 ACTIVITY AT THE END OF CYCLE 2 (Ge-Li Gamma Scanning Data, Assembly Averages)

FIG. 5.1 - STEAM GENERATOR SCHEMATIZATION FOR THE F.111 RID CODE ANALYSIS.

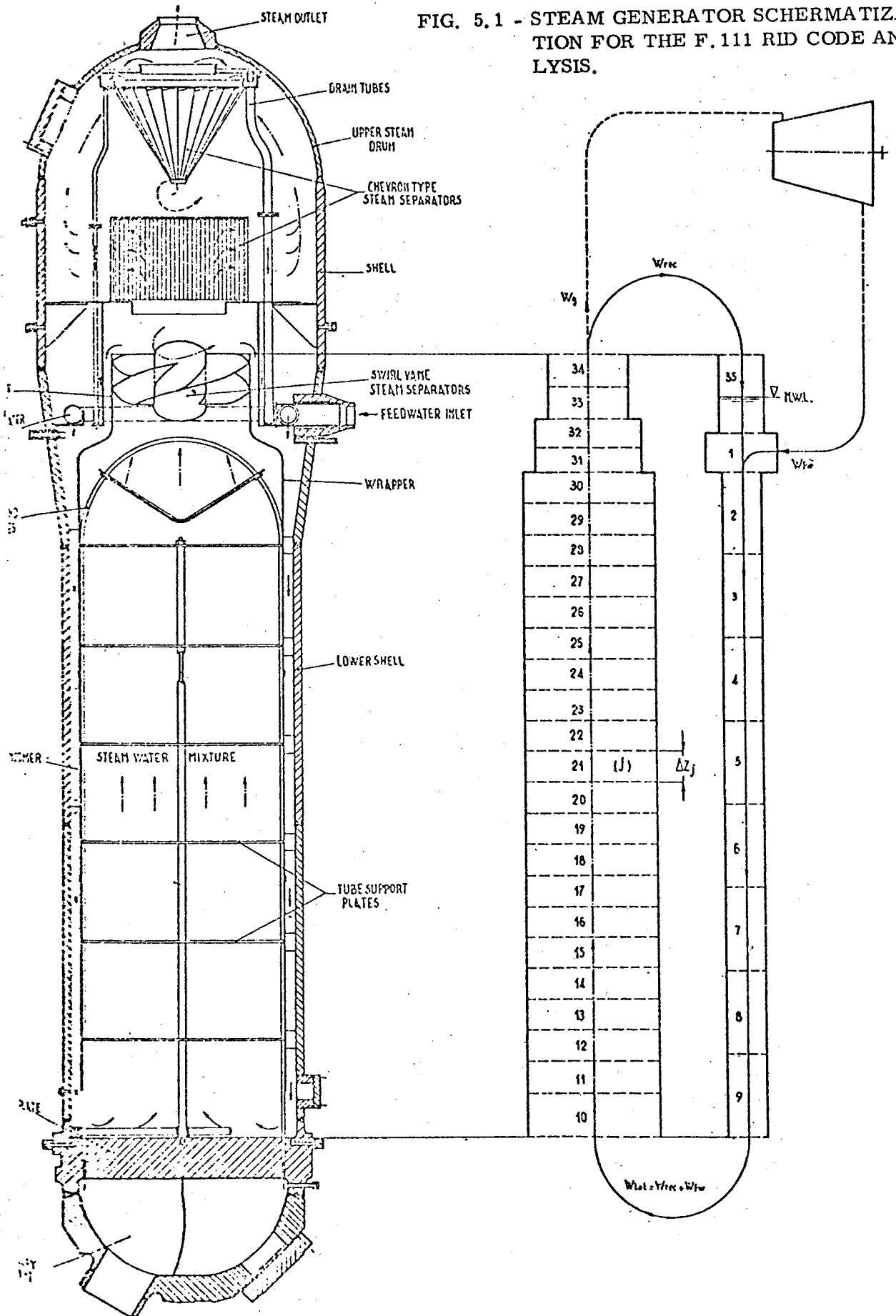


FIG. 5.2 (a) - SIMPLIFIED DIAGRAM OF HIGH PRESSURE STEAM LINES OF THE TRINO VERCELLESE PLANT.

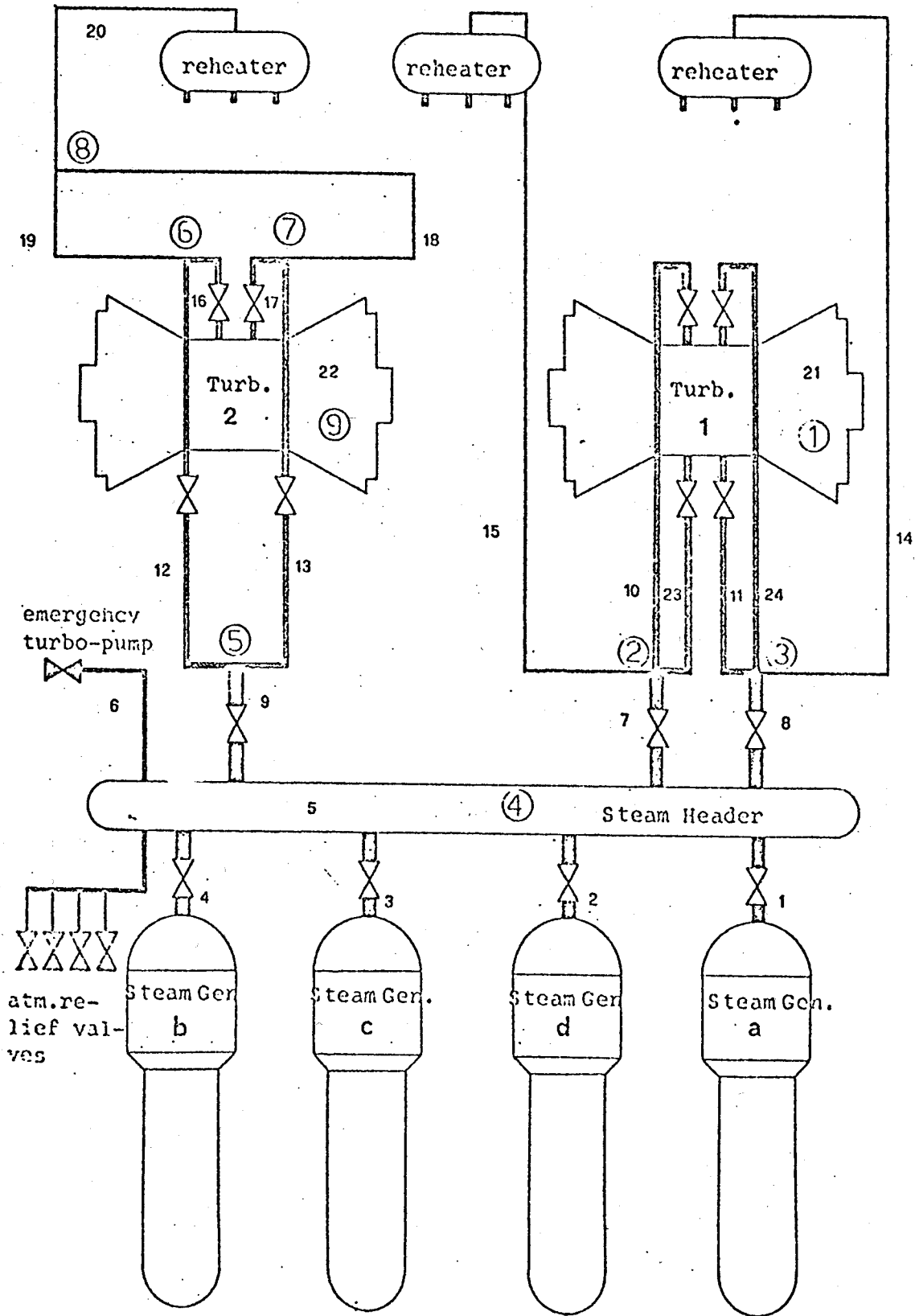


FIG. 5.2 (b) - EQUIVALENT ELECTRIC NETWORK FOR THE ARIA CODE
(Cfr. Fig. 5.2 a)

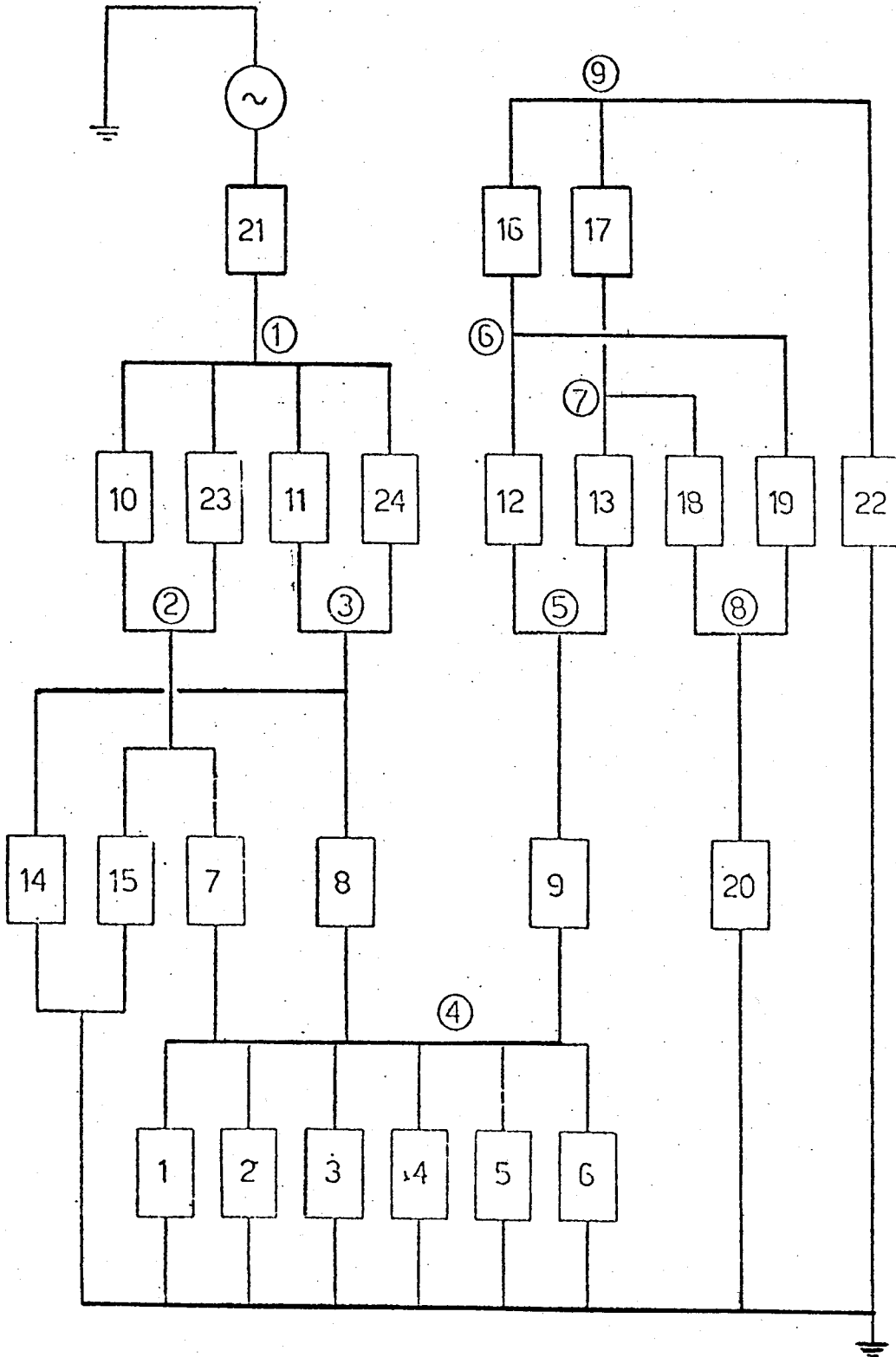


FIG. 5.3 - TIME VARIATION OF STEAM FLOW RATE, STEAM QUALITY AND LIQUID VELOCITY IN THE FIRST ELEMENT (940 MWt).

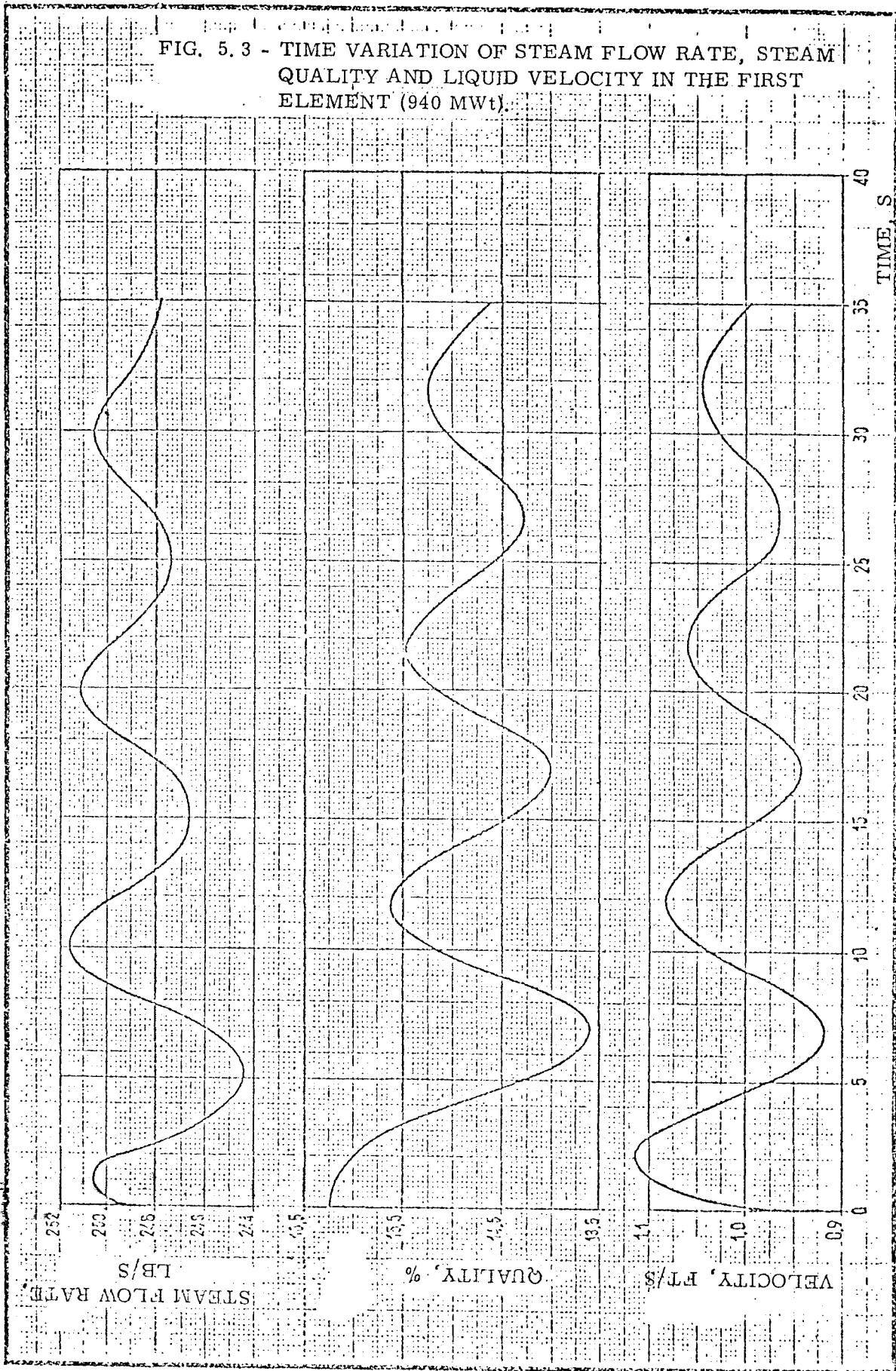
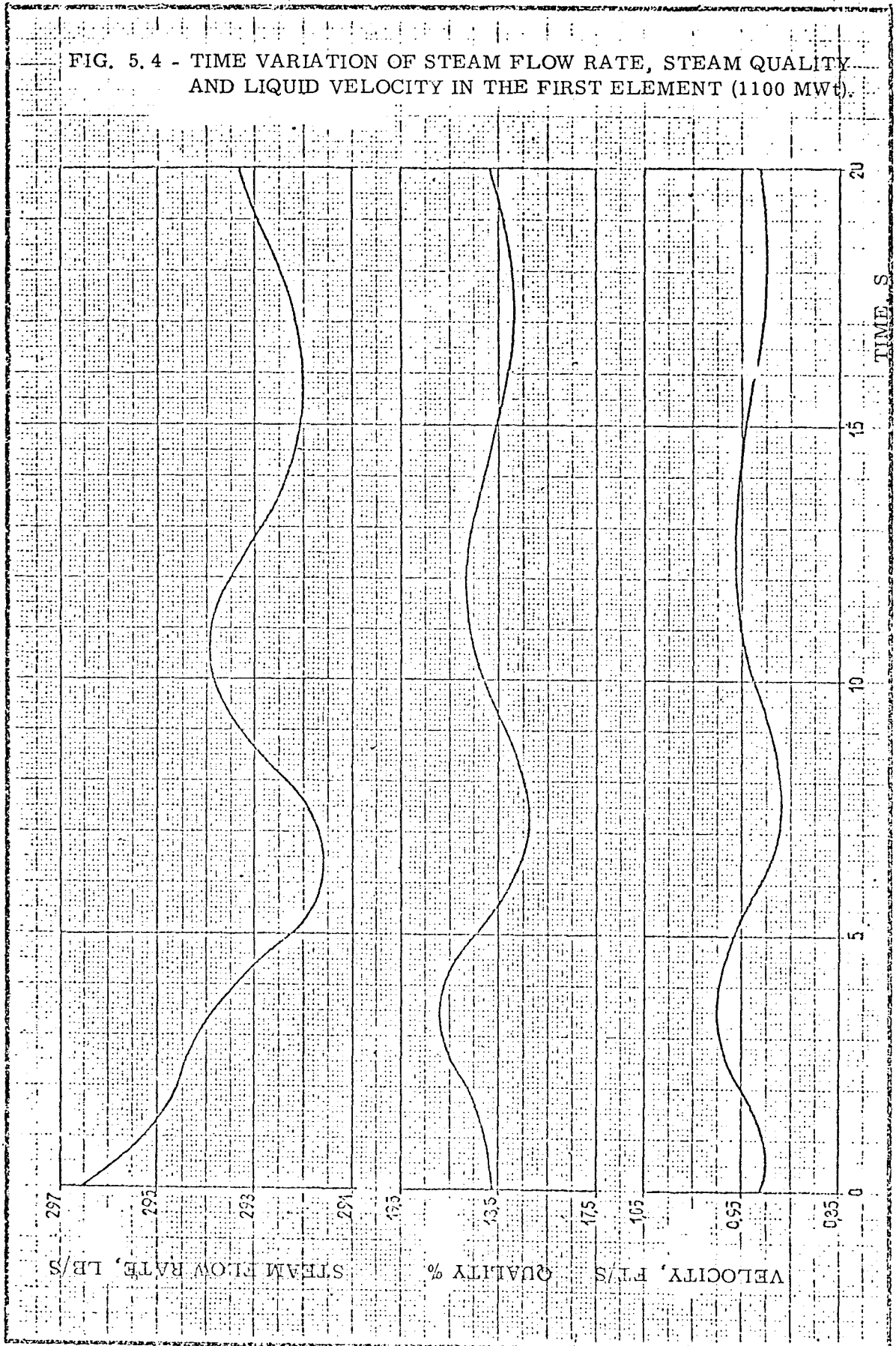


FIG. 5.4 - TIME VARIATION OF STEAM FLOW RATE, STEAM QUALITY AND LIQUID VELOCITY IN THE FIRST ELEMENT (1100 MWt).



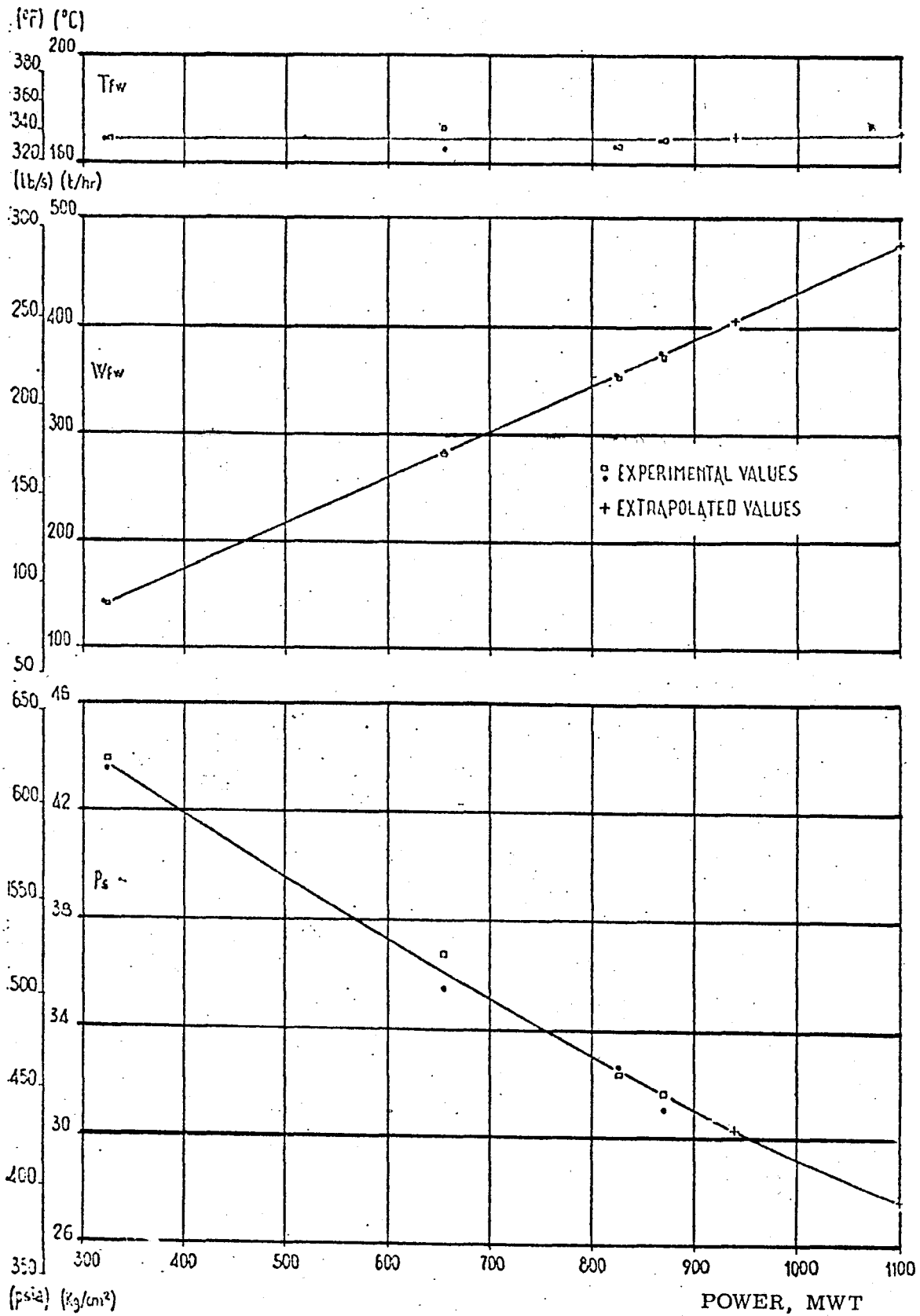


FIG. 5.5 - FEEDWATER TEMPERATURE (T_{fw}), FEEDWATER FLOW RATE (W_{fw}) AND SECONDARY PRESSURE (P_s) VS. POWER

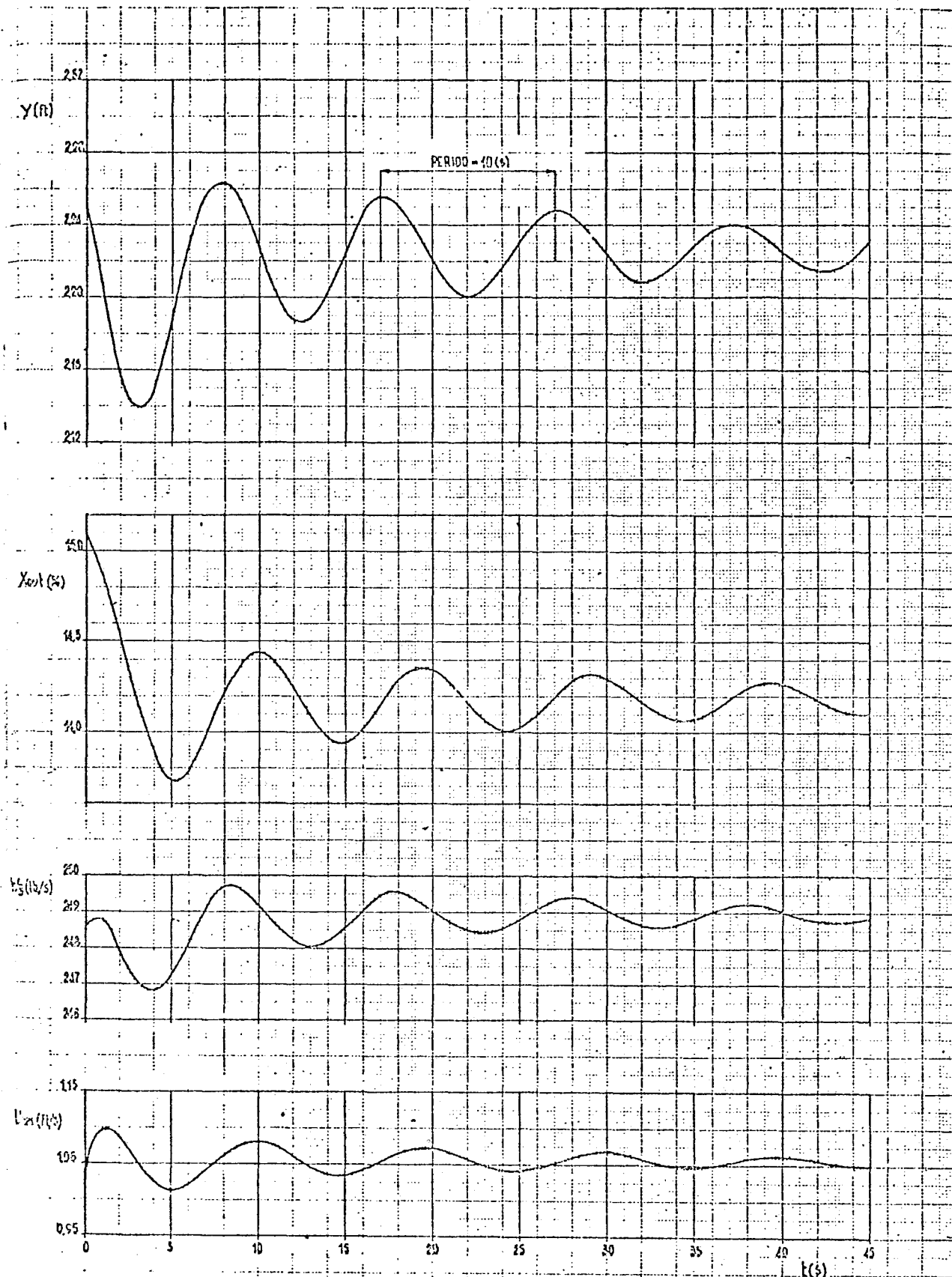


FIG. 5.6 - TIME VARIATION OF WATER LEVEL (Y), STEAM QUALITY (X_{out}), STEAM FLOW RATE (W_g) AND LIQUID VELOCITY (U) IN THE FIRST ELEMENT (940 MWt)

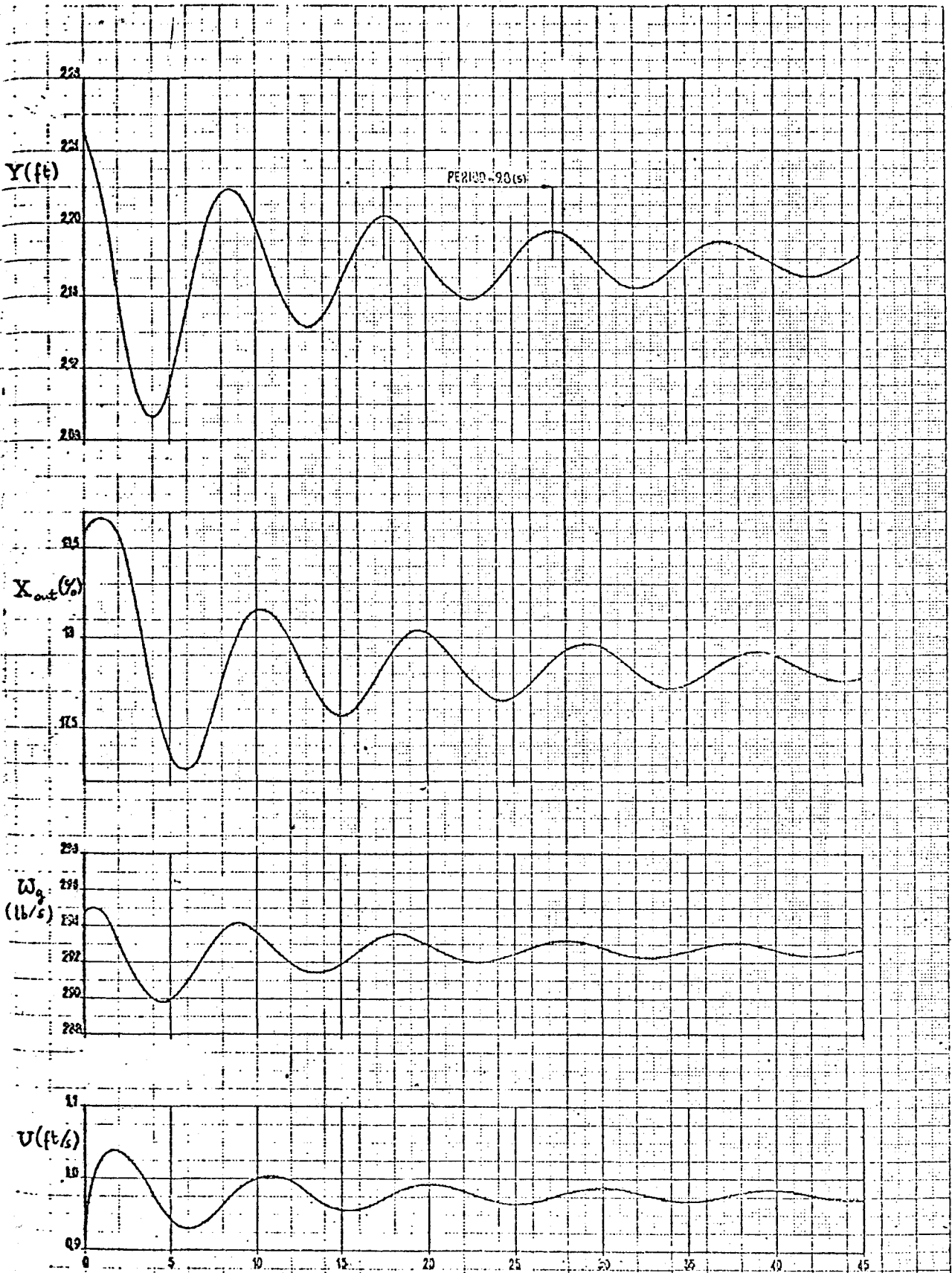


FIG. 5.7 - TIME VARIATION OF WATER LEVEL (Y), STEAM QUALITY (X_{out}), STEAM FLOW RATE (W_g) AND LIQUID VELOCITY (U) IN THE FIRST ELEMENT (1100 MWt).

FIG. 5.8 - TIME VARIATION OF STEAM FLOW RATE, STEAM QUALITY AND LIQUID VELOCITY IN THE FIRST ELEMENT (1200 AND 1250 MWt).

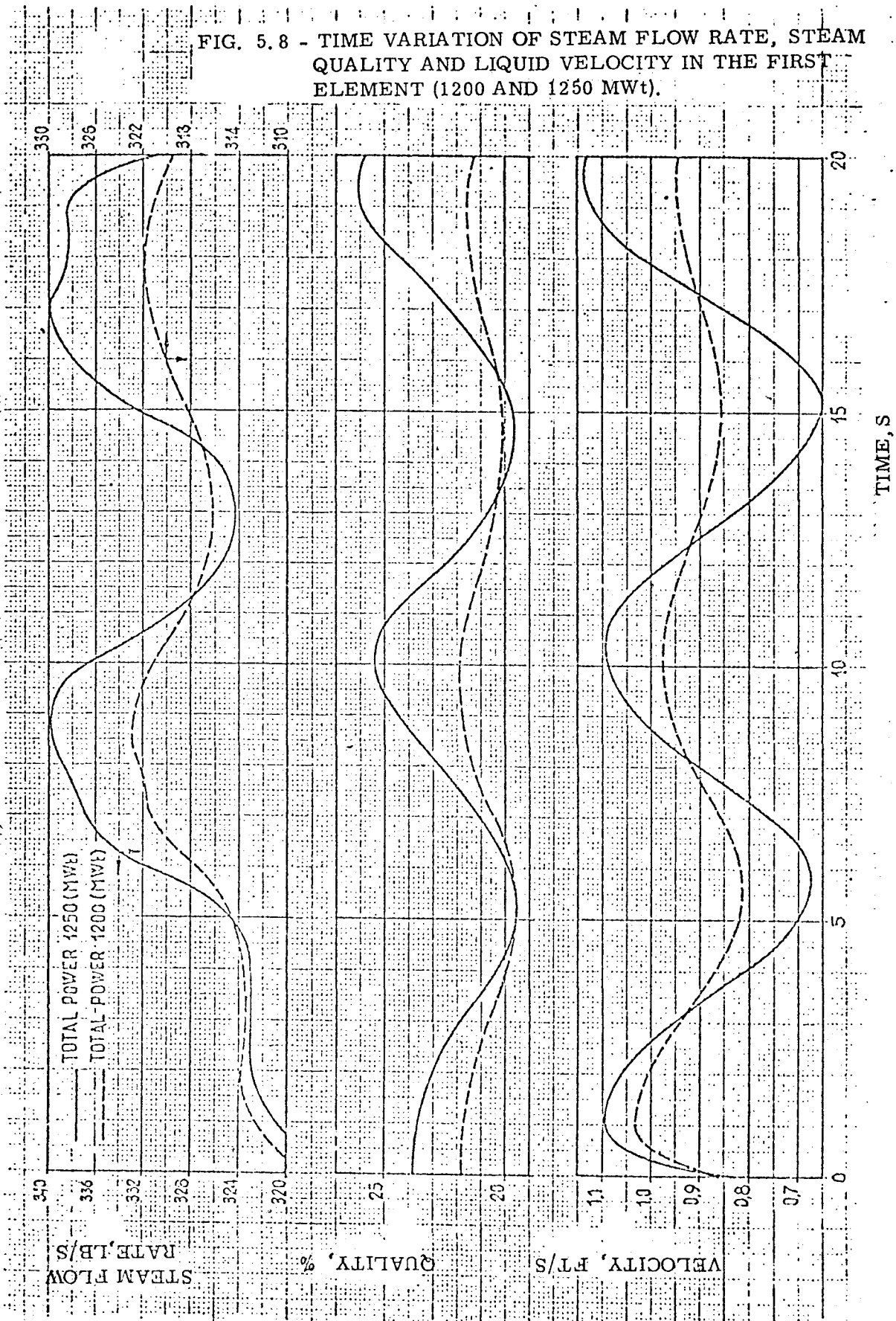


FIG. 5.9 - AMPLITUDES OF STEAM GENERATORS LEVEL OSCILLATIONS (NORMALIZED TO STEAM GENERATOR A OSCILLATION AT 825 MWt) VERSUS POWER.

NOMINAL LEVEL SET POINT

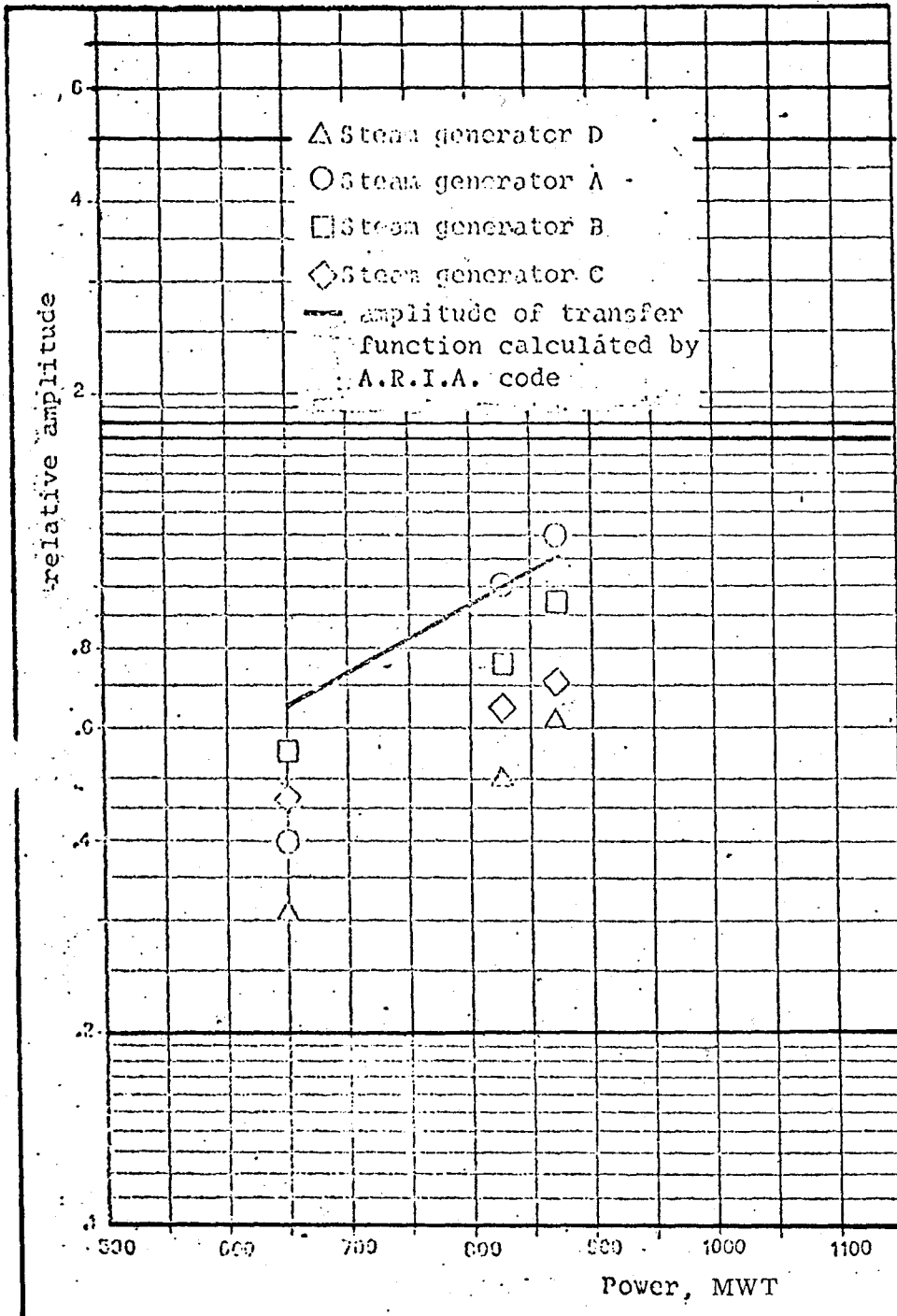


FIG. 5.10 - AMPLITUDES OF STEAM GENERATORS LEVEL OSCILLATIONS (NORMALIZED TO STEAM GENERATOR A OSCILLATION AT 825 MWt AND NOMINAL LEVEL SET POINT) VERSUS POWER, + 30 CM LEVEL SET POINT

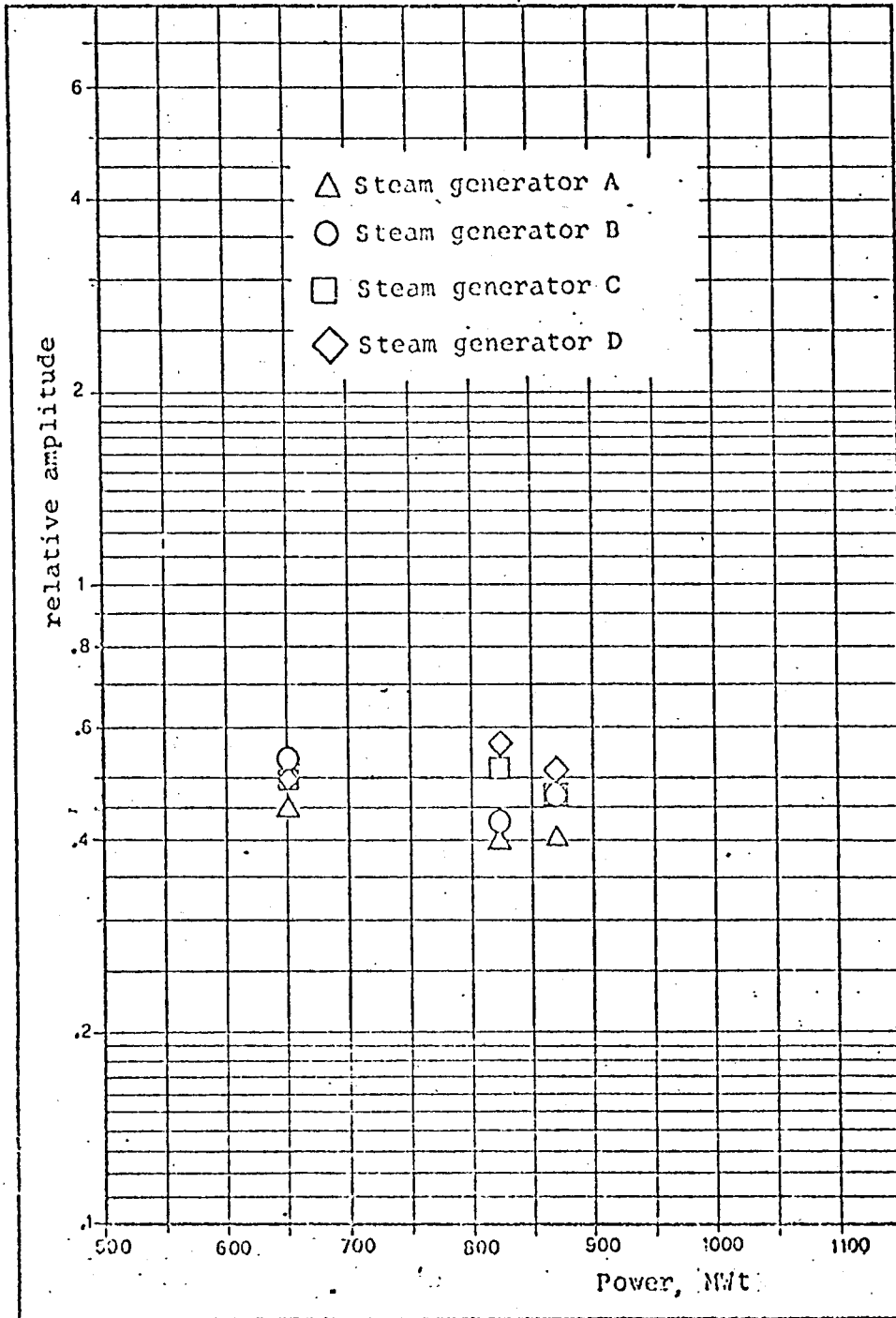
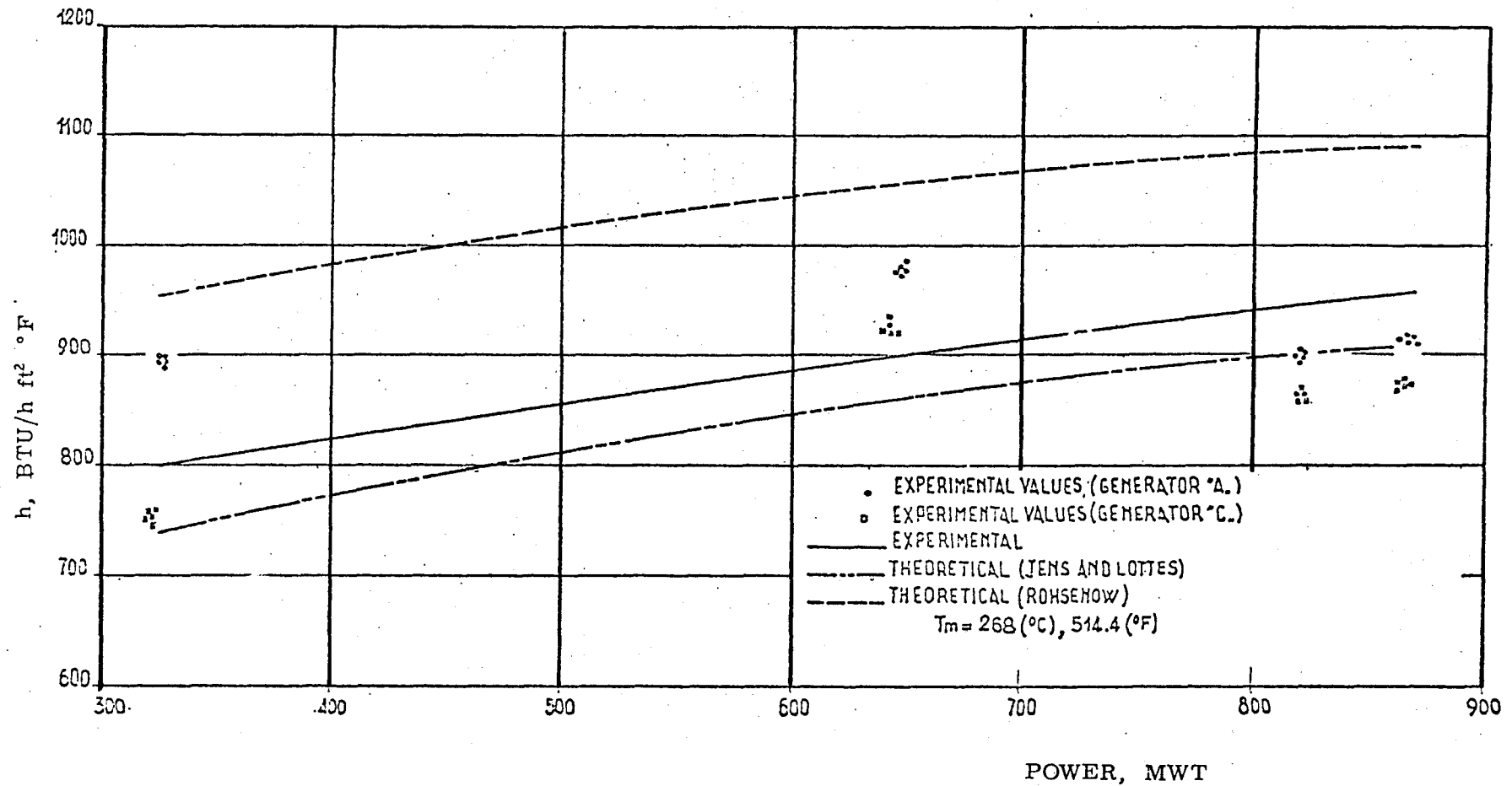
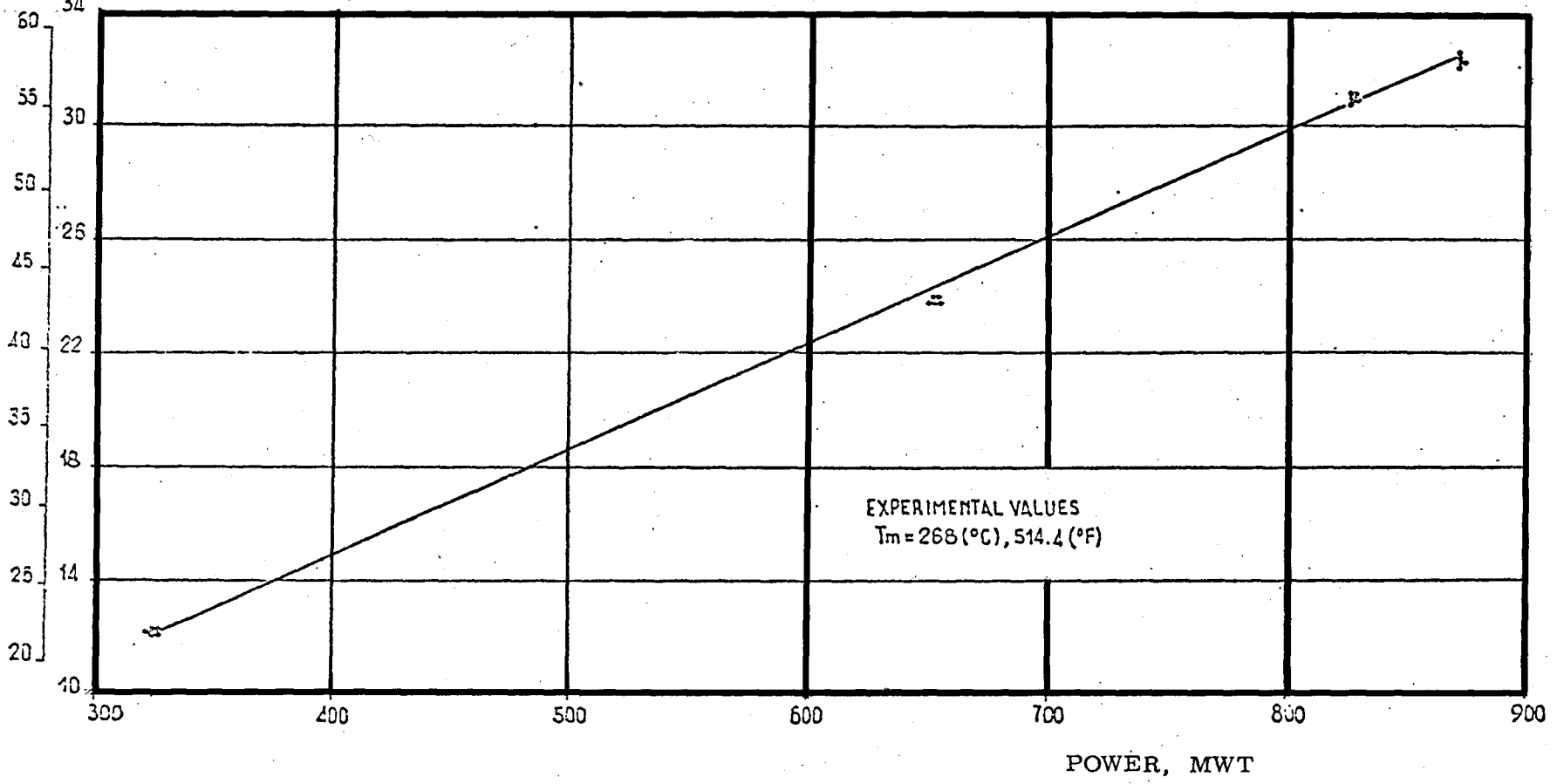


FIG. 5.11 - OVERALL HEAT TRANSFER COEFFICIENT VS. POWER



ΔT_p
(°F) (°C)

FIG. 5.12 - EXPERIMENTAL ΔT_p VS. POWER



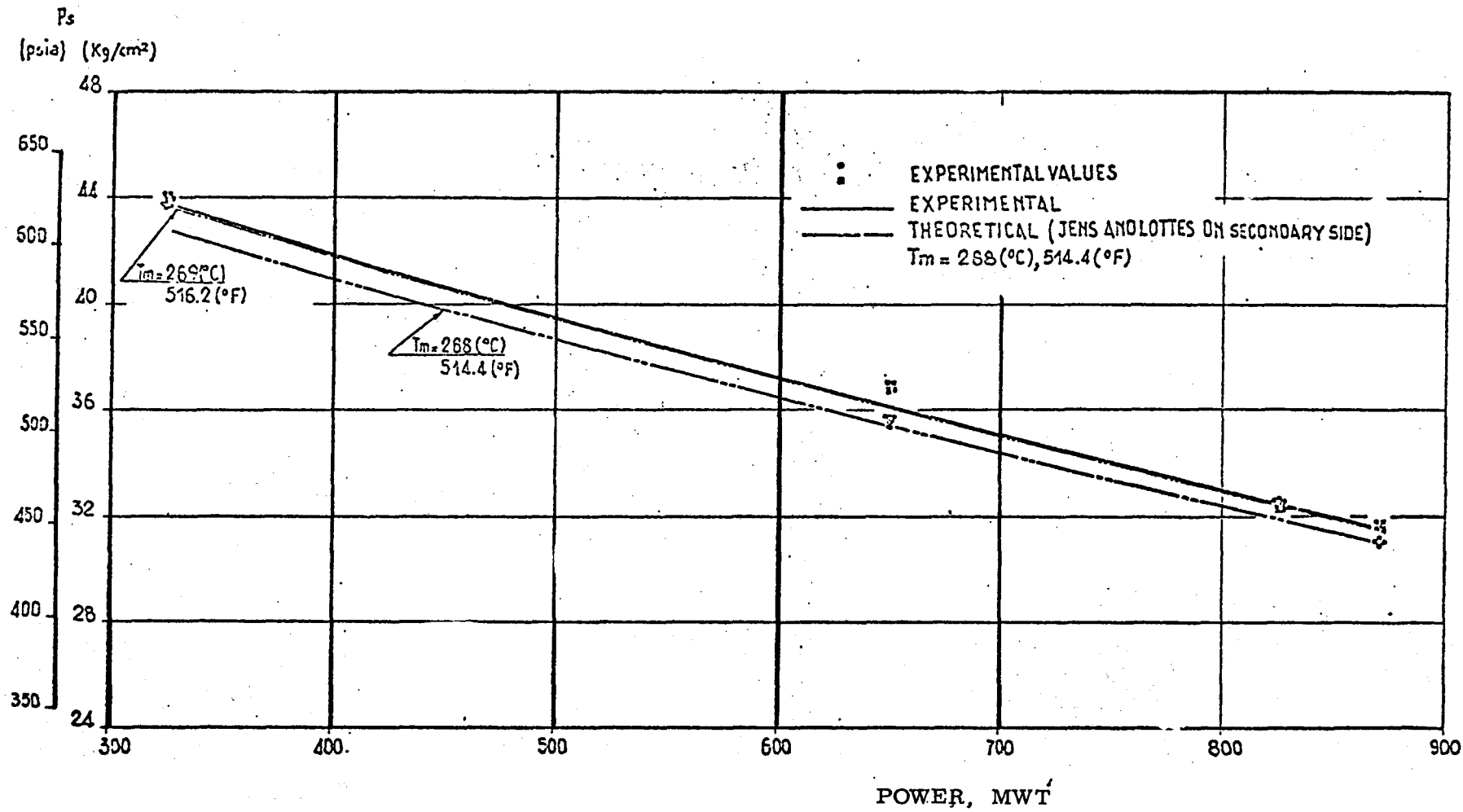


FIG. 5.13 - SECONDARY PRESSURE (P_s) VS. POWER

FIG. 5.14 - STEAM PRESSURE AND HEAT TRANSFER COEFFICIENT VS PRIMARY AVG. TEMPERA-
 TURE FOR VARIOUS POWER LEVELS

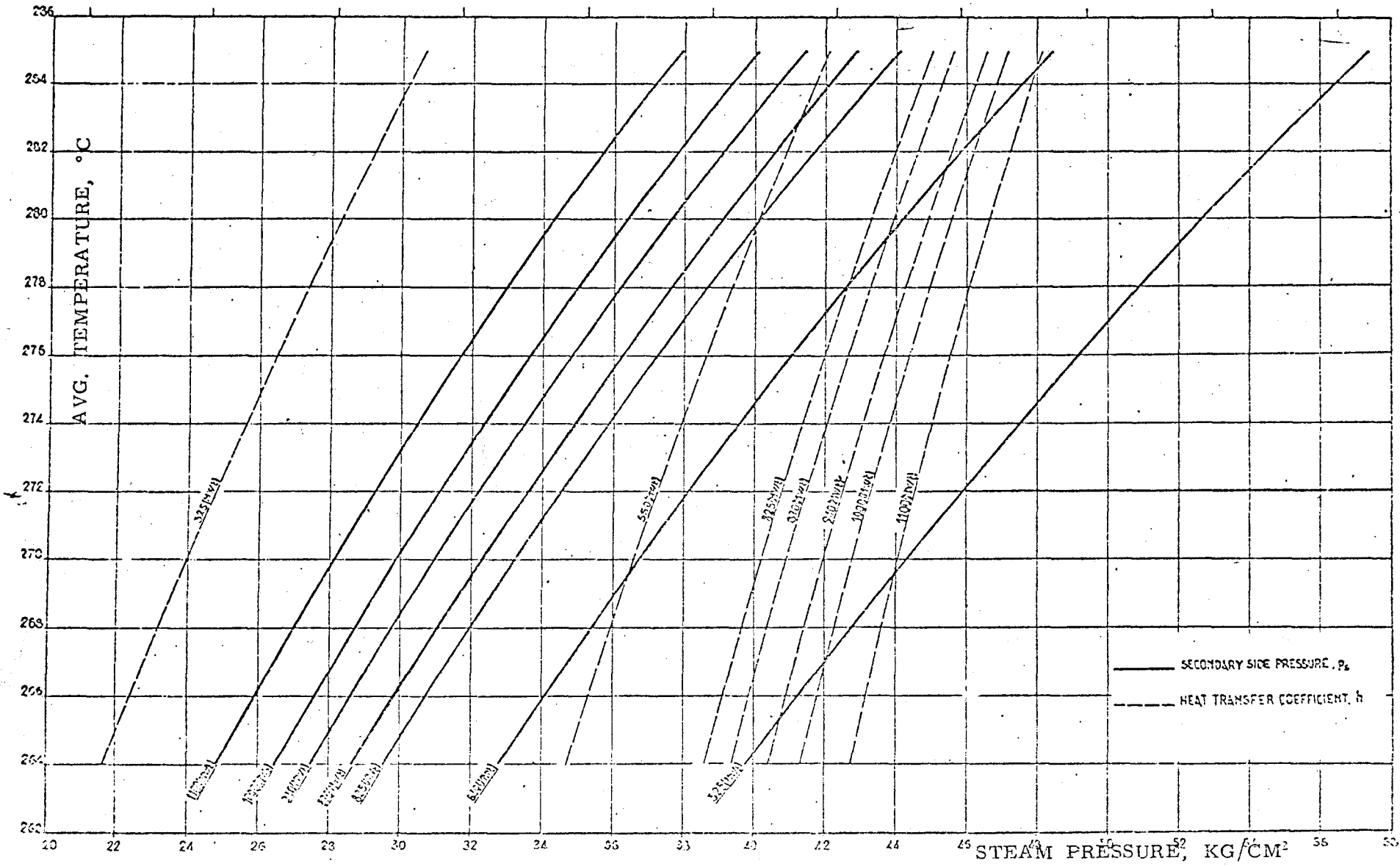
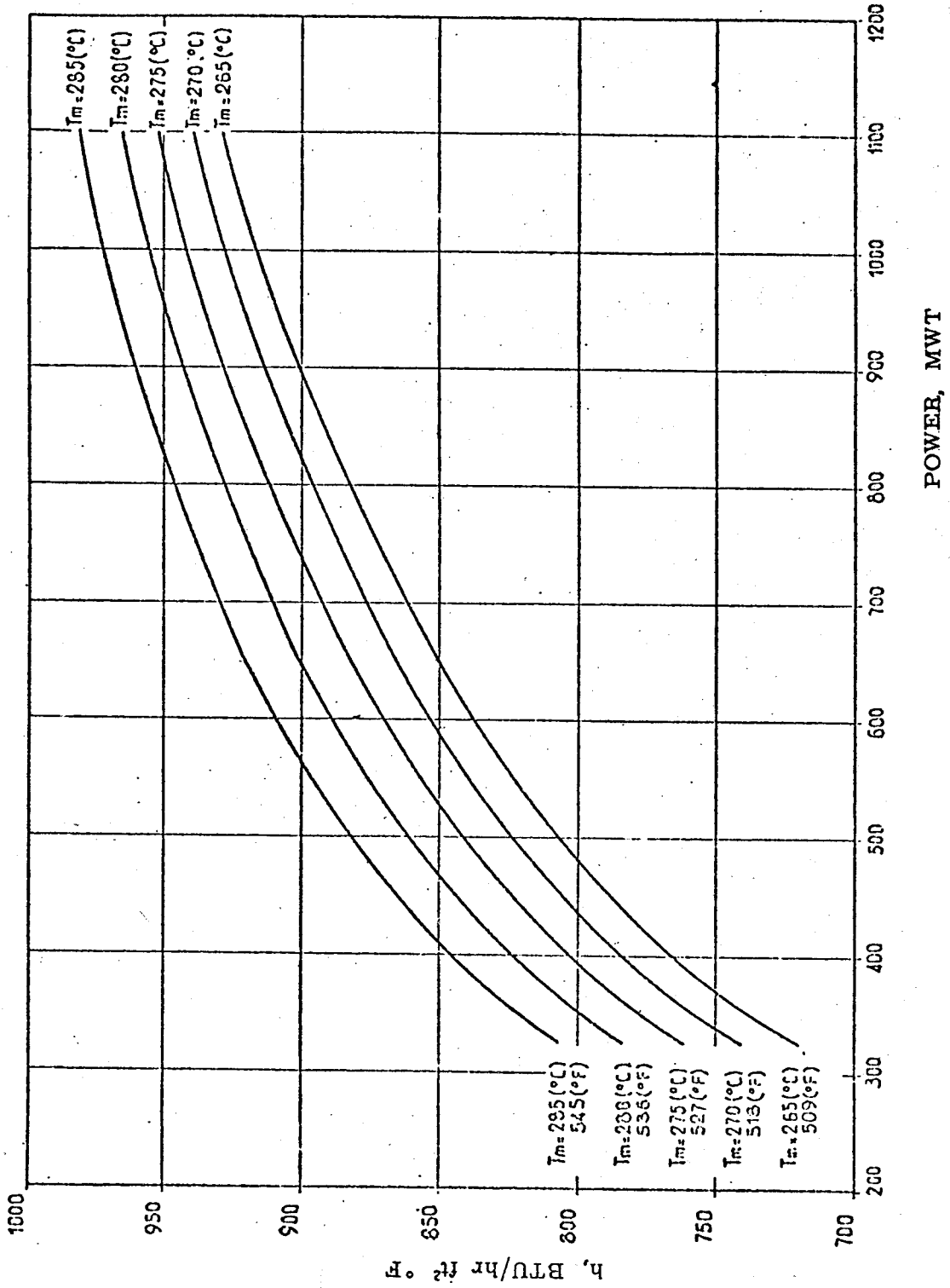


FIG. 5.15 - OVERALL HEAT TRANSFER COEFFICIENT VS. POWER FOR VARIOUS AVERAGE TEMPERATURES (T_m)



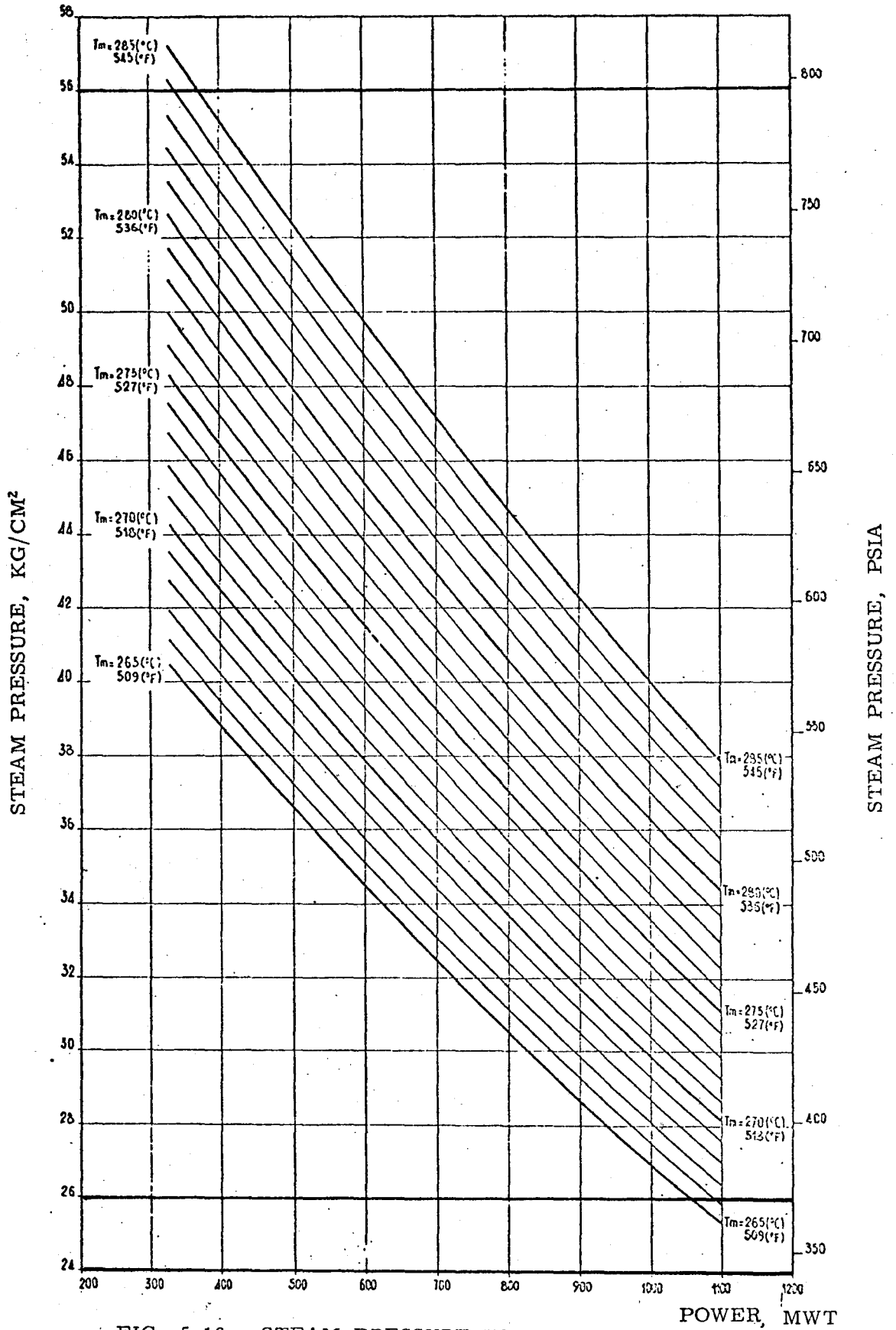


FIG. 5.16 - STEAM PRESSURE VS. POWER

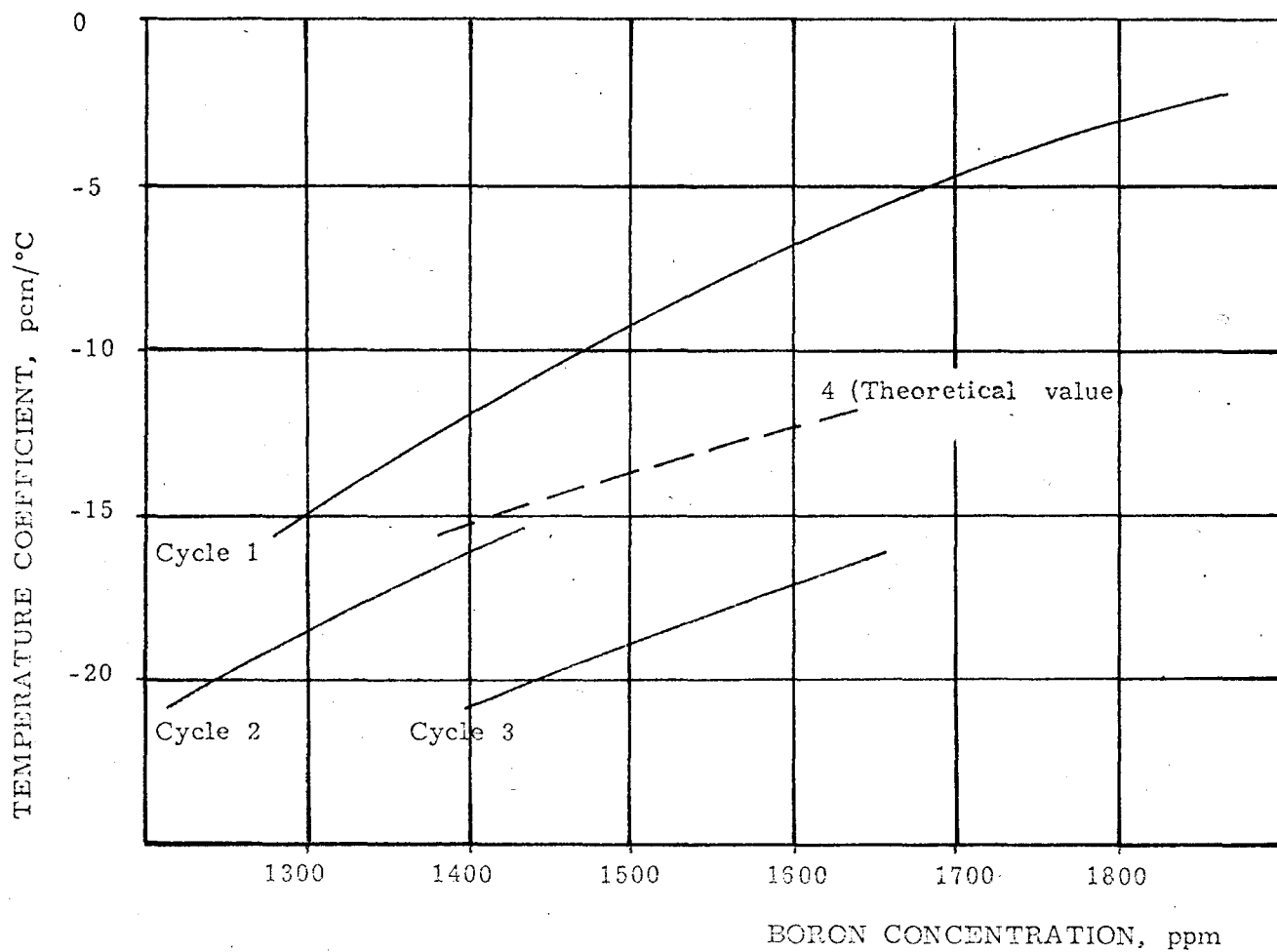


FIG. 6.1 - MODERATOR TEMPERATURE COEFFICIENT VS. BORON CONCENTRATION (HOT, ZERO POWER, BEGINNING OF CYCLE)

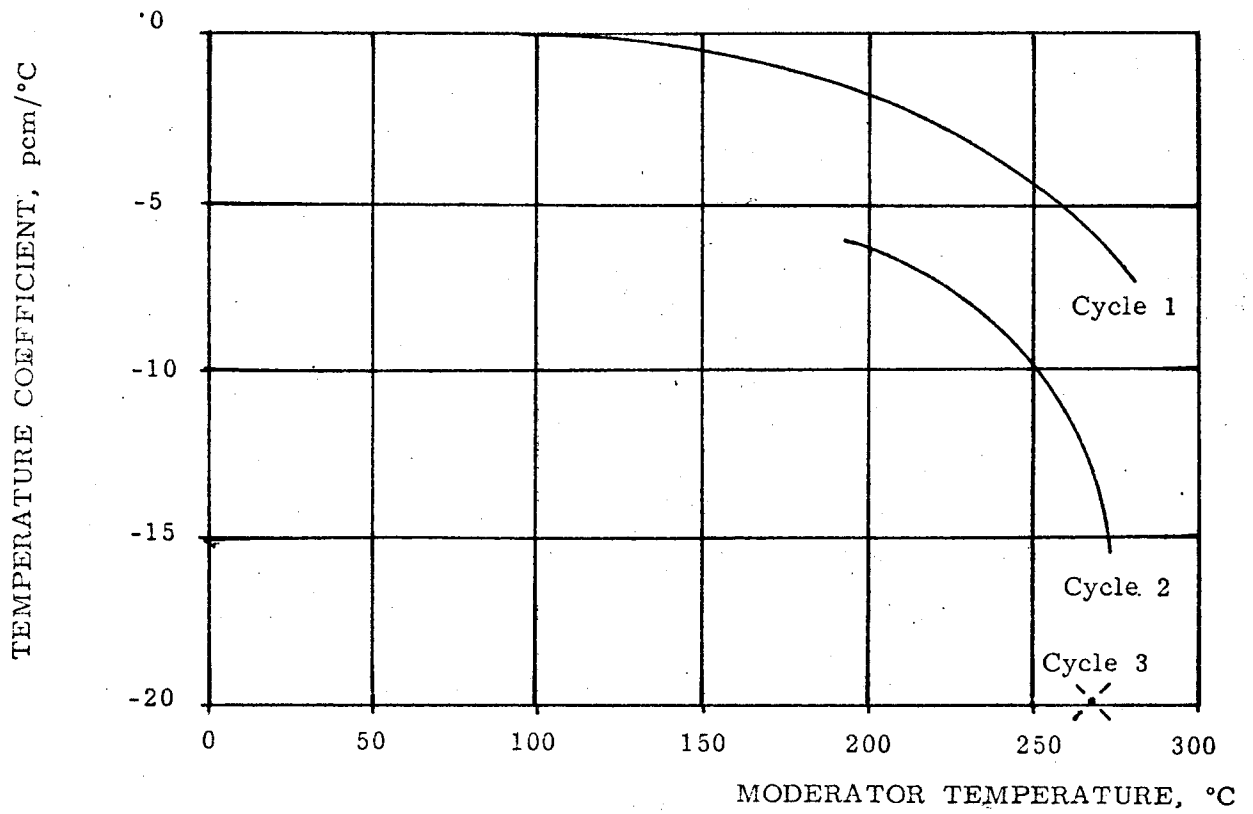


FIG. 6.2 - MODERATOR TEMPERATURE COEFFICIENT VS. MODERATOR TEMPERATURE (HOT, ZERO POWER, BEGINNING OF CYCLE)

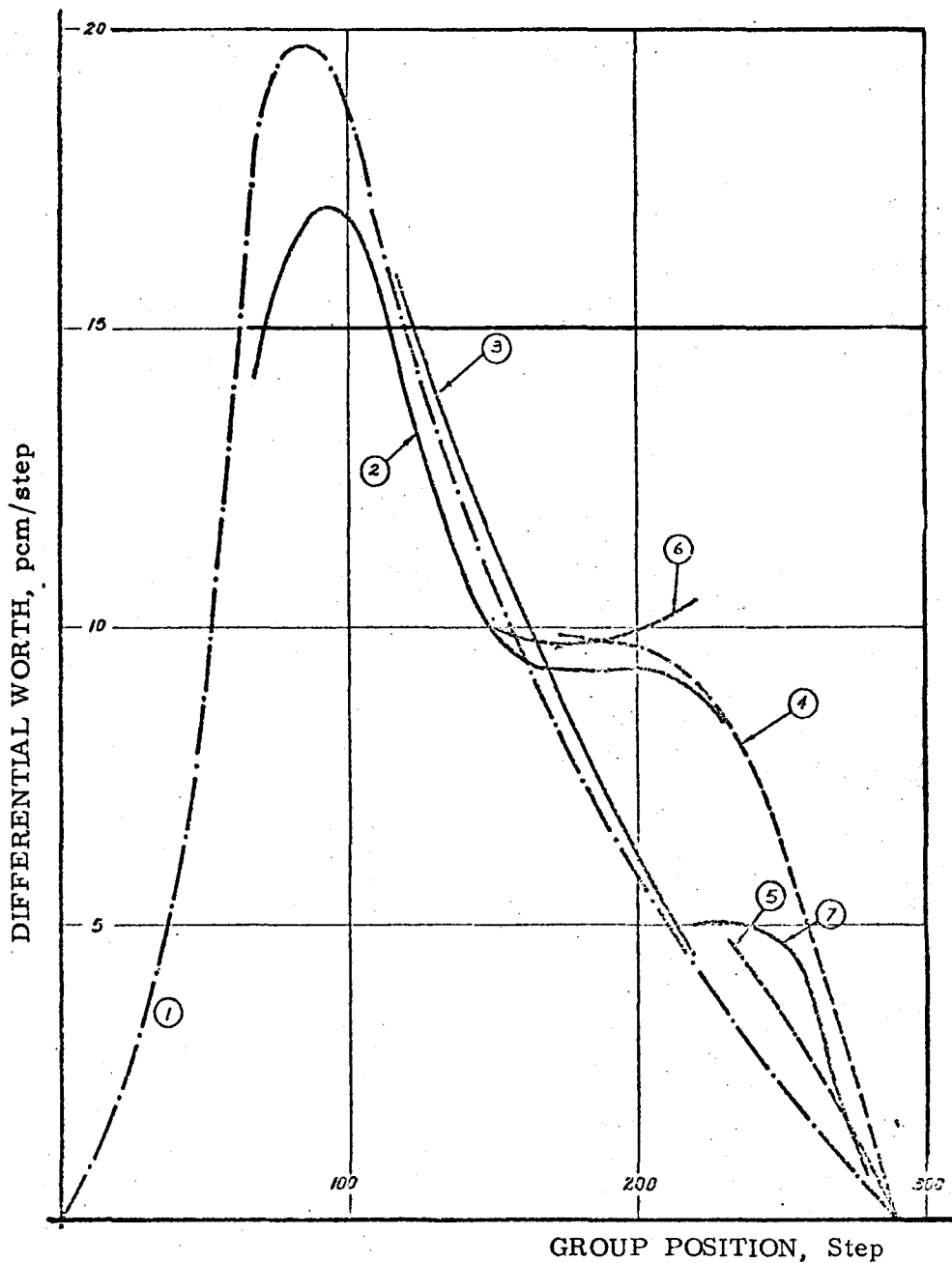


FIG. 6.3 - CONTROL GROUP DIFFERENTIAL WORTH.

- (1) HOT, ZERO POWER, BEGINNING OF LIFE
- (2) HOT, ZERO POWER, DURING XENON TRANSIENT (HIGH Xe CONCENTRATION)
- (3) HOT, ZERO POWER, DURING XENON TRANSIENT (LOW Xe CONCENTRATION)
- (4) HOT, 560 MWth, RODS INITIALLY IN (183 STEPS, 1150 MWD/MTU)
- (5) HOT, 560 MWth, RODS INITIALLY OUT (1150 MWD/MTU)
- (6) HOT, DURING POWER CHANGE
- (7) HOT, 825 MWth, RODS INITIALLY OUT (10,900 MWD/MTU)

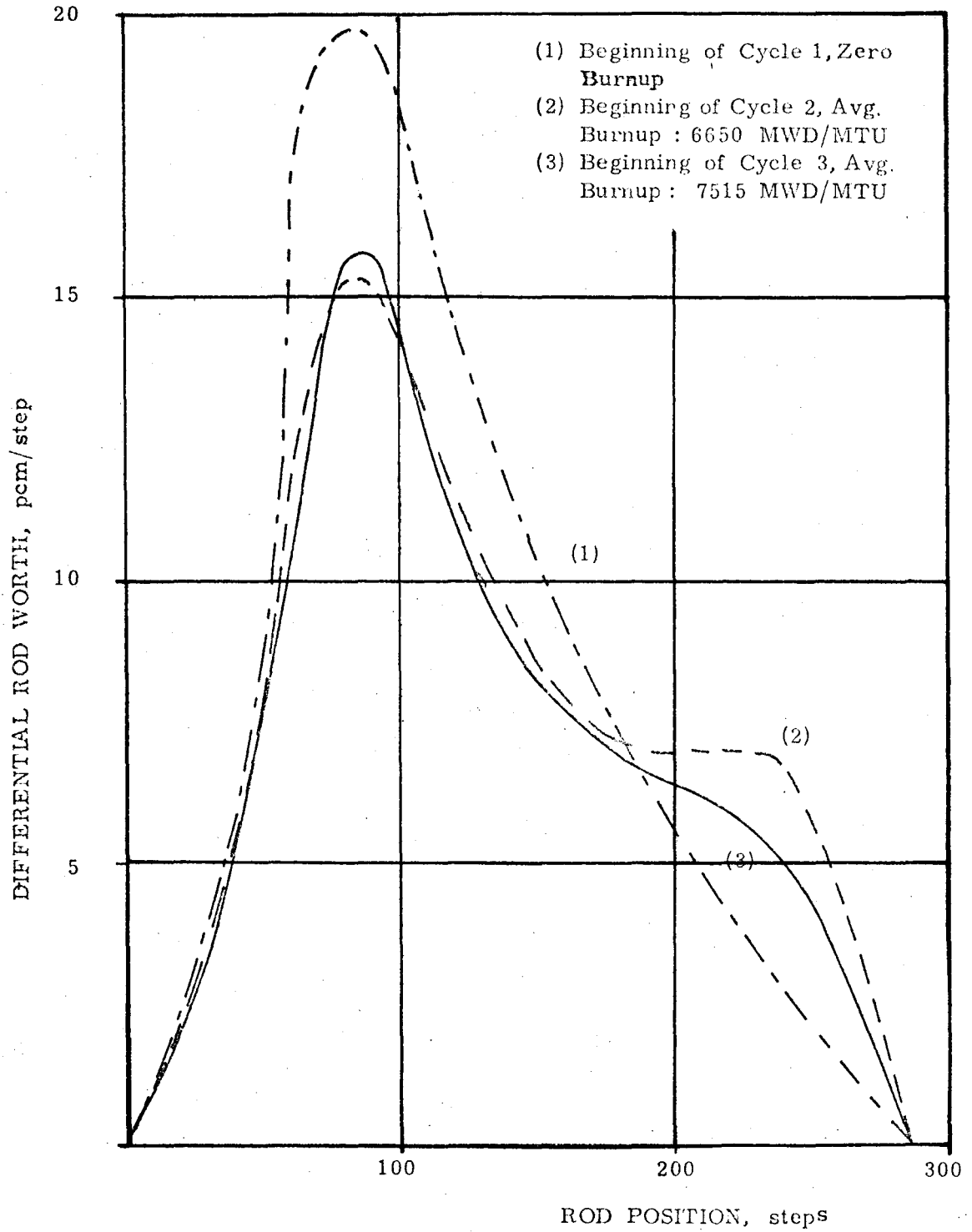


FIG. 6.4 - DIFFERENTIAL CONTROL ROD WORTH

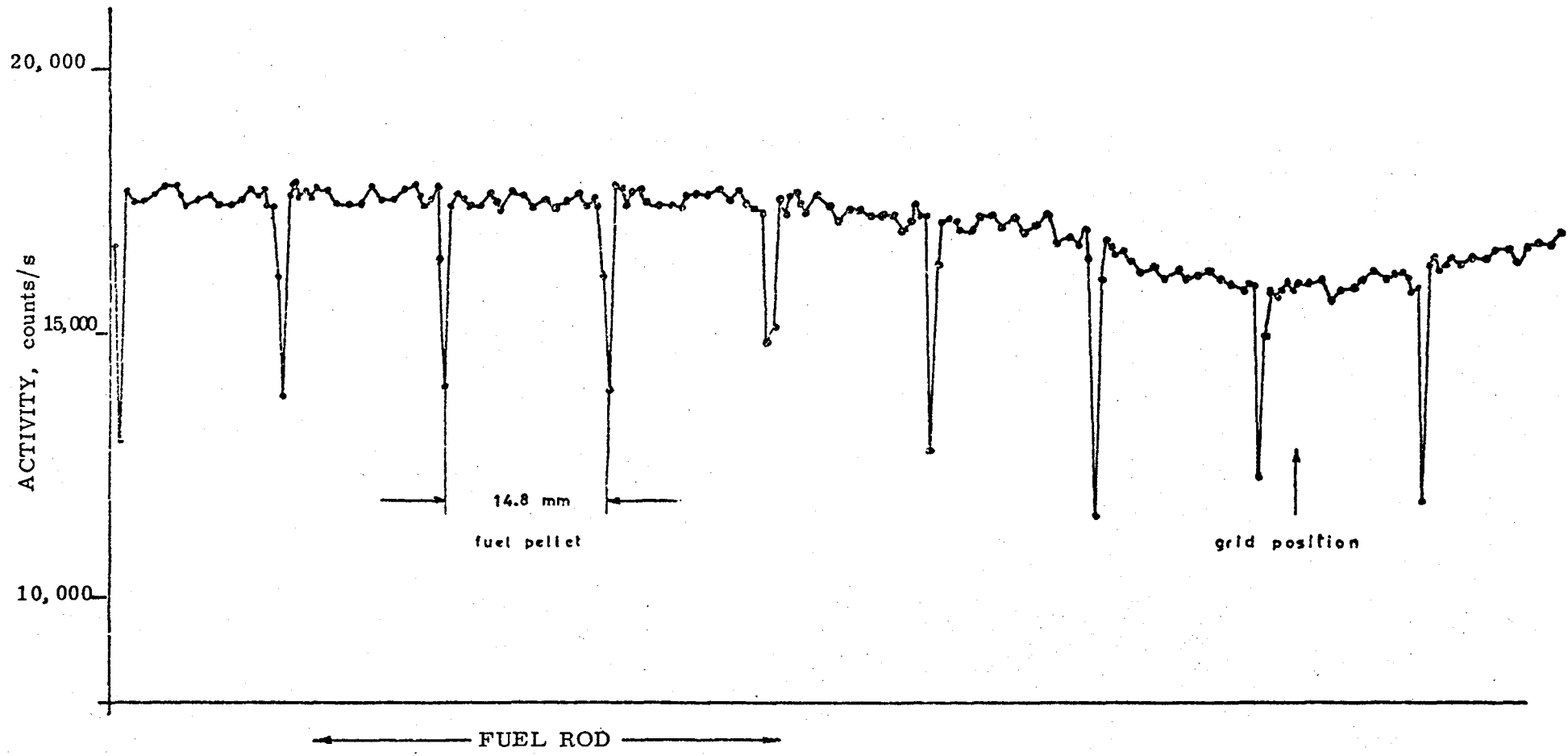


FIG. 7.1 - TOTAL GAMMA-ACTIVITY, PART OF TYPICAL ROD

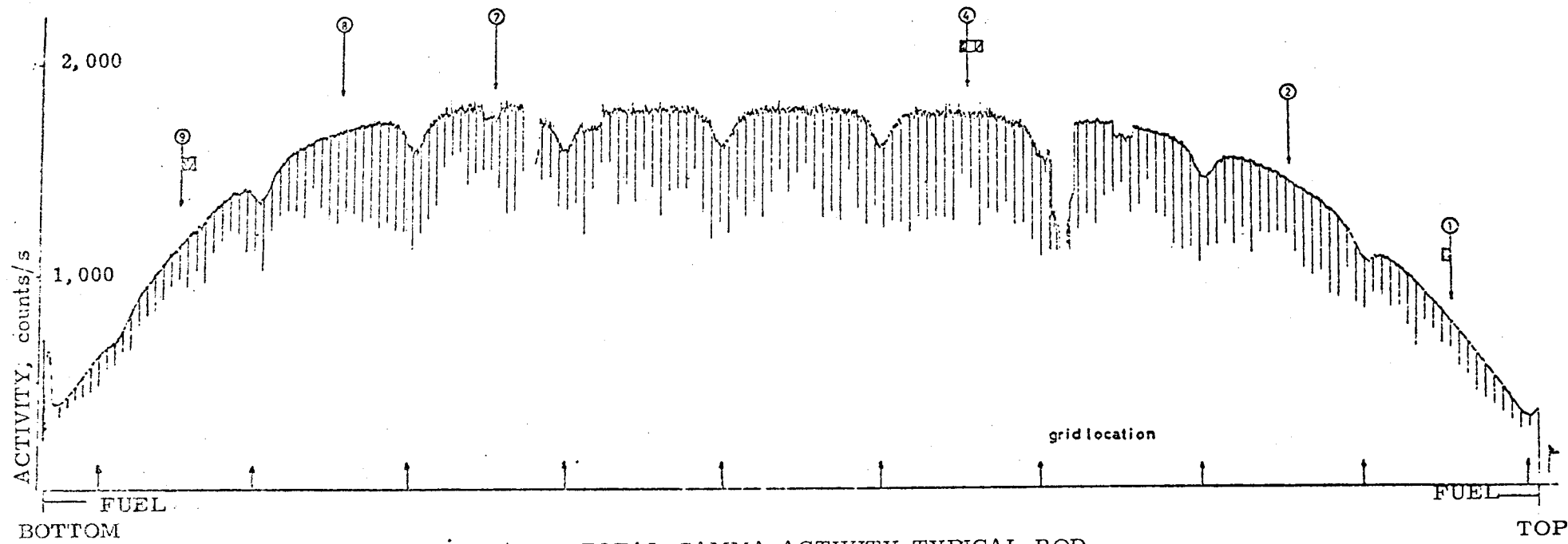


FIG. 7.2 - TOTAL GAMMA ACTIVITY, TYPICAL ROD

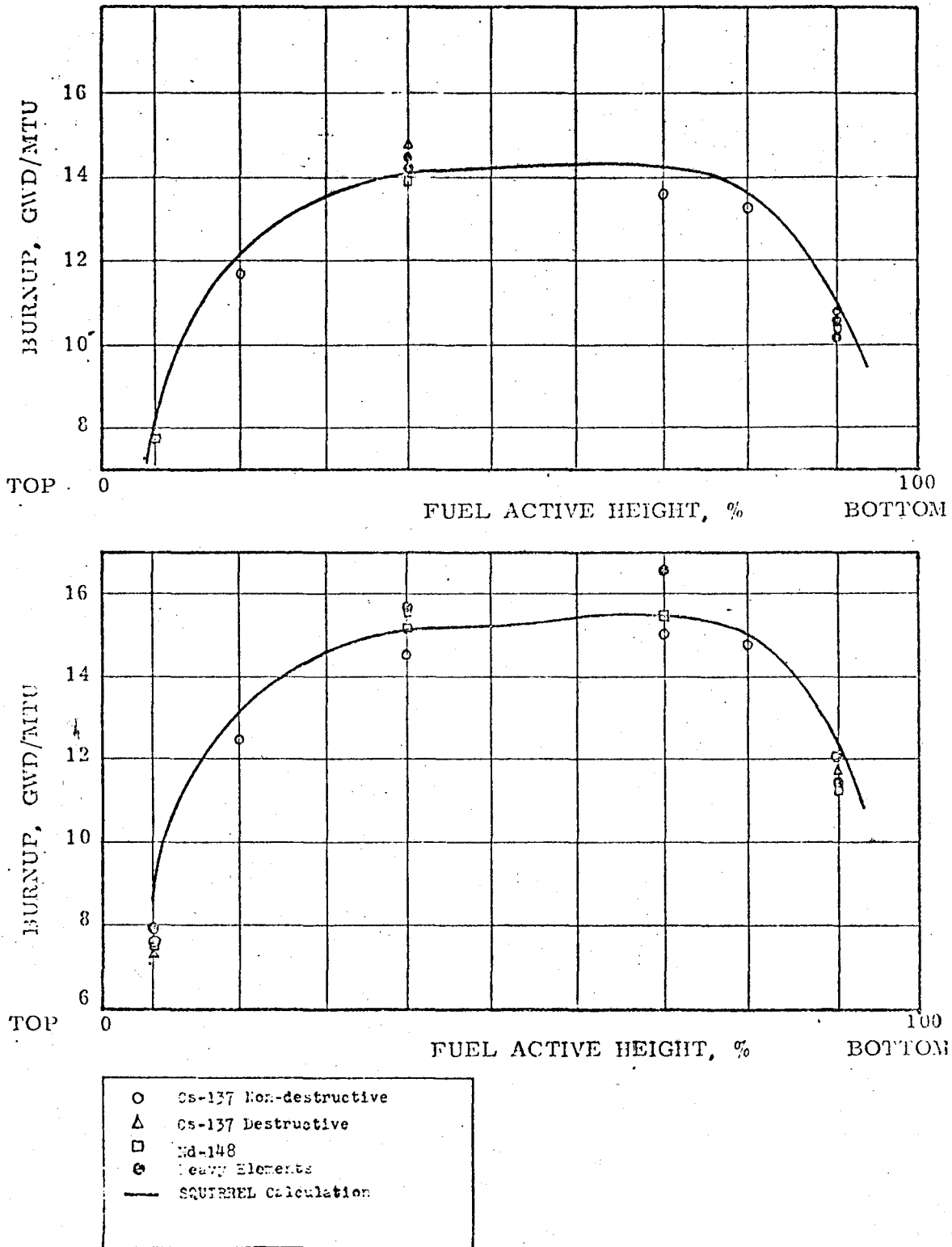


Fig. 7.3 COMPARISON OF EXPERIMENTAL AND THEORETICAL AXIAL BURNUP DISTRIBUTIONS IN TWO FUEL RODS AT THE END OF CYCLE 1 (Initial Enrichments: 2.72 and 3.13 w/o Respectively)

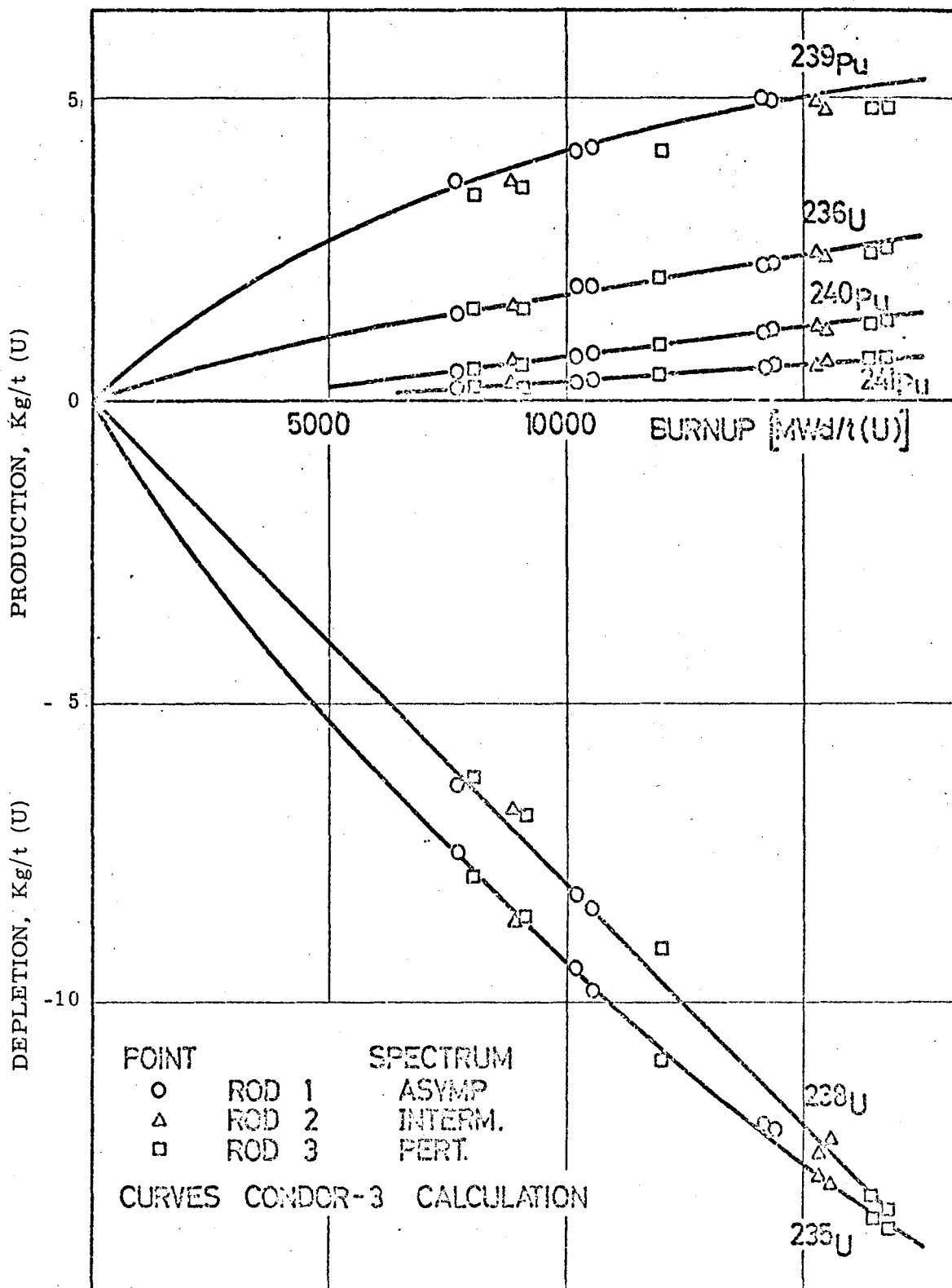


FIG. 7.4 (a) - ISOTOPIC PRODUCTION AND DEPLETION VS. BURN-UP FOR THE INNER CORE REGION.

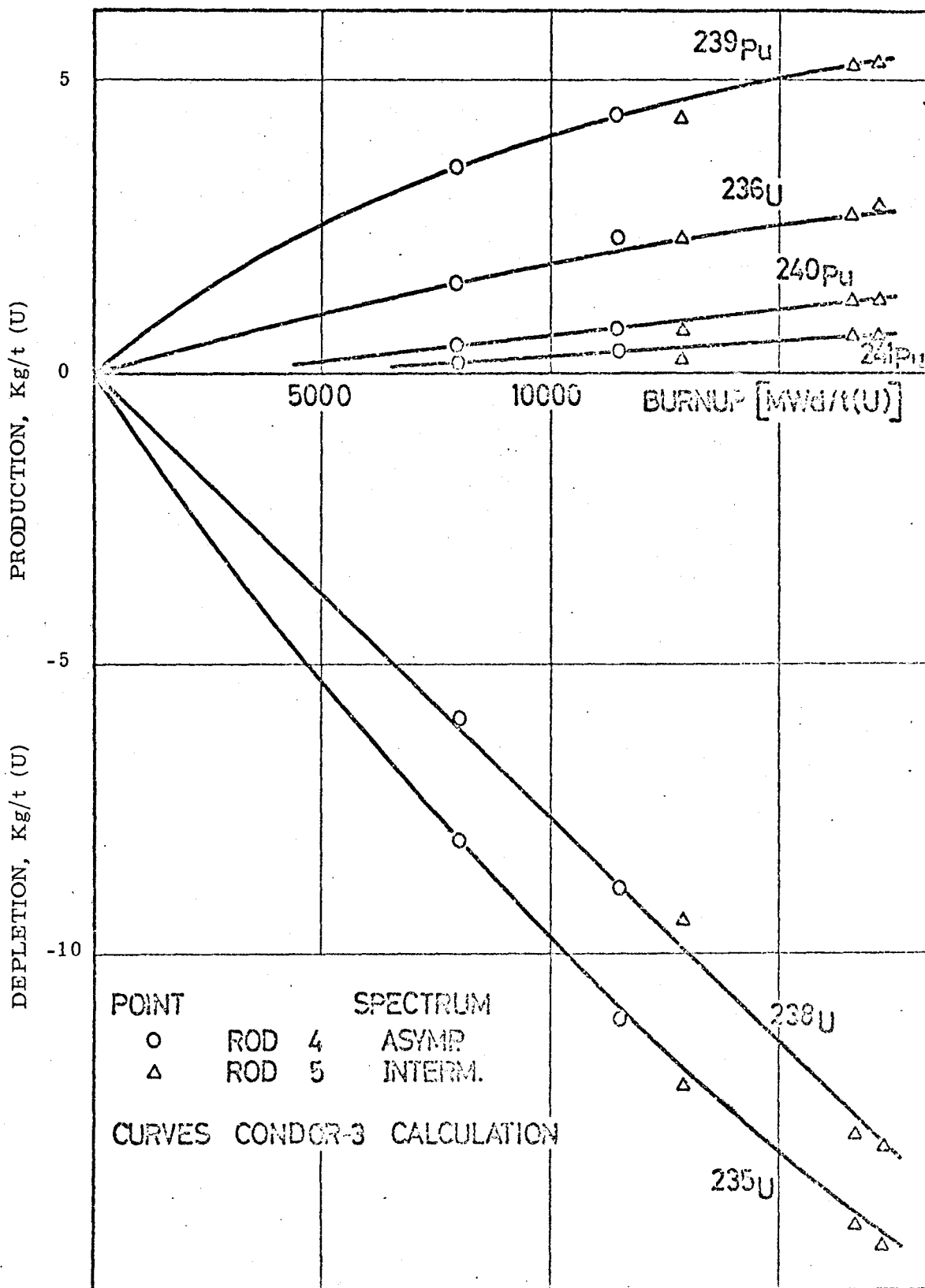


FIG. 7.4 (b) - ISOTOPIC PRODUCTION AND DEPLETION VS. BURN-UP FOR THE INTERMEDIATE CORE REGION.

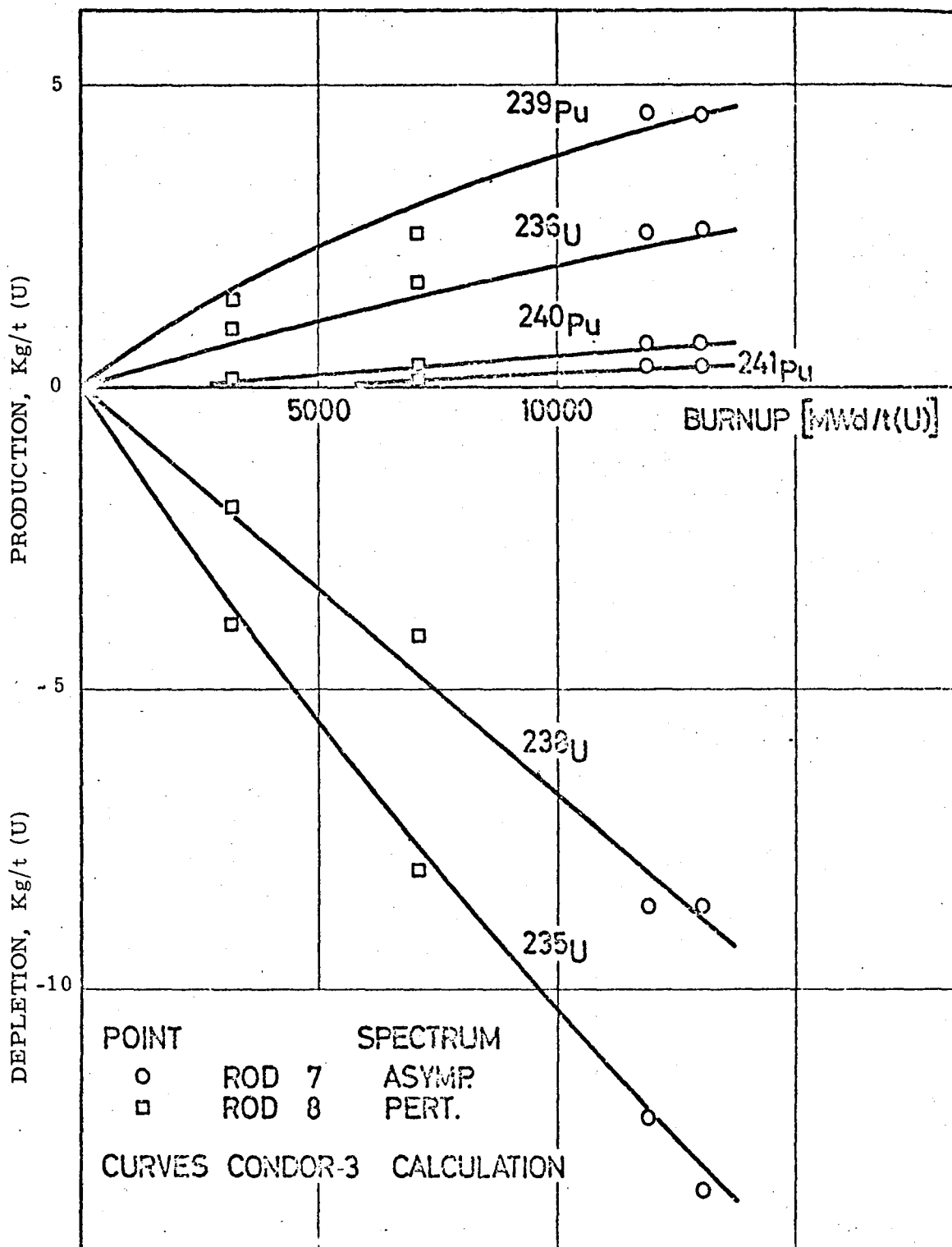


FIG. 7.4 (c) - ISOTOPIC PRODUCTION AND DEPLETION VS. BURN-UP FOR THE OUTER CORE REGION.

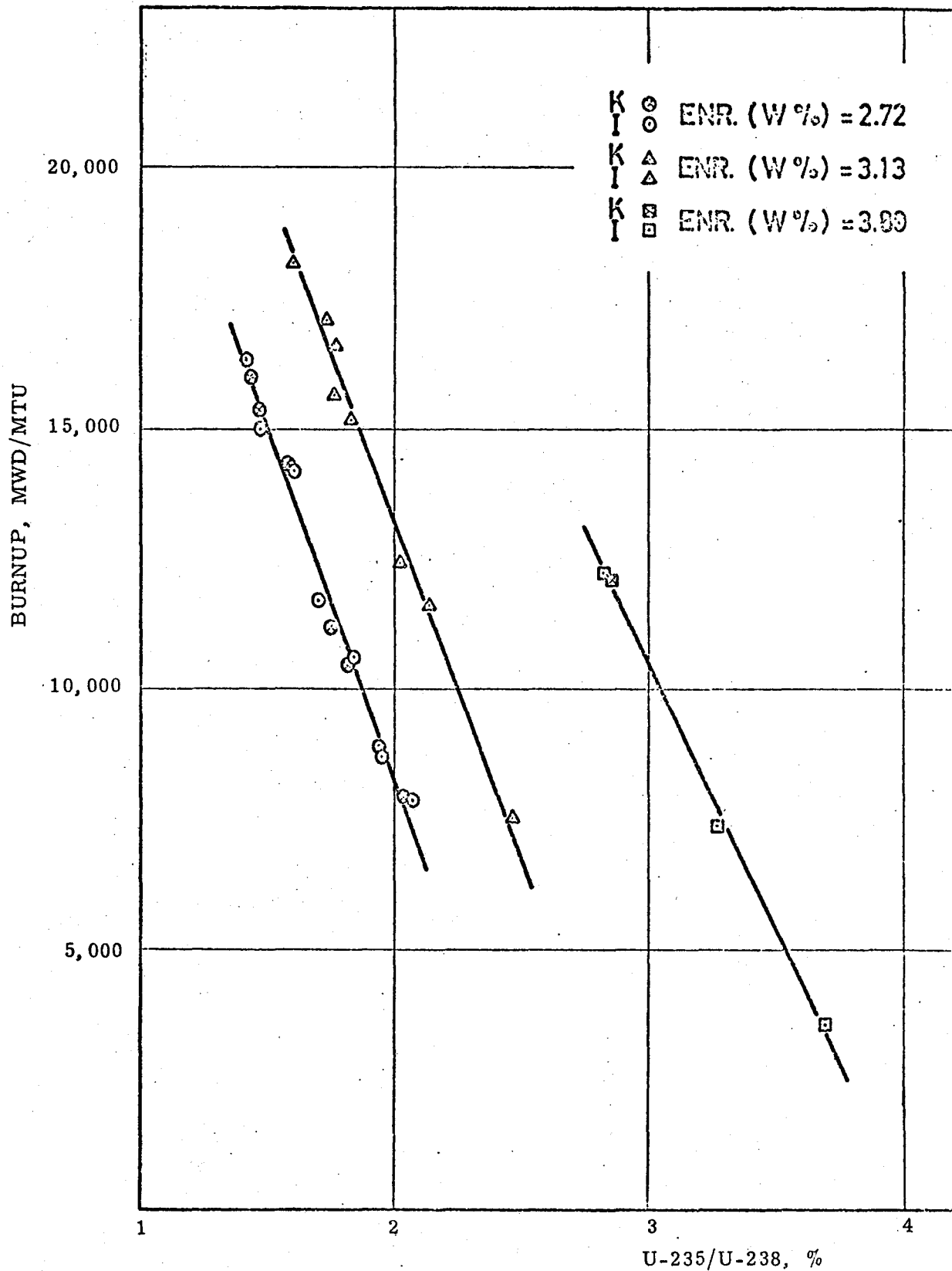


FIG. 7.5 - CORRELATION BETWEEN BURNUP AND U-235/U-238

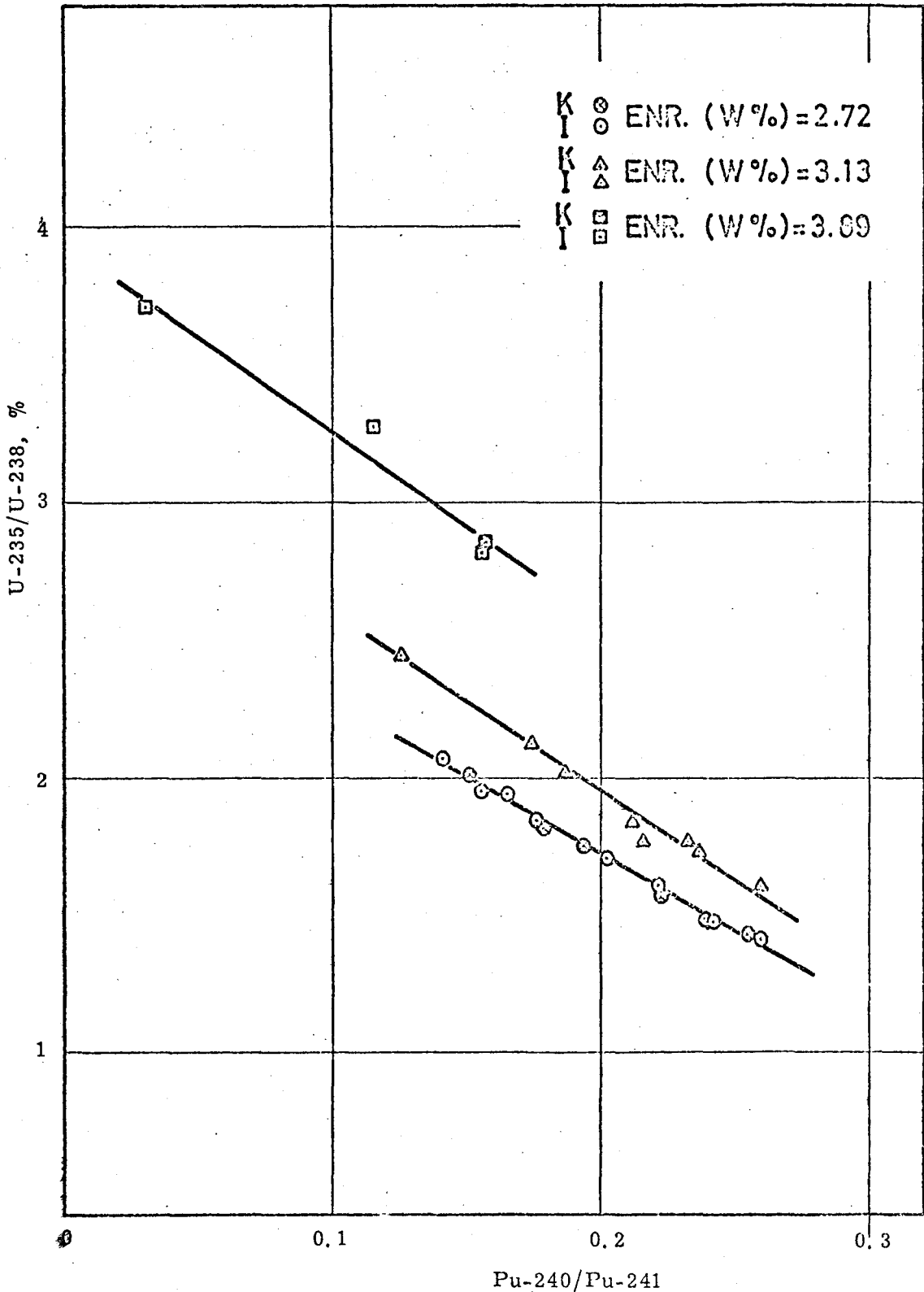


FIG. 7.6 - CORRELATION BETWEEN U-235/U-238 AND Pu-240/Pu-239

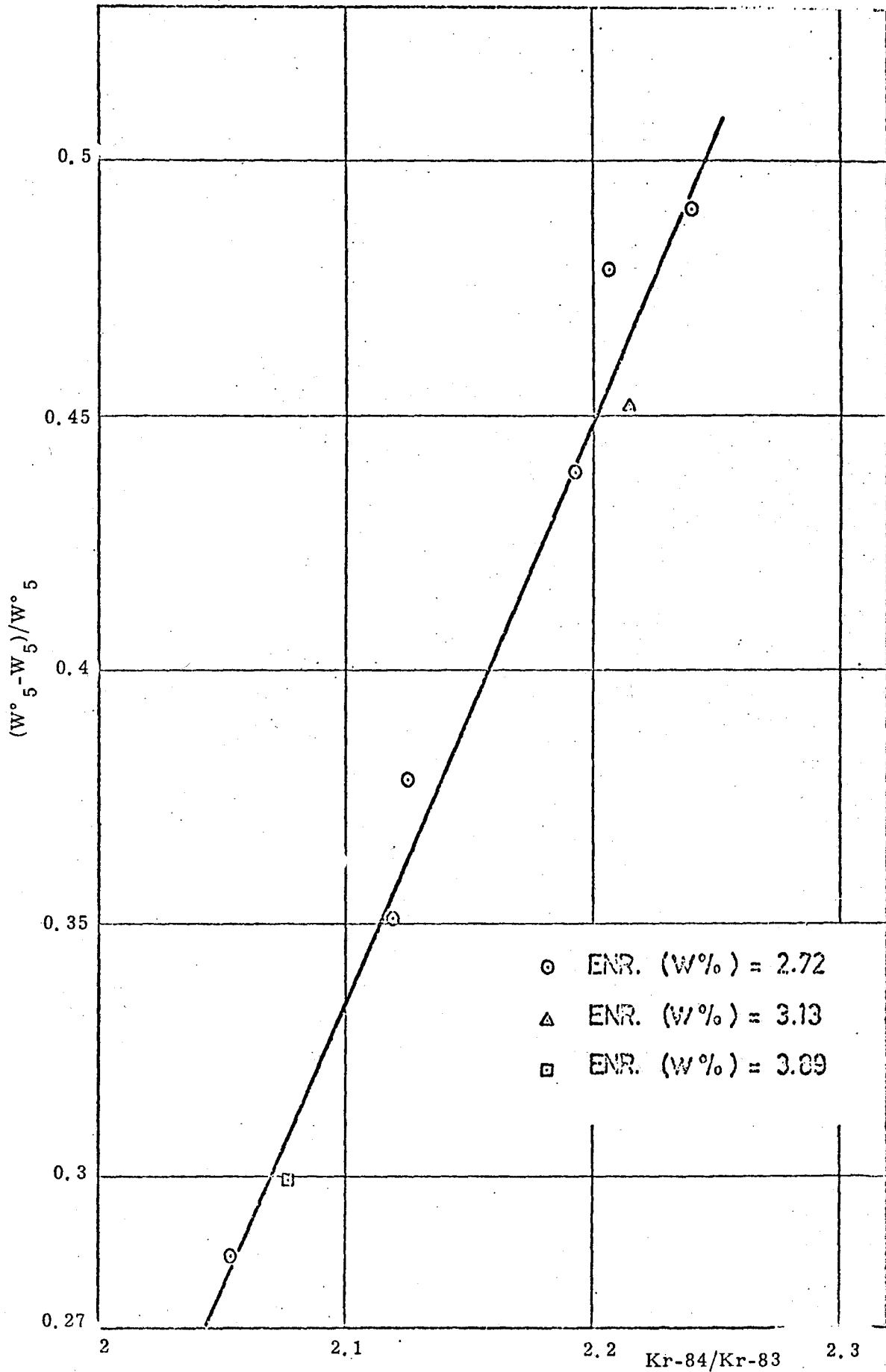


FIG. 7.7 - CORRELATION BETWEEN URANIUM DEPLETION AND Kr-84/Kr-83

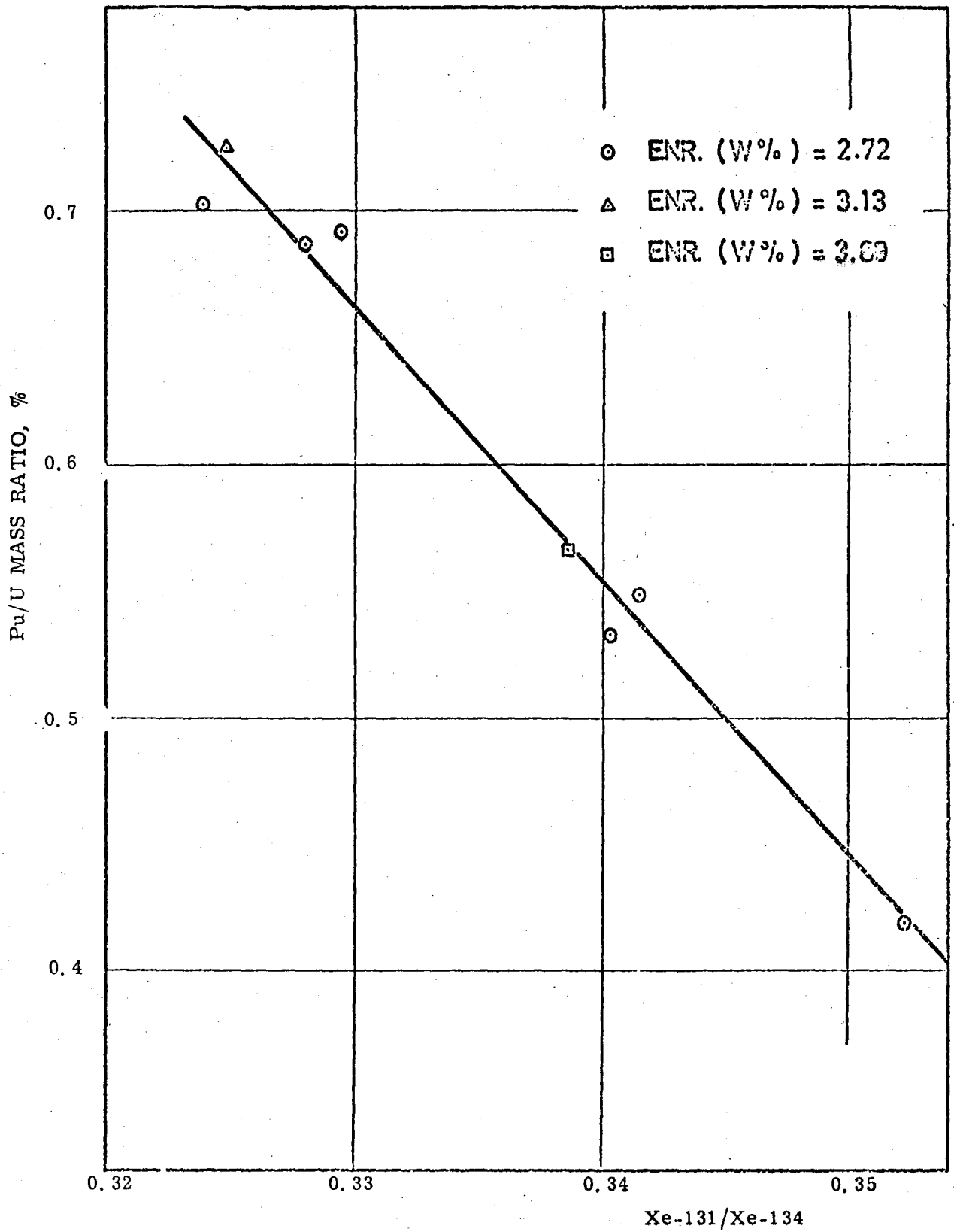


FIG. 7.8 - CORRELATION BETWEEN Pu/U AND Xe-131/Xe-134.

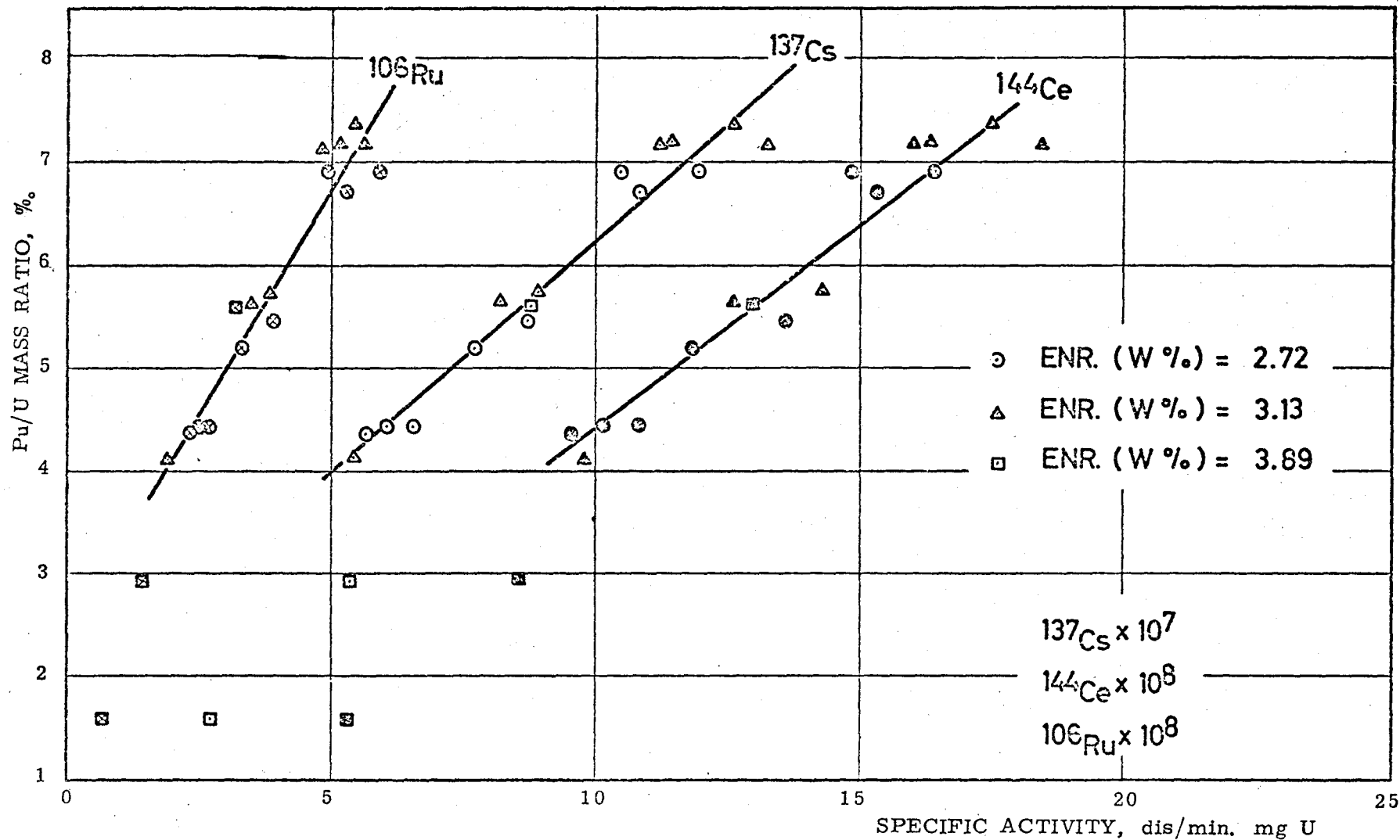


FIG. 7.9 - CORRELATION BETWEEN Pu/U AND Cs-137, Ce-144, Ru-106 SPECIFIC ACTIVITIES

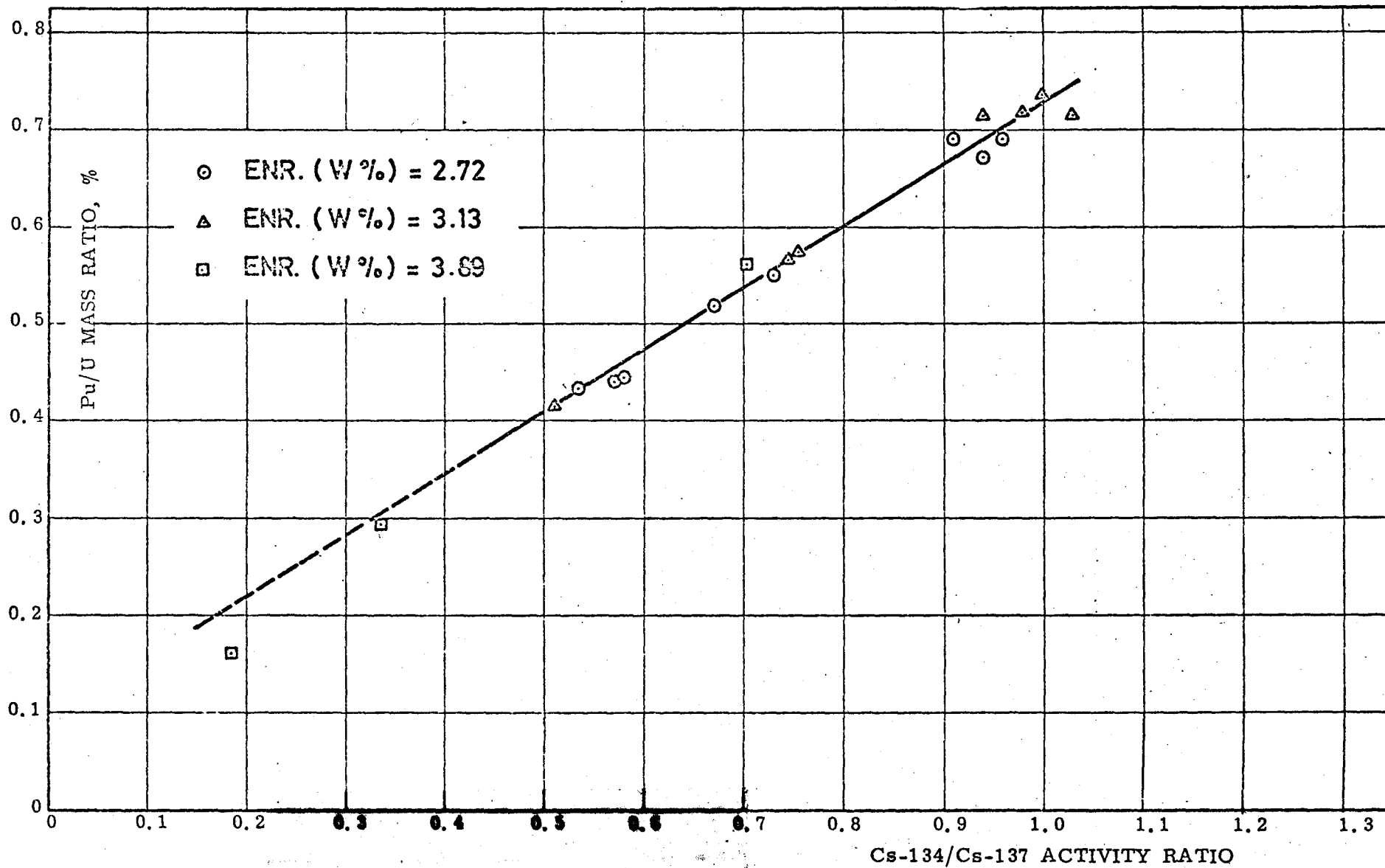


Fig. 7.10 Correlation between Pu/U and Cs-134/Cs-137 activity ratio

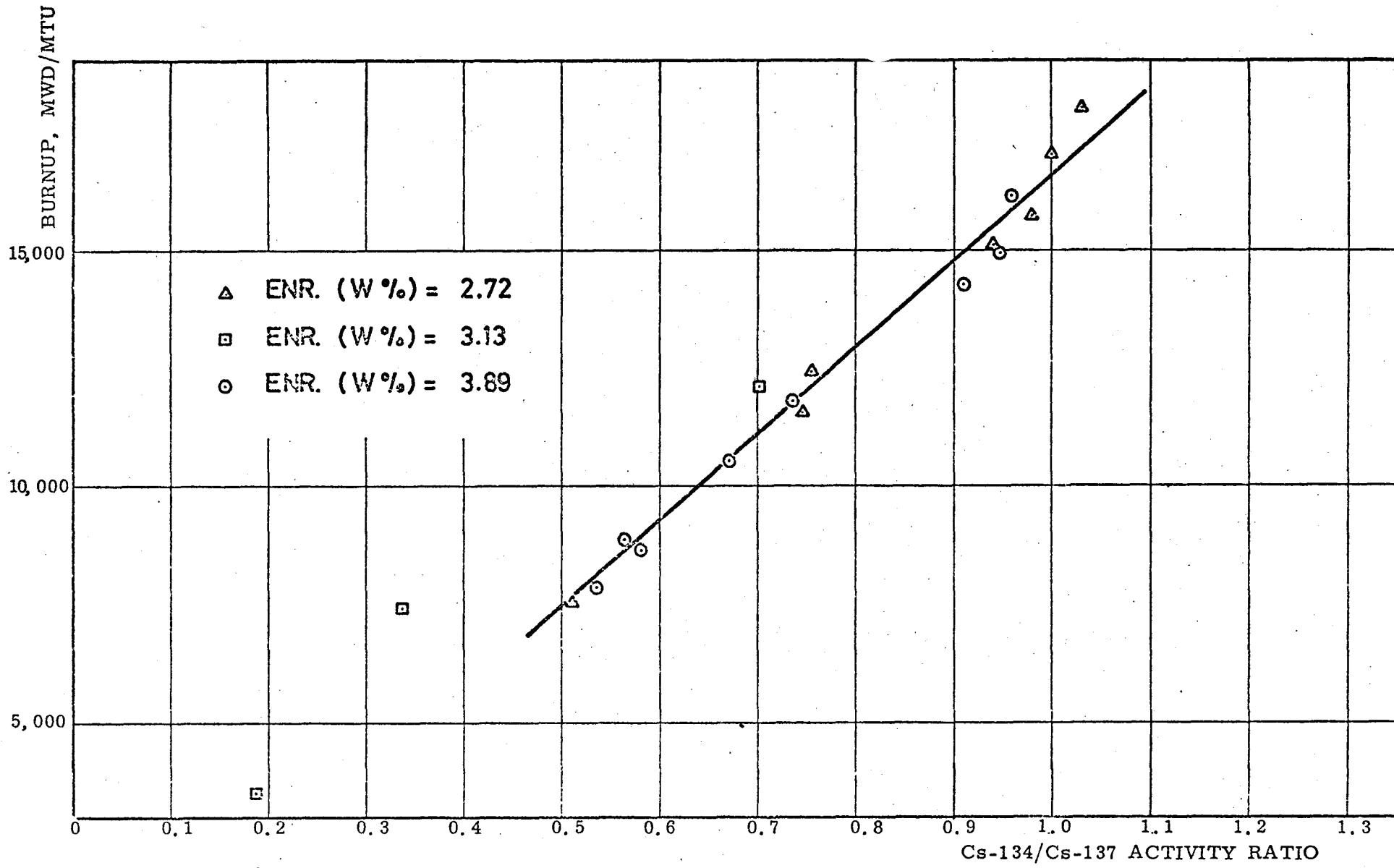


FIG. 7.11 - CORRELATION BETWEEN BURNUP AND Cs-134/Cs-137 ACTIVITY RATIO

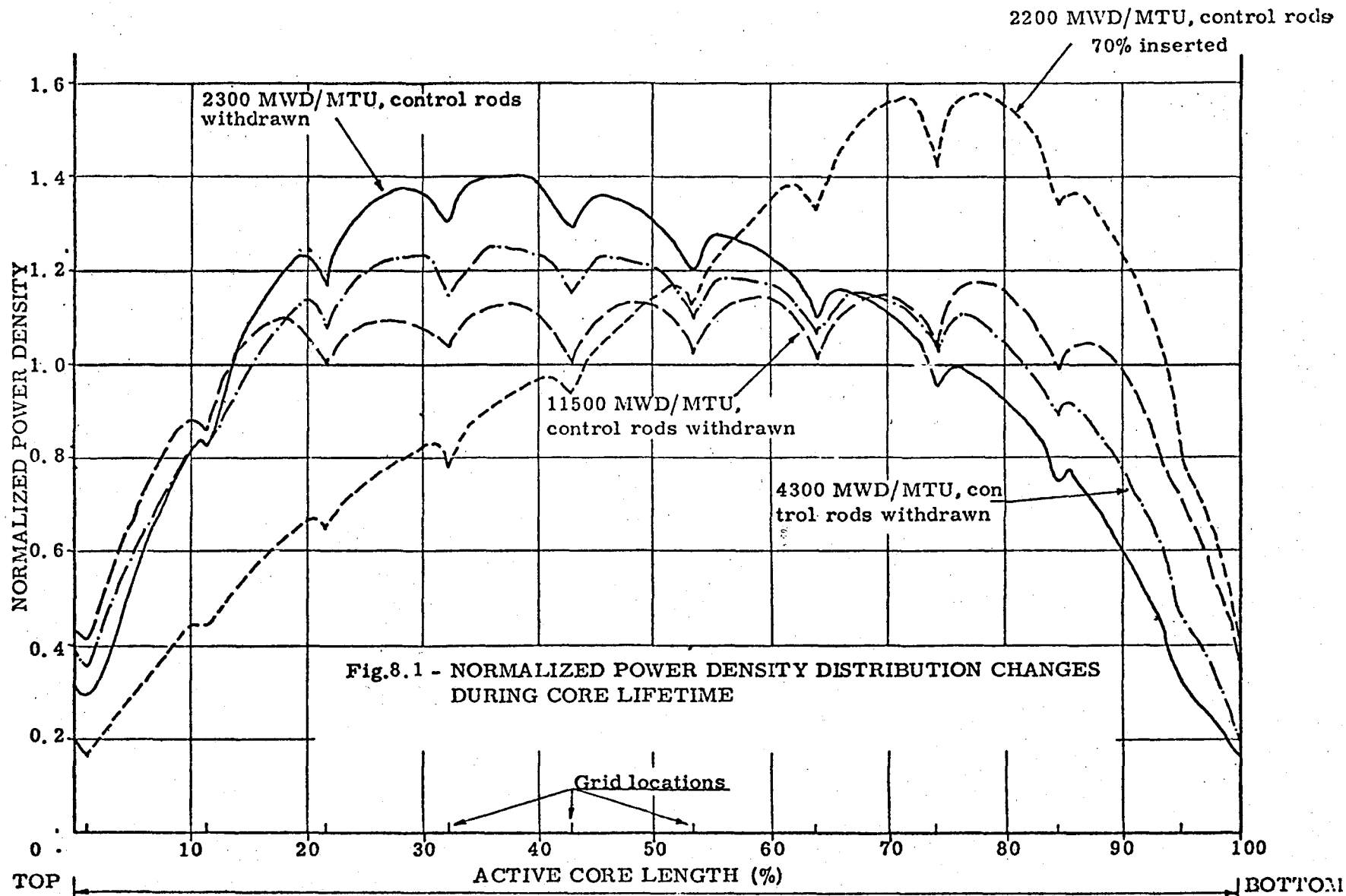


Fig.8.1 - NORMALIZED POWER DENSITY DISTRIBUTION CHANGES DURING CORE LIFETIME

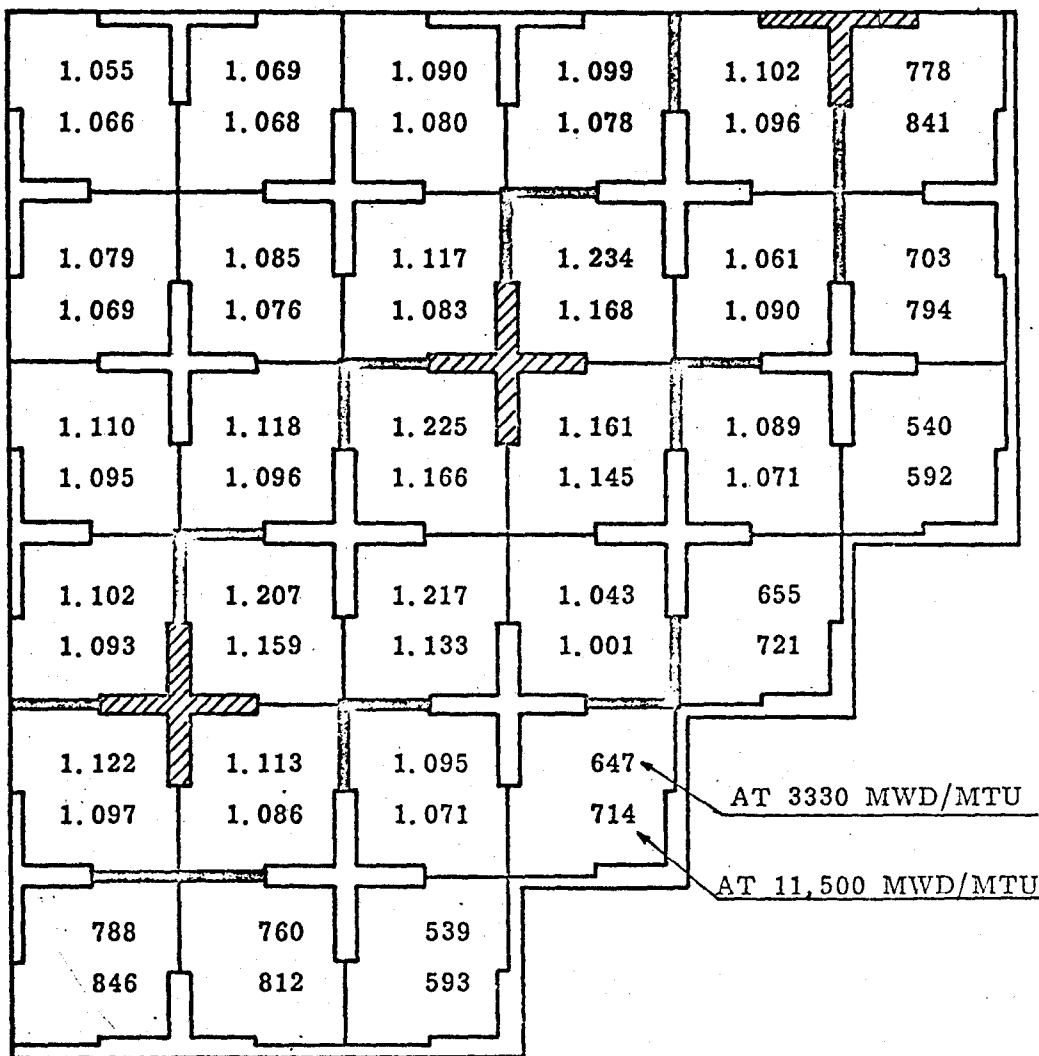
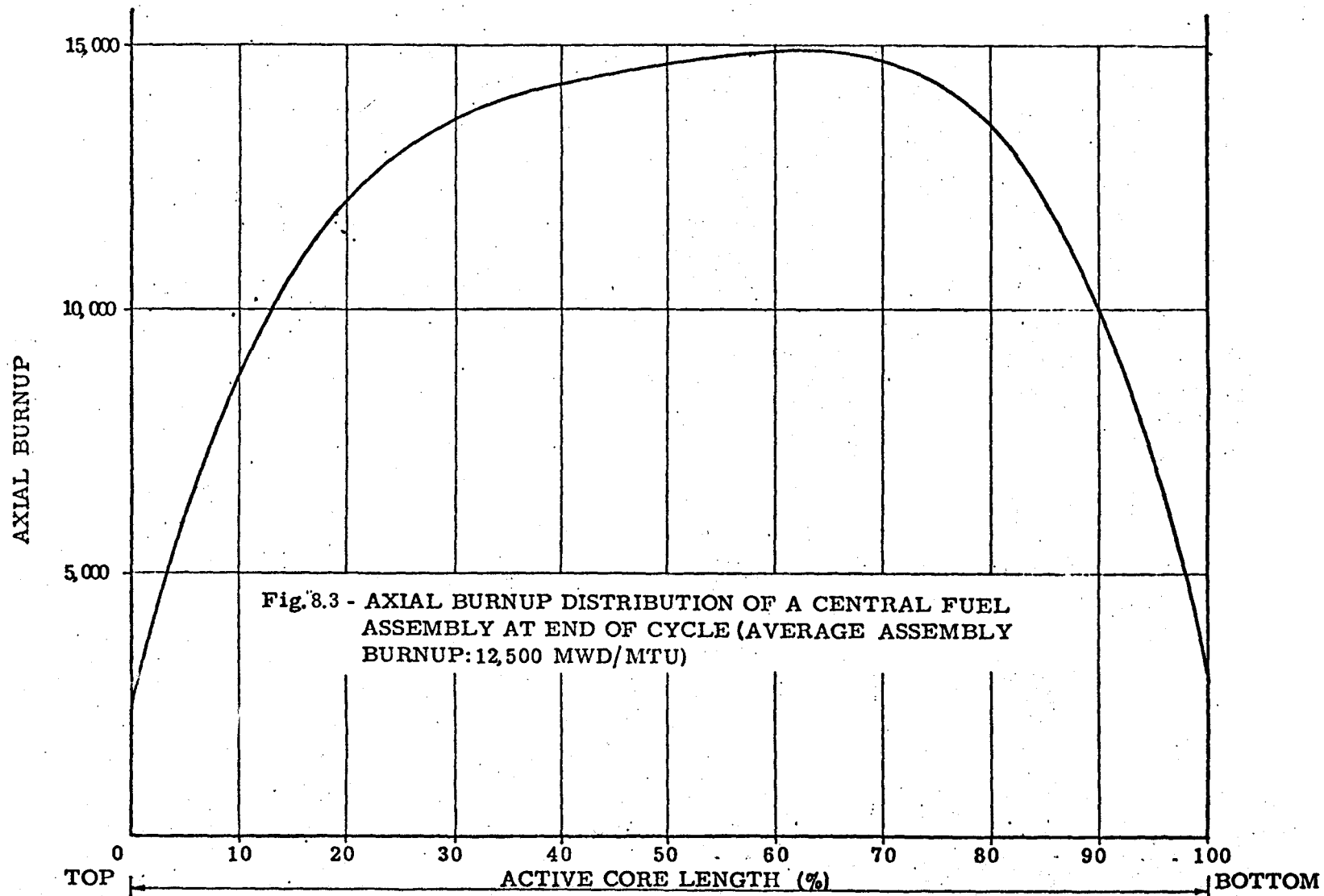
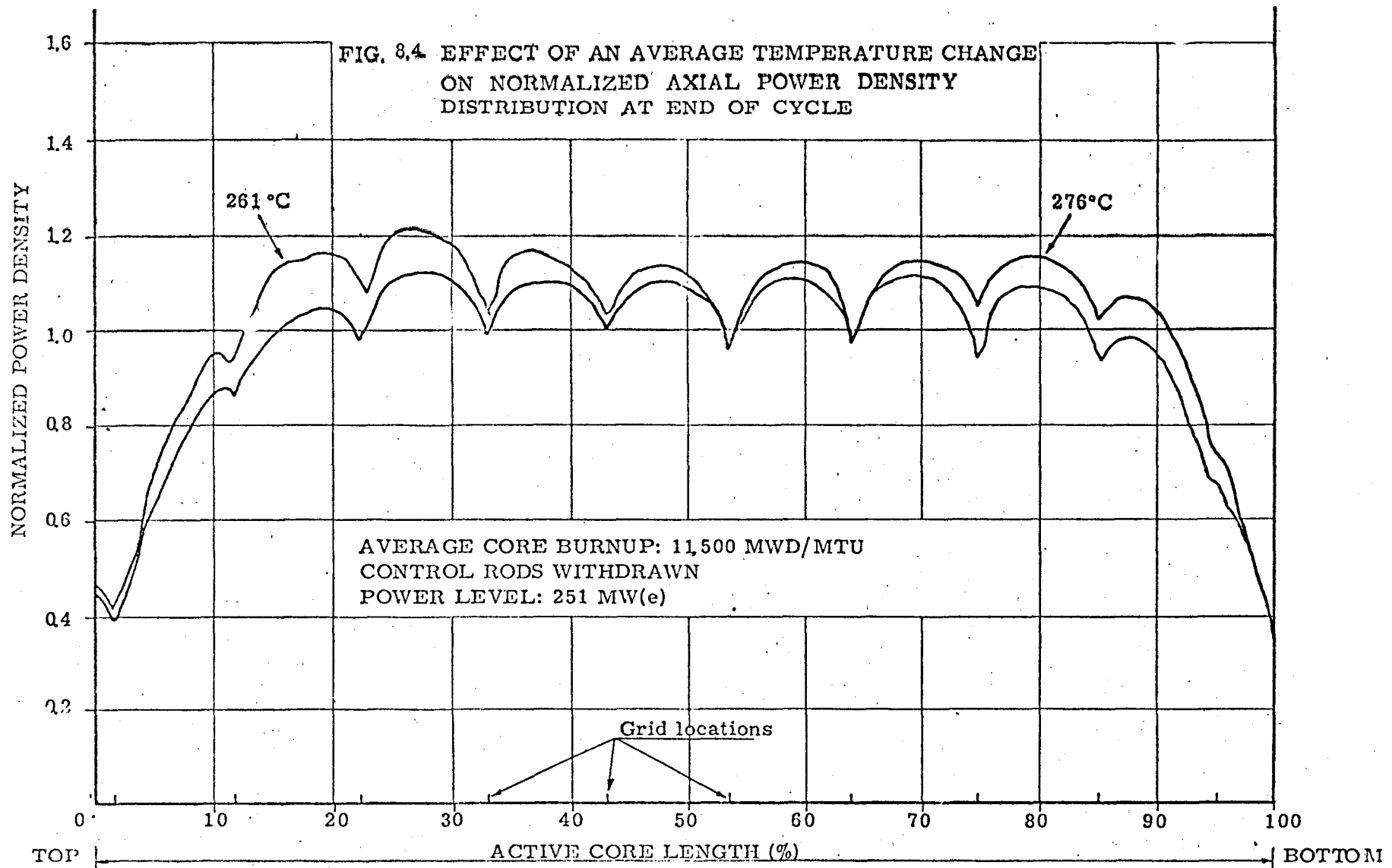
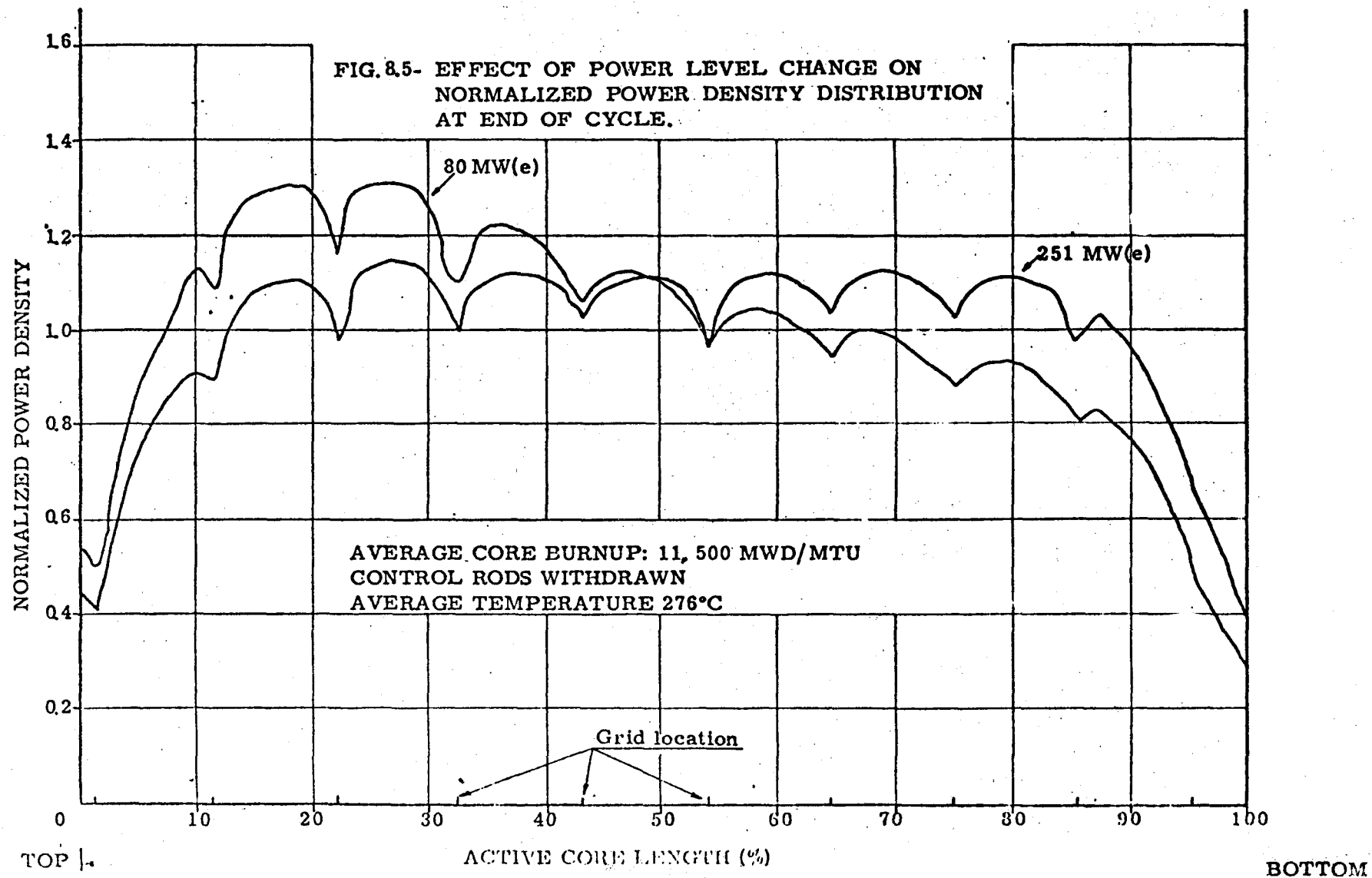


FIG.8.2 - ASSEMBLYWISE RADIAL POWER DISTRIBUTIONS AT 3330 MWD/MTU AND AT END OF CYCLE (11,500 MWD/MTU) (FULL POWER, DATA NORMALIZED TO UNIT AVERAGE)



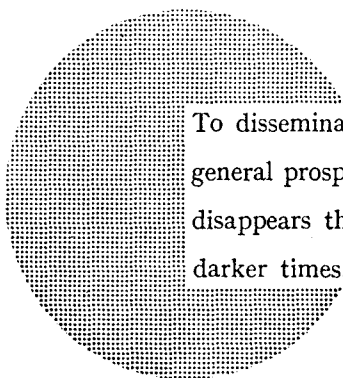




NOTICE TO THE READER

All scientific and technical reports published by the Commission of the European Communities are announced in the monthly periodical "euro-abstracts". For subscription (1 year: B.Fr 1 025,—) or free specimen copies please write to .

**Office for Official Publications
of the European Communities
Boîte postale 1003
Luxembourg
(Grand-Duchy of Luxembourg)**



To disseminate knowledge is to disseminate prosperity — I mean general prosperity and not individual riches — and with prosperity disappears the greater part of the evil which is our heritage from darker times.

Alfred Nobel

SALES OFFICES

The Office for Official Publications sells all documents published by the Commission of the European Communities at the addresses listed below, at the price given on cover. When ordering, specify clearly the exact reference and the title of the document.

UNITED KINGDOM

H.M. Stationery Office
P.O. Box 569
London S.E. 1 — Tel. 01-928 69 77. ext. 365

BELGIUM

Moniteur belge — Belgisch Staatsblad
Rue de Louvain 40-42 — Leuvenseweg 40-42
1000 Bruxelles — 1000 Brussel — Tel. 512 00 26
CCP 50-80 — Postgiro 50-80

Agency:
Librairie européenne — Europese Boekhandel
Rue de la Loi 244 — Wetstraat 244
1040 Bruxelles — 1040 Brussel

DENMARK

J.H. Schultz — Boghandel
Møntergade 19
DK 1116 København K — Tel. 14 11 95

FRANCE

*Service de vente en France des publications
des Communautés européennes — Journal officiel*
26, rue Desaix — 75 732 Paris - Cédex 15*
Tel. (1) 306 51 00 — CCP Paris 23-96

GERMANY (FR)

Verlag Bundesanzeiger
5 Köln 1 — Postfach 108 006
Tel. (0221) 21 03 48
Telex: Anzeiger Bonn 08 882 595
Postscheckkonto 834 00 Köln

GRAND DUCHY OF LUXEMBOURG

*Office for Official Publications
of the European Communities*
Boîte postale 1003 — Luxembourg
Tel. 4 79 41 — CCP 191-90
Compte courant bancaire: BIL 8-109/6003/200

IRELAND

Stationery Office — The Controller
Beggar's Bush
Dublin 4 — Tel. 6 54 01

ITALY

Libreria dello Stato
Piazza G. Verdi 10
00198 Roma — Tel. (6) 85 08
CCP 1/2640

NETHERLANDS

Staatsdrukkerij- en uitgeverijbedrijf
Christoffel Plantijnstraat
's-Gravenhage — Tel. (070) 81 45 11
Postgiro 42 53 00

UNITED STATES OF AMERICA

European Community Information Service
2100 M Street, N.W.
Suite 707
Washington D.C. 20 037 — Tel. 296 51 31

SWITZERLAND

Librairie Payot
6, rue Grenus
1211 Genève — Tel. 31 89 50
CCP 12-236 Genève

SWEDEN

Librairie C.E. Fritze
2 Fredsgatan
Stockholm 16
Post Giro 193, Bank Giro 73/4015

SPAIN

Libreria Mundi-Prensa
Castello 37
Madrid 1 — Tel. 275 51 31

OTHER COUNTRIES

*Office for Official Publications
of the European Communities*
Boîte postale 1003 — Luxembourg
Tel. 4 79 41 — CCP 191-90
Compte courant bancaire: BIL 8-109/6003/300